COMMONWEALTH OF AUSTRALIA
DEPARTMENT OF EXTERNAL AFFAIRS

AUSTRALIAN NATIONAL ANTARCTIC RESEARCH EXPEDITIONS

A.N.A.R.E. REPORTS

SERIES C

VOLUME II

COSMIC RAYS

Cosmic Ray Studies at Macquarie Island and Heard Island, 1948 - 51

By

F. JACKA, N. R. PARSONS, P. W. FORD and R. M. JACKLYN

ISSUED BY THE ANTARCTIC DIVISION, DEPARTMENT OF EXTERNAL AFFAIRS, MELBOURNE
JANUARY, 1959

PREFACE

This report is concerned with an examination of variations in sea level cosmic ray intensity measured with Geiger counter telescopes at the Australian National Antarctic Research Expeditions' stations at Heard Island (geographic co-ordinates 53·0°S., 73·4°E.; geomagnetic co-ordinates 61°S., 130°E.) and Macquarie Island (geographic co-ordinates 54·5°S., 159·0°E.; geomagnetic co-ordinates 61°S., 243°E.).

As large variations in barometric pressure are frequent at Heard Island and Macquarie Island these stations afforded an opportunity to study the variations in cosmic ray intensity associated with variations in atmospheric structure. Also, because of their high geomagnetic latitudes, it was hoped that new information might be obtained on variations associated with solar and geomagnetic disturbances. Measurements similar to those at Heard Island and Macquarie Island were also made on H.M.A.S. *Wyatt Earp* (Caro, Law and Rathgeber, 1948) and on M.V. *Duntroon* (Law, Mackenzie and Rathgeber, 1949) in a study of the latitude effect and other problems.

The proposal to carry out these measurements came from Dr. H. D. Rathgeber (then of the University of Melbourne) who directed the work in its initial stages. Dr. D. E. Caro (also of University of Melbourne) took responsibility for much of the original equipment design.

The design and construction of the equipment was carried out in the Physics Department, University of Melbourne; the authors are greatly indebted to Professor L. H. Martin for providing the necessary laboratory and workshop facilities and for his interest in the project.

The Heard Island measurements were made by F. Jacka and the late J. E. Jelbart. The Macquarie Island measurements were made by C. L. Speedy and K. C. Hines (1948), N. R. Parsons (1950) and P. W. Ford (1951).

The material of chapters 7 and 8 of this report has already been published (Jacklyn 1954-55).

The manuscript of the report was submitted in June, 1955.

F. JACKA
Chief Physicist
Antarctic Division, Department of External Affairs

CONTENTS

1. INTRODUCTION. F. JACKA 1
   Outline of the problem 1
   Variations of atmospheric origin 1
   Variations associated with solar and geomagnetic disturbances 2

2. DESCRIPTION OF EQUIPMENT. F. JACKA AND N. R. PARSONS 4
   Abstract 4
   Introduction 4
   Equipment used at Heard Island and Macquarie Island, 1948 6
   Equipment used at Macquarie Island, 1950-52 8
   Notation used for coincidence rates 13
   Counting errors 14

3. STATISTICAL ANALYSIS. F. JACKA 15
   Abstract 15
   Introduction 15
   Regression analysis 15
   Simple regression—error term normally distributed 16
   Multiple regression—error term normally distributed 17
   Effect of non-independence of successive values of ε 17
   Simple regression—X_1 a Poisson variate 18
   Accuracy of the regression model 20
   Computing methods 20

4. COSMIC RAY INTENSITY VARIATIONS OF ATMOSPHERIC ORIGIN. F. JACKA. 21
   Abstract 21
   Introduction 21
   The barometer and temperature effects—experimental results 23
   Significance of the barometer and temperature coefficients 23
   Barometer effect for mesons—theoretical treatment 37
   Barometer effect—discussion 42
   Cosmic ray intensity and upper air data—experimental results 47
   Significance of results 48
   Duperier temperature effect—theoretical treatment 58
   Duperier temperature effect—discussion 64
   μ-meson decay effect (barometric pressure constant) 69
   Barometer effect for μ-mesons (height of production constant) 72
   Conclusions 74
   Appendix: Comments on a paper by Olbert (1953) 76

5. COSMIC RAY INTENSITY VARIATIONS ASSOCIATED WITH SOLAR AND GEOMAGNETIC DISTURBANCES. F. JACKA 80
Abstract 80
Introduction 80
Variations associated with magnetic storms 81
Cosmic ray intensity and solar radio noise 81
Conclusions 83

6. DIURNAL VARIATION IN COSMIC RAY INTENSITY. P. W. FORD AND N. R. PARSONS 85

7. THE BAROMETER COEFFICIENT AND AIR MASS EFFECTS ON COSMIC RAYS AT MACQUARIE ISLAND. R. M. JACKLYN 89
Abstract 89
Introduction 89
Data and methods of analysis 90
The front effects 90
The mechanism of the front effects and the variability of the barometer coefficient 92
Conclusions 95

8. COSMIC RAYS AND AIR MASS EFFECTS AT MACQUARIE ISLAND. R. M. JACKLYN 96

ACKNOWLEDGEMENTS 99

REFERENCES 100

1. INTRODUCTION

by F. JACKA

Outline of the problem. Since the work of Myssowsky and Tuwim (1928) established the dependence of cosmic ray intensity on barometric pressure, many workers have made systematic measurements with ionization vessels and more recently with Geiger counter telescopes in order to study the variations with time of the cosmic ray intensity. These studies have revealed the existence of several distinct time variations, which may be divided into two main groups: (a) Variations of atmospheric origin; (b) Variations associated with solar and geomagnetic disturbances. In addition there is some evidence for a very small sidereal diurnal variation (Elliot and Dolbear, 1951).

It is the purpose of the present work to examine the variations in cosmic ray intensity measured at Heard Island and Macquarie Island under the headings (a) and (b) above.

An outline of present knowledge of these variations is given below:

Variations of atmospheric origin

(a) Barometer effect. A negative correlation between cosmic ray intensity and barometric pressure has been demonstrated by many workers (Hogg, 1949). This effect is ascribed to absorption in the atmosphere and to decay of μ-mesons, the probability of which increases with increase in their height of production. If μ-meson production is assumed to occur at a definite atmosphere depth, x_o gm. cm.$^{-2}$, then since $x_s = x_o \exp S_s/H$ the intensity at sea level will decrease with increase in x_s for fixed H. (x_s gm. cm.$^{-2}$ = atmospheric depth at sea level, S_s = distance from level x_o to level x_s and H cm. = scale height of the atmosphere.)

It will be shown in § 4·4 that an accurate treatment of the problem along these lines yields values of the barometer coefficient which do not agree with the experimental estimates.

(b) Sea level temperature effect. At many localities the cosmic ray intensity and air temperature are negatively correlated (Hogg, 1949). This effect is ascribed to variation of S_s associated with variation of H at fixed x_s. Air temperature at sea level has in some places a fairly high positive correlation with mean temperature of the atmosphere and hence with H. Increase in H increases S_s which increases the probability of μ-mesons decaying before reaching sea level.

(c) Meson decay effect and Duperier positive temperature effect. Duperier (1951 and earlier references given in this paper) has shown that the sea level hard component intensity may be represented by a linear function of barometric pressure, height of the μ-meson production level (assumed to be at about 100 millibar) and mean temperature in an interval below this level, the temperature coefficient being positive. The effects of variation of barometric pressure and height of μ-meson production are mentioned above; the positive temperature effect is ascribed by Duperier to nuclear capture in the atmosphere of π-mesons, the probability of which increases with density (i.e. decreases with increase in temperature), thus decreasing the number which decay into μ-mesons. Duperier's experimental results are not in good agreement with his theoretical calculations.

Variations associated with solar and geomagnetic disturbances.

(a) Magnetic storm effect. Magnetic storms are sometimes accompanied by a decrease in cosmic ray intensity (Forbush 1938) of several per cent followed by a gradual return to normal intensity, the form of the variation being similar to, but not highly correlated with, that of the horizontal component of the earth's magnetic field. Several writers (e.g. Hayakawa et al. 1950) have examined the possibility of explaining this variation in terms of the effects on the trajectories of the primary cosmic ray particles of the magnetic field associated with a ring current around the earth of the type suggested by Chapman and Ferraro (1933) in their theory of magnetic storms. Alfvén (1950) attributes the variation to the change in energy of the primary cosmic ray particles on passing through the solar ionized corpuscular stream which is responsible for the magnetic storm. This stream has a transverse electric field due to its motion through the assumed magnetic field of the sun.

Smaller variations (both increases and decreases) show a 27-day recurrence tendency of form roughly similar to that of magnetic activity (Hogg, 1949).

(b) Solar flare effect. Increases in cosmic ray intensity of from a few per cent to more than 100 per cent have been observed in association with intense solar flares (Forbush, Stinchcomb and Schein, 1950). Several theories of this effect are summarized by Elliot (1952). Dolbear, Elliot and Dawton (1951) have shown that a similar effect of much smaller magnitude also occurs in association with Dellinger type radio fade-outs which are usually associated with solar flares of moderate intensity.

(c) Solar daily variation. Several writers have reported a diurnal variation in cosmic ray intensity at sea level (Lange and Forbush, 1948). This variation may be in part due to variation in the atmosphere, but its amplitude is enhanced and its phase advanced on days of high geomagnetic

activity (Sekido and Kodama, 1952). Thambyahpillai and Elliot (1953) have further shown that the phase of this variation has undergone a considerable change in the last 20 years. It appears likely that this change is part of a 22-year variation coinciding with the 22-year sun-spot cycle.

Elliot and Dolbear (1951) in Manchester, using two counter telescopes, one pointing to the north at 45° zenith angle and the other pointing south at the same zenith angle, have shown that the south-minus-north difference, which is independent of atmospheric structure, shows a daily variation with significant 24-hour and 12-hour components. This variation is enhanced on days of high geomagnetic activity. Assuming this effect to be due to variation in primary cosmic ray intensity they then calculated the expected east-minus-west daily variation and found this to be in good agreement with their observed east-minus-west daily variation.

2. DESCRIPTION OF EQUIPMENT

by F. JACKA AND N. R. PARSONS

Abstract. The cosmic ray programme of the Australian National Antarctic Research Expeditions at Heard Island and Macquarie Island is described. Some of the practical difficulties encountered in establishing the Heard Island cosmic ray laboratory are mentioned.

The cosmic ray intensity recording equipment used at Heard Island and Macquarie Island is described; circuit diagrams of the basic units of the final form of the equipment are given. Errors in counting are found to be too small to be of importance in the interpretation of the records.

Introduction. The decision to include cosmic ray studies in the programme of the Australian National Antarctic Research Expeditions was made in July, 1947, and development of suitable equipment was commenced immediately in the physics laboratories of the University of Melbourne. As this project was the first of its kind undertaken in this country, intensive work was necessary to prepare equipment in time to leave for Heard Island in November, 1947, and later for Macquarie Island and the Antarctic (on H.M.A.S. *Wyatt Earp*). However, some success had already been achieved in the development of Geiger counters suitable for cosmic ray studies.

The proposed equipment consisted of three Geiger counter telescopes with associated recording circuits, a spherical ionization chamber of 20 litre capacity filled with argon at 50 atmospheres pressure, using β ray compensation and registering on a Lindemann electrometer with photographic recording (Jelbart, 1949), and also a further Geiger counter array and circuits for recording extensive showers.

However, the Macquarie Island ionization chamber suffered a gas leak which prevented its use and the Heard Island Lindemann electrometer suffered damage which in spite of protracted attempts could not be repaired with the facilities available at Heard Island. Later work was carried out to develop a vibrating disc electrodynamic electrometer (Norman, 1950) for use with the ionization chambers. However, difficulties with insulation in this electrometer have prevented it from functioning satisfactorily. Further work on this instrument has been resumed recently.

Since the extensive showers were to be recorded photographically with the ionization record and because of unsatisfactory behaviour of the shower recording circuits due mainly to the long (20 μ-sec.) resolving time of the coincidence circuits no satisfactory shower measurements were made at Heard Island or Macquarie Island with this equipment. New circuits were

developed at Heard Island, but because the required components were not available they could not be put into use; these formed the basis of the circuits used later in the equipment which was to go to Macquarie Island in 1950.

The Heard Island cosmic ray laboratory was constructed from a 9-ft. by 9-ft. prefabricated hut designed for use in the tropics. The original high gable roof was replaced by a flat, almost horizontal, roof built from light timber obtained mainly from packing cases. This flat roof proved very satisfactory from the point of view of avoiding snow deposition which would have affected the cosmic ray records. With the very windy conditions that prevail at Heard Island snow frequently packed hard on sloping roofs but not on this flat roof.

A 6-ft by 9-ft. dark room was added to the building using the material of the original gable roof, timber obtained from packing cases and some fibro-cement sheets. Later a small porch was built from further scrap material. The outer walls of the whole building were weather-proofed with bituminous felt, the walls and roof were insulated with rock-wool and lined with hard-board.

Work benches, storage shelves, a film-drying cupboard and seats were constructed mainly from packing-case timber. Two 44-gallon petrol drums (mounted inside the darkroom to avoid freezing) were used for water tanks. Pipe fittings and taps from the expedition's wrecked aircraft were used. The darkroom sink was formed from a sheet of aluminium and a pressed steel wash-dish.

After installing the cosmic ray recorder, all Geiger counters and circuits were tested. Very little damage had occurred in transit from Melbourne. However, during the first few months of operation many difficulties arose. Parts of the recording circuits proved insufficiently reliable; these were replaced with new circuits, some of which were developed at Heard Island and others at Melbourne, the details being radioed to Heard Island. Later in the year, because of inadequacy of supplies, many used valves had to be re-used, necessitating alterations in other component values in order to maintain reliable operation.

Because their life was shorter than expected, the electro-mechanical counters used for registering the output pulse rate from the cosmic ray recorder had to be repaired. The "carry-over" mechanism on the units drums which were die-cast from white metal became worn. This was built up with soft solder which was then filed and scraped to shape. After several such repairs most of the original metal had been replaced with soft solder and this method was no longer satisfactory. It then became necessary to make complete new drums; the bodies of these (approximately $\frac{1}{2}$ in. diameter) were turned from 1 in. diameter brass on a watchmaker's lathe and

the carry-over mechanism was formed by cutting away the excess metal by hand. Later it was necessary to make new hard steel driving gears which had to be filed to shape.

During the winter months failure of Geiger counters occurred through deposition on the glass surface of a film of tar-like material which was found to come from the rather inefficient kerosene-burning heater in the building. After removing the heater, the recording camera frequently failed due to the combined effects of excessive wear and low temperatures. This necessitated rebuilding the camera and replacing several parts which had to be hand-made.

In spite of the many equipment failures ten months reliable records were obtained with only occasional short breaks in the series.

At Macquarie Island during 1948 the facilities were similar to those described above and many of the same difficulties were encountered.

During 1949 the whole equipment was rebuilt (Parsons, 1951) in the light of experience gained at Heard Island. The new equipment was installed at Macquarie Island in 1950 in a new, well-built prefabricated laboratory measuring 36 ft. by 12 ft. This was well equipped and adequate supplies of spare parts were stocked; very few difficulties occurred in maintaining the equipment.

At Heard Island and Macquarie Island regular checks were made in the performance of Geiger counters and recording circuits. Photographic records were processed regularly and examined to ascertain that no peculiarities had passed unnoticed. Meteorological data (pressure, temperature and radio-sonde data) were obtained regularly from the station meteorologist.

Equipment used at Heard Island and Macquarie Island, 1948. The Heard Island and Macquarie Island (1948) recorders contained six trays of Geiger counters arranged as shown in Fig. 1. Each tray contained six counters connected in parallel. Threefold coincidences were recorded between trays 1, 2 and 3, giving the total intensity over a half-angle of 33° by 33° directed vertically; the average coincidence rate was approximately 4,500 per hour. Threefold coincidences, averaging approximately 3,300 per hour, between trays 2, 3 and 4 gave the hard component intensity over the same solid angle; the soft component (mainly electrons) was stopped in the 10 cm. of lead between trays 3 and 4. Twofold coincidences between trays 5 and 6 recorded the total intensity over nearly the full hemisphere, the average coincidence rate being approximately 21,200 per hour.

The Geiger counters used were of pyrex glass construction. The cathode was a film of copper evaporated onto the glass from the central 0·004-in. tungsten wire anode which had been previously electroplated with copper.

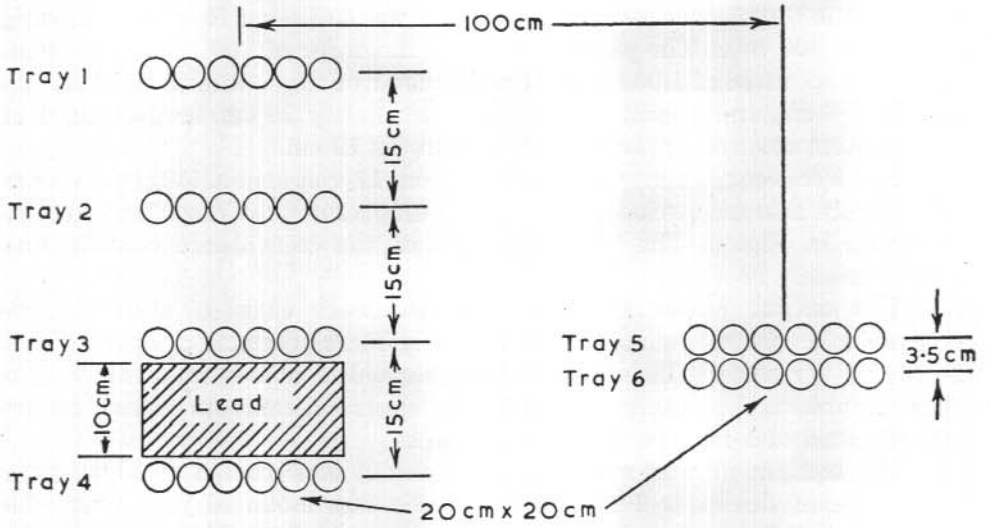

FIG. 1.

Arrangement of Geiger counters in the Heard Island cosmic ray recorder.

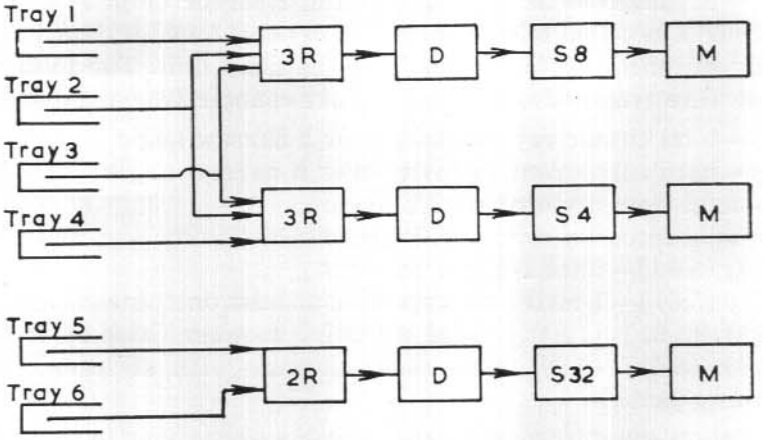

FIG. 2.

Block diagram of circuits of the Heard Island cosmic ray recorder.
Legend: 3R, 3 fold coincidence; 2R, 2 fold coincidence; D, discriminator; Sr, scale of r; M, driving circuit and mechanical register.

The counters were self-quenching, being filled with argon and ethyl ether in the ratio 8 to 1. The total gas pressure was adjusted to give a starting voltage of 900 volts. The plateaux were of the order of 200 volts. The counters were operated at 1,000 volts. The diameter of the counters was approximately 3·4 cm. and sensitive length approximately 20 cm. so that trays of six counters covered approximately 20 cm. by 20 cm.

The whole equipment was operated from 12-volt lead-acid accumulators which were charged periodically. A block diagram of the recording circuits is shown in Fig. 2. The resolving time of the coincidence circuits was approximately 20 μ-sec.

The output pulses from the circuits were counted with electromechanical counters (telephone message registers) capable of operation at 25 counts per second. These were photographed at hourly intervals with a 16 mm. camera, the timing being made by electrical contacts carried on the minute hand of a marine-type chronometer.

The equipment was mounted in a cabinet constructed of aluminium with walls of thickness 0·7 gm. cm.$^{-2}$. This was mounted just under the laboratory roof, which consisted of approximately 2 gm. cm.$^{-2}$ of organic matter (wood, hardboard, etc.)

Equipment used at Macquarie Island, 1950-52. The 1950-52 Macquarie Island cosmic ray recorder contained eight trays of Geiger counters. Trays 1 to 6 were arranged as in the Heard Island recorder (Fig. 1) and trays 7 and 8 formed a two-fold telescope similar to trays 5 and 6; this was placed at varying distances up to 200 m. from the main unit. The following coincidences were recorded (the numbers are counter tray numbers):

(1,2,3)—total cosmic ray intensity over a narrow angle
(2,3,4)—hard component intensity over a narrow angle
(5,6)—total intensity over a wide angle
(7,8)—total intensity over a wide angle
[(1,2,3), (5,6)]—total 1-metre showers
[(2,3,4), (5,6)]—1-metre showers with at least one penetrating particle
{[(1,2,3), (5,6)], (7,8)} —total extensive showers (base up to 200 m.)
{[(2,3,4), (5,6)], (7,8)} —extensive showers with at least one penetrating particle

The Geiger counters used were of similar dimensions to those used in the Heard Island apparatus. During the first twelve months of operation, the cathodes in most of them were evaporated gold and, in the remainder, were platinum deposited from "liquid bright platinum" which was painted on then heated in a stream of air. The filling contained argon and ethylene in the ratio 9 to 1. During the last ten months of operation, evaporated gold cathodes were used, the filling being argon and ethyl ether in the ratio 9 to

1·1. In each case the total pressure was adjusted to give a starting voltage of 1,000 volts. The plateaux were all longer than 200 volts.

After several months use some deterioration of the counters became apparent and the argon-ethylene and argon-ether filled counters behaved quite differently. Deterioration of the argon-ether counters usually led to greater frequency of multiple and spurious pulses and shortened plateaux. The argon-ethylene counters on the other hand gave smaller and smaller pulses at the normal operating voltage, the plateaux remaining roughly the same length but drifting to a higher voltage range. Tests performed on aged argon-ethylene counters showed that on first applying the normal operating voltage the pulses were of normal size but after a few minutes decreased in size, reaching a stable level after a further few minutes. Pulses of normal size could be obtained by increasing the voltage and this led also to an increase in starting voltage. This behaviour suggested the presence of a semi-insulating material on the electrodes, probably polymerization products from the breakdown of the ethylene quenching vapour.

Facilities were not available at Macquarie Island to open, clean and refill the counters. However, it was found that, after connecting the ends of the anode wire directly across a 12-volt accumulator, bringing the wire to a bright red heat for two to three seconds, most of the aged counters returned to normal characteristics with a further useful life of three to four months. Most of these rejuvenated counters then failed in the same way and some of them responded satisfactorily to a second rejuvenation treatment.

The argon-ether filled counters after deterioration did not respond to this treatment. In order to increase their useful life it was found necessary to operate at a lower over-voltage and to modify the pulse-shaping circuits to accept smaller counter pulses.

A block diagram of the recording circuits of the apparatus is shown in Fig. 3. The functions of the various units are briefly described below; all valves used were miniature pentodes, type 6AK5.

(a) Power units. The equipment incorporated three separate vibrator power units operated from banks of 12-volt lead-acid accumulators which were continuously charged through selenium rectifiers. Battery operation was considered desirable because of the relatively poor regulation and occasional interruptions of the 230-volt A.C. output from the station supply.

In the main rack one power unit provided the high tension for Geiger counter operation (trays 1 to 6), a stabilized —75-volt bias supply and an unregulated + 220-volt supply for operation of the power tubes driving the mechanical registers. A second unit provided a stablized + 150-volt output.

In the remote unit a single power unit provided high tension for Geiger counter operation (trays 7 and 8), a stablized + 150-volt output for operation of the pulse shaping and coincidence circuits and an unregulated +220-

volt supply to operate the cathode followers feeding pulses along the coaxial cable to the main unit.

All valve heaters were operated directly from the accumulators, the centre points of which were earthed.

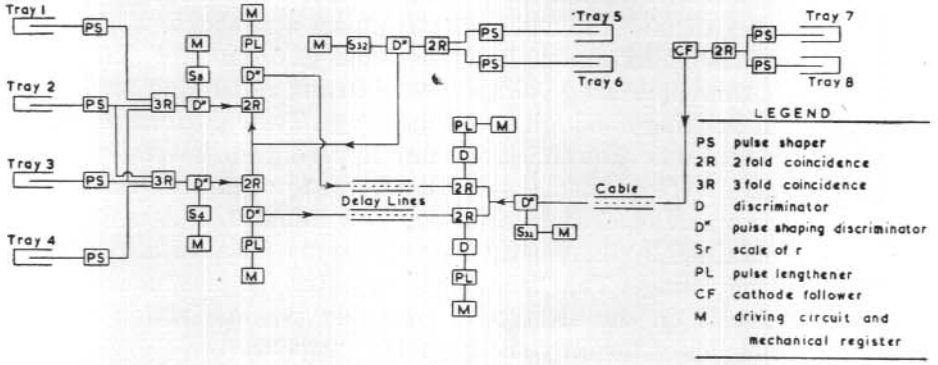

FIG. 3.

Block diagram of circuits of the Macquarie Island (1950-51) cosmic ray recorder.

Vibrators in the power units were replaced about once per month, usually as a routine procedure rather than because of failure. This was found desirable because of interference with other recording equipment at the station caused by poor waveforms generated by operation of the vibrators under high load conditions for longer periods.

Power consumptions in the main unit and remote unit were approximately 120 watt and 40 watt respectively.

(b) Pulse shaping circuits. Pulses from each tray of Geiger counters were fed to a pulse shaping circuit shown in Fig. 4. The output from this circuit was a single negative-going half-cycle with practically zero overshoot. The effective width of this standard output pulse at the grid of the coincidence circuit was 2 μ-sec.

(c) Coincidence circuits. In these circuits (Figs. 5 and 6) a cathode load was used. This enabled slightly better discrimination between the cases, all tubes cut off and not all tubes cut off simultaneously; it also made a useful reduction in total current drain on the 150-volt line.

(d) Discriminators and pulse-shaping discriminators. Details of the pulse-shaping discriminator are given in Fig. 7. The output from this circuit was similar to that from the pulse-shaping circuit described under (b) above. In the discriminators which do not feed to a coincidence circuit the inductive anode load was replaced by a 50,000-ohm resistor.

(e) Delay lines. Since transmission time along the 200-metre coaxial cable from the remote unit was approximately 1·75 μ-sec., it was necessary

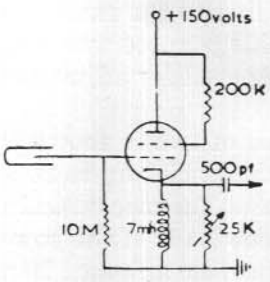

FIG. 4.
Pulse-shaping circuit.

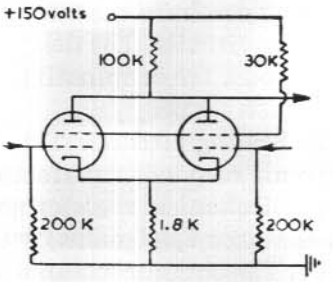

FIG. 5.
Two-fold coincidence circuit.

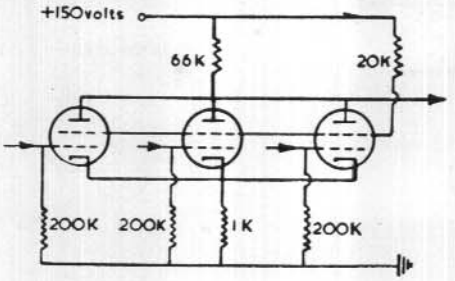

FIG. 6.
Three-fold coincidence circuit.

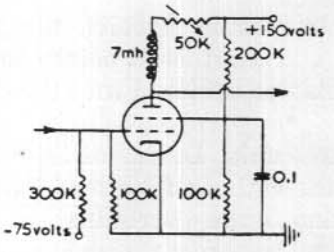

FIG. 7.
Circuit of pulse-shaping discriminator.

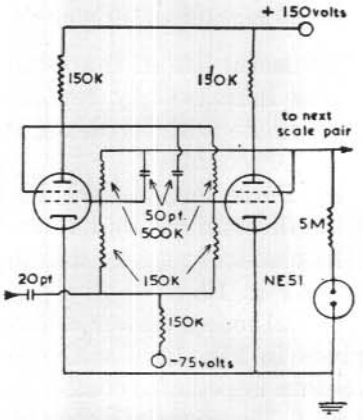

FIG. 8.
Circuit of scale of two.

to delay pulses from the main unit before feeding to the extensive shower coincidence circuits. The delay lines used for this purpose were made up of five π-sections, the terminating impedance being used for adjustment of the output pulse shape.

(f) Scaling circuits. The circuit of a scale of two is shown in Fig. 8. This circuit responds satisfactorily at pulse frequencies up to 20 kc/sec.

(g) Mechanical register and driving circuit. The mechanical registers (coil resistance 8,000 ohms) were wired as anode loads of the power valves (Fig. 9). The circuit constants were chosen to provide a $\frac{1}{15}$ sec., 20 ma. pulse through the coil for reliable operation. Each power tube had its own isolating resistance—capacitance filter on the 220-volt supply line.

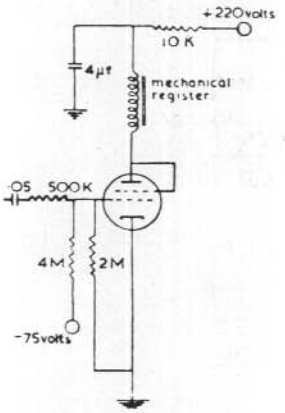

FIG. 9.
Mechanical register and driving circuit.

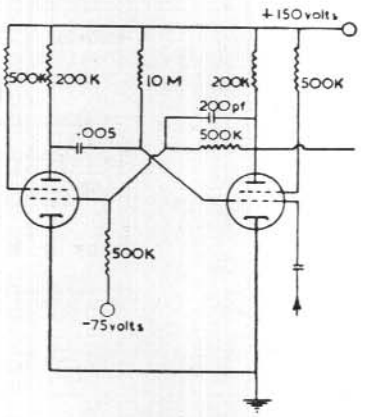

FIG. 10.
Circuit of pulse lengthener.

The useful life of the mechanical registers (telephone message registers) was increased by replacing the units and tens drums with drums specially made with hardened steel sections. The registers then had a life of 10^7 to 10^8 counts.

(h) Pulse lengthener. In the shower recording circuits, the pulses from the discriminators had to be inverted and lengthened before feeding to the mechanical register driving circuit. This was achieved with the circuit shown in Fig. 10.

(i) Cathode follower circuit of the remote unit. Details of this circuit are given in Fig. 11. Positive pulses from the cathode followers feed into the 75-ohm impedance coaxial cable connecting to the discriminators in the main unit. The discriminator bias was reduced to accept the smaller pulses which are attenuated in the cable.

(j) Test equipment. A test pulse generator was built into the main unit to provide negative pulses of adjustable amplitude and repetition rate. The

test pulse was preceded (by a variable time interval) by a short positive pulse used to trigger an oscilloscope.

(k) Camera recording system. The eight mechanical registers in the main unit were illuminated and photographed at hourly intervals with a single-shot electrically-driven 35-mm. camera, the operation of which was controlled, through a system of relays, by a marine-type chronometer carrying platinum contacts on the minute-hand and dial.

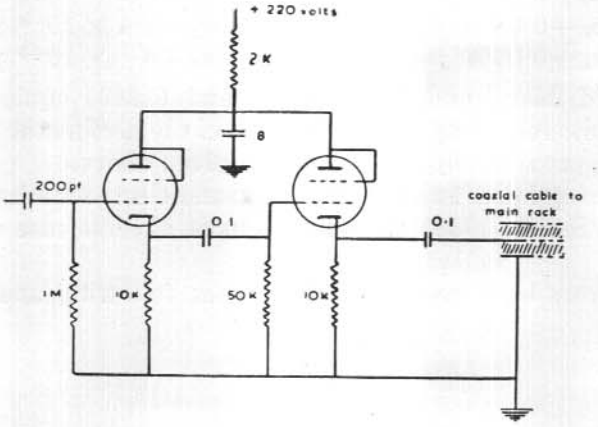

FIG. 11.
Cathode follower circuit of the remote unit.

The main unit containing trays 1 to 6 was mounted in an aluminium cabinet with walls of 0·7 gm. cm.$^{-2}$ mounted close under the laboratory roof which consisted of about 2 gm. cm.$^{-2}$ of organic matter (wood, "onozote", etc.). The remote unit containing trays 7 and 8 was mounted in an aluminium cabinet with walls of 0·7 gm. cm.$^{-2}$; this was protected from the weather by a canvas sheet.

Notation for coincidence rates. In the remainder of this report the following notation will be used:

Number per hour of coincidences	(1,2,3)	$= c_1$
" " " " "	(2,3,4)	$= c_2$
" " " " "	(5,6)	$= c_3$
" " " " "	(7,8)	$= c_4$
" " " " "	$c_1 - c_2$	$= D$
" " " " "	[(1,2,3), (5,6)]	$= s_1$
" " " " "	[(2,3,4), (5,6)]	$= s_2$
" " " " "	{[(1,2,3), (5,6)], (7,8)}	$= s_3$
" " " " "	{[(2,3,4), (5,6)], (7,8)}	$= s_4$

The measurements of shower intensities s_1, s_2, s_3 and s_4 have been discussed by Parsons (1951) and are not examined in this report.

Counting errors. Each tray of six Geiger counters had a background counting rate of approximately 1,100 per minute. With a resolving time of 2 μ-sec. in each coincidence circuit the mean accidental rates for the Macquarie Island (1950-52) equipment were:

c_1 —0·04%	s_1 —2%
c_2 —0·06%	s_2 —5%
c_3 —0·03%	s_3 —$1{\cdot}4 \times 10^{-4}$ per hour
c_4 —0·03%	s_4 —4 $\times 10^{-5}$ per hour

For the Heard Island and Macquarie Island (1948) equipment with coincidence circuit resolving times of 20 μ-sec. the accidental rates for c_1, c_2 and c_3 were approximately 10 times those given above.

The counting losses in scaling circuits and electro-mechanical registers (Alaoglu and Smith, 1938) were in the most adverse case about 0·03 per cent.

These errors have been neglected in the following analysis of observations.

3. STATISTICAL ANALYSIS

by F. JACKA

Abstract. Maximum likelihood estimates of regression coefficients are calculated in the cases where, for given values of the independent variables, the dependent variable has (i) a normal distribution and (ii) Poisson's distribution. In case (i) these estimates are identical with the "least squares" estimates while in case (ii) they are not. However, in case (ii) it is found that, even when the range of variation of the expected value of the independent variable is large and its mean value small, the difference between the "maximum likelihood" and "least squares" estimates is small compared with the sampling errors in these estimates. It is concluded that the "least squares" estimates of regression coefficients are sufficiently accurate for all problems treated in following chapters in which the dependent variable is a measure of cosmic ray intensity.

Results are quoted for confidence limits of regression coefficients and for tests of "goodness of fit" of the regression equations. In cases where successive values of the error term of the regression model are not independently distributed these tests are unreliable.

The practical procedures adopted for computing regression coefficients are described.

Introduction. Statistical analysis involves setting up a mathematical model which describes the variables under consideration, estimating the constants of this model from the observed values of the variables and comparing these with values expected according to a particular (physical) theory. In chapter 4 the main problem will be that of representing (or predicting) a measure of the cosmic ray intensity by a linear function of a set of variables such as barometric pressure, height of meson production level, etc., estimating the constants of this linear function from the observed data, and later comparing the theoretically expected values with these estimates —a problem in regression analysis.

It is the purpose of the present section to outline the statistical principles and methods used in treating this problem.

Regression analysis. It is known that over short periods during which the primary cosmic ray intensity may be assumed constant and during which no changes in atmospheric structure occur, the number of cosmic ray particles counted per unit time interval with a particular apparatus is a

Poisson variate. The expected value of the cosmic ray intensity may be given by an expression of the form

$$\alpha + \beta_2 x_2 + \beta_3 x_3 + \ldots\ldots; \quad x_j = X_j - \overline{X}_j$$

where X_2, X_3, ... are measures of physical quantities which affect the cosmic ray intensity. This description of the variables constitutes the mathematical model—in this case a "regression model".

Given a series of associated observations of cosmic ray intensity, X_1 and X_2, X_3, ... it is required to estimate α, β_2, β_3 ...., and to make statements about the estimates in order to know with what confidence it may be said they are or are not consistent with the theoretically calculated values. Before discussing this problem consider the case where for given X_2, X_3, ..., etc., X_1, is a normal variate.

Simple regression—error term normally distributed. Assume

$$X_1 = \alpha + \beta_2 x_2 + \epsilon$$

where successive values of the error term ϵ are distributed independently of each other and of X_2. Further assume ϵ to be a normal variate of zero expectation and constant variance, σ^2.

If X_2 takes the value X_{2i} the probability that X_1 assumes a value in the interval X_{1i} to $X_{1i} + dX_{1i}$ is

$$\phi\,(X_{1i})\,dX_{1i} = (2\pi\sigma^2)^{-\frac{1}{2}} \exp\left[-\frac{1}{2\sigma^2}\,(X_{1i}-\alpha-\beta_2 x_{2i})^2\right] dX_{1i}$$

If then a series of observations is made in which X_2 takes the values X_{21}, X_{22}, ... X_{2i}, ... X_{2n}, the probability that the values of X_1 will fall in the intervals X_{1i} to $X_{1i} + dX_{1i}$ is given by

$$P\,(X_{11}, X_{12}, \cdots X_{1i}, \cdots X_{1n})\,dX_{11}dX_{12} \cdots dX_{1n} = \prod_{i=1}^{i=n} \phi\,(X_{1i})\,dX_{1i}$$

so that $P = (2\pi\sigma^2)^{-\frac{n}{2}} \exp\left[-\frac{1}{2\sigma^2}\sum_{i=1}^{n}(X_1-\alpha-\beta_2 x_{2i})^2\right]$

Now, using the method of maximum likelihood, best estimates of α, β_2 and σ^2 are those values which make P (or log P) a maximum for the values X_{1i}, X_{2i} actually obtained in the sample of observations.
This gives

$$\frac{\partial \log P}{\partial \alpha} = 0, \qquad \frac{\partial \log P}{\partial \beta_2} = 0, \qquad \frac{\partial \log P}{\partial \sigma^2} = 0$$

which leads to $\alpha^* = \overline{X}_1$, $\beta^* = \Sigma x_{1i}\, x_{2i}/\Sigma x_{2i}^2$
for the maximum likelihood estimates of α and β_2. These are the estimates obtained by the least squares method. For the maximum likelihood estimate of σ^2

$$\sigma^{*2} = s_{1.2}^2 = s_1^2\,(1-r_{12}^2)$$

is obtained where $s_{1.2}^2$ is the variance of the residuals (deviations of X_{1i} from the regression line), s_1^2 is the variance of x_{1i} and $r_{12} = [(\Sigma x_1\, x_2)^2/\Sigma x_1^2\, \Sigma x_2^2]^{\frac{1}{2}}$ is the coefficient of correlation between x_{1i} and x_{2i} in the sample.

It can be shown (Cramer, 1946, Ch. 37) that $n\sigma^{*2}/\sigma^2$ is distributed like χ^2 with n—2 degrees of freedom and that $s_2\ (n-2)^{\frac{1}{2}}\ (\beta^* - \beta)/\sigma^*$ has Student's distribution with $n-2$ degrees of freedom. This gives for the $(100-p)\%$ confidence limits of β the value $\beta^* \pm t_p\ \sigma^*/s_2(n-2)^{\frac{1}{2}}$ where t_p is taken with n—2 degrees of freedom.

Multiple regression—error term normally distributed. Now assume

$$X_1 = \alpha+\beta_2 x_2+\beta_3 x_3+ \cdots +\beta_k x_k+\epsilon$$

where successive values of ϵ are distributed independently of each other and of $X_1, X_2, \ldots . X_k$. Further, assume ϵ to be normally distributed with zero expectation and constant variance, σ^2. Following the procedure above, maximum likelihood estimates are obtained

$$\alpha^* = \overline{X}_1,\ \beta_i^* = -\frac{s_1}{s_i}\cdot\frac{w_{1i}}{w_{11}},\ i = 2,3, \cdots k,$$

$$\sigma^{*2} = s^2{}_{1\,(2,\ \cdots\ k)} = s_1{}^2\,(1-R_1{}^2{}_{(2,3,\ \cdots\ k)})$$

where s_i^2 is the variance of x_i in the sample, $s_1{}^2{}_{(2,\ \ldots .\ k)}$ is the variance of residuals, w is the determinant $|\ r_{ij}\ |$ and w_{ij} is the co-factor of r_{ij} in w. $R_{1(2,\ 3,\ \ldots .\ k)}$ is called the coefficient of multiple correlation between X_1 and its estimate.

In this case it can be shown (Cramer, 1946, Ch. 37) that $n\sigma^{*2}/\sigma^2$ is distributed like χ^2 with $n-k$ degrees of freedom and that $s_{i(j)}\sqrt{n-k}\ \dfrac{\beta_i^*-\beta_i}{\sigma^*}$ (where (j) represents all subscripts 2, 3, ... k but omitting i) has Student's distribution with $n-k$ degrees of freedom. The $(100-p)\%$ confidence limits of β_i are then given by

$$\beta_i^* \pm t_p\ \frac{\sigma^*}{s_{i(j)}\sqrt{n-k}}$$

Effect of non-independence of successive values of ϵ. Durbin and Watson (1950) have pointed out that if successive values of the error term are not distributed independently of each other

(1) The estimates of the regression coefficients, though unbiased, need not have least variance (in this sense they are not "best estimates").

(2) The usual formula for the variance of an estimate is no longer applicable and is liable to give a serious underestimate of the true variance.

(3) The t and F distributions, used for making confidence statements, lose their validity.

They have also devised a statistic for use in testing for non-independence (serial correlation) of successive errors. The statistic chosen is $d = \Sigma(\triangle Z)^2/\Sigma Z^2$ where Z denotes the deviation from regression and $\triangle$Z's are first differences of Z. In a further paper Durbin and Watson (1951) tabulate significance points of lower and upper bounds, d_L and d_U, of d such

that sample values of d less than $d_{L(p\%)}$ indicate significant positive serial correlation at the $p\%$ level, while values of d greater than $d_{U(p\%)}$ indicate that the value is not significant at the $p\%$ level. If d lies between d_L and d_U the test is inconclusive.

In cases where the dependent variate, X_1, is an accurate measure of a stochastic variable, serial correlation of errors can be due only to incorrectness of the regression equation, that is, incorrect mathematical representation of the physical situation.

Simple regression — X_1 a Poisson variate. Now return to the case where for fixed values of the independent variates the dependent variate has Poisson's distribution and treat only the case of one independent variate. If X_2 takes a particular value X_{2j} the probability that X_1 takes the value X_{1j} is given by

$$\phi\,(X_{1j}) = \exp\,(-\alpha-\beta x_{2j})(\alpha+\beta x_{2j})X_{1j}/X_{1j}!$$

If then a series of observations is made in which X_2 takes the values X_{21}, X_{22}, $\ldots . X_{2i}$, $\ldots .$ X_{2n} the probability that X_1 will have the values X_{11}, X_{12}, $\ldots .$ X_{1i}, $\ldots .$ X_{1n} is given by

$$P\,(X_{11}, X_{12}, \cdots . X_{1i} \cdots . X_{1n}) = \prod_{i=1}^{n} \phi(X_{1i})$$

so that

$$\log P = \sum_{i=1}^{n}\left[-\alpha-\beta x_{2i}+X_{1i} \log\,(\alpha+\beta x_{2i})-\log X_{1i}!\right]$$

To estimate α and β using the maximum likelihood method put

$$(1)\quad \frac{\partial \log P}{\partial \alpha} = \sum \frac{X_1-\alpha-\beta x_2}{\alpha+\beta x_2} = 0$$

$$(2)\quad \frac{\partial \log P}{\partial \beta} = \sum \frac{X_1 x_2}{\alpha+\beta x_2} = 0$$

From (1) is obtained

$$(3)\quad n\,\frac{\overline{X}_1-\alpha}{\alpha} + \frac{\overline{X}_1\beta^2\Sigma x_2^{\,2}}{\alpha^3} - \frac{\overline{X}_1\beta^3\Sigma x_2^{\,3}}{\alpha^4} + \cdots . - \frac{\beta\Sigma x_1 x_2}{\alpha^2} + \frac{\beta^2\Sigma x_1 x_2^{\,2}}{\alpha^3} \cdots . = 0$$

and from (2) is obtained

$$(4)\quad \frac{\overline{X}_1\beta^2\Sigma x_2^{\,2}}{\alpha^3} - \frac{\overline{X}_1\beta^3\Sigma x_2^{\,3}}{\alpha^4} + \cdots . - \frac{\beta\Sigma x_1 x_2}{\alpha^2} + \frac{\beta^2\Sigma x_1 x_2^{\,2}}{\alpha^3} - \cdots . = 0$$

Subtracting (3) and (4) gives

$$\alpha^* = \overline{X}_1$$

as the maximum likelihood estimate for α. This is the estimate obtained by the least squares method. For β however the maximum likelihood estimate, β^*, is (from (1)) the solution of the equation

$$(5)\qquad \sum \frac{X_1}{\overline{X}_1+\beta x_2} = n$$

which is different from the least squares estimate. This equation may be solved either graphically or by an iterative procedure starting with the least squares estimate, $\Sigma x_1 x_2/\Sigma x_2^2$, as a first approximation. If β_i is an approximation for β^* and $\beta_i + 1$, the next approximation

$$\beta_{i+1} = \beta_i + \Delta_i$$

Insert this value in (5)

$$\sum \frac{X_1}{\bar{X}_1 + \beta_i x_2 + \Delta_i x_2} \simeq \sum \frac{X_1}{\bar{X}_1 + \beta_i x_2}\left(1 - \frac{\Delta_i x_2}{\bar{X}_1 + \beta_i x_2}\right) \simeq n$$

giving

$$\Delta_i \simeq \frac{\sum \frac{X_1}{\bar{X}_1 + \beta_i x_2} - n}{\Sigma x_1 x_2/(\bar{X}_1 + \beta_i x_2)^2}$$

One would expect the least squares estimate b and the maximum likelihood estimate β^* to be similar, especially in cases where α is large and the range of variation of βx_2 in the sample small compared with α. The analysis of cosmic ray intensity variations in chapters 4 and 5 is concerned with cases of this type and the least squares estimates are used.

In order to gain some idea of the accuracy of the approximation $b \simeq \beta^*$ in other cases a number of samples was examined. These were obtained as follows: Two Geiger counters some distance apart in the horizontal plane were connected to a two-fold coincidence circuit, the output of which was fed to an electronic counting device. A radioactive γ ray source was placed near the Geiger counters, its position and the separation between the counters being adjusted to give a coincidence pulse rate of about 10 per minute. The number of coincidences, X_1, occurring in various time intervals, X_2, were then measured. The coincidence rate X_1/X_2 remained constant over a long period, its value being 0·160. The expected value of X_1 then, should be given by $\alpha + \beta x_2$ with β very close to 0·160 and $\alpha = \beta X_2$, X_1 being a Poisson variate for fixed X_2. Some information on each sample of observations and the estimates b and β^* of β are given in Table 1.

TABLE 1

Number in Sample	$\beta\bar{X}_2$	Range of βx_2 / $\beta\bar{X}_2$	$\bar{X}_1/\bar{X}_2$	b	β^*
11	3·196	1·00	0·164	0·218	0·182
11	3·196	1·00	0·164	0·118	0·120
11	3·196	1·00	0·150	0·214	0·283
16	7·191	0·667	0·167	0·198	0·214
16	7·191	0·667	0·165	0·114	0·113
16	7·191	0·667	0·160	0·139	0·124
31	52·73	0·182	0·159	0·142	0·140

It will be seen that the difference $\beta^* - b$ is generally small compared with the difference $\beta^* - \beta$. Even in these samples then it is not important whether b or β^* is chosen to estimate β.

Accuracy of the regression model. It was pointed out in a previous section that if for given values of the independent variates the dependent variate is normally distributed with variance σ^2, $ns_1^{2}{}_{(2,3,\ldots.k)}/\sigma^2$ is distributed like χ^2 with $n-k$ degrees of freedom. If the dependent variate X_1 has Poisson's distribution, it would then be expected that $\chi_s^2 = ns_1^{2}{}_{(2,3,\ldots.k)}/\overline{X}_1$ would be distributed approximately as χ^2 with $n-k$ degrees of freedom provided a is large and the range of variation of $\beta_2 x_2 + \beta_3 x_3 + \ldots. + \beta_k x_k$ in the sample is small compared with a. If the dependent variate is of the form $X_1 = g \times$ a Poisson variate, χ_s^2 will be given by $\chi_s^2 = \dfrac{ns_1^{2}{}_{(2,3,\ldots.k)}}{g\overline{X}_1}$

These conditions are satisfied in the samples considered in Chapter 4 where χ_s^2 is compared with χ^2 to test the hypothesis that the regression model is correct. If $\chi_s^2 > \chi_{p\%}^2$ the hypothesis is discredited at the $p\%$ significance level; that is, the variations of X_1 are not fully accounted for by the assumption that X_1 (or $\frac{1}{g} X_1$) is a Poisson variate and X_1 has expectation

$$a + \beta_2 x_2 + \ldots. + \beta_k x_k.$$

Computing methods. In order to facilitate the computation of regression coefficients, etc., discussed in chapter 4, the observed values of the variables (after subtraction of suitable constants to reduce the figures to a more convenient magnitude) were entered in the form of punched holes on Hollerith cards. Additional entries denoting the place of observation, year, month, date and time enable identification and sorting of the records. All sums and sums of products were then determined with Hollerith sorting and tabulating machines using the method of "progressive digiting" (Baehne, 1935).

These values were then transferred to a printed work sheet. The remainder of the computations was carried out with electrically-driven desk calculators.

4. COSMIC RAY INTENSITY VARIATIONS OF ATMOSPHERIC ORIGIN

by F. JACKA

Abstract. Using data from Heard Island and Macquarie Island, barometer and temperature coefficients are determined for the hard component, the total intensity and the soft component of cosmic rays at sea level. The temperature coefficients are not significant. After eliminating the barometric effect, systematic variations in the cosmic ray intensity remain.

Barometer coefficients for the hard component are calculated using the assumption that the pressure—height distribution in the atmosphere is exponential and that μ-mesons are produced at a definite atmospheric depth. Whatever the assumed depth of production in the range 300 to 80 mb., the theoretical values obtained are numerically too high.

It is found that on using a linear function of barometric pressure, height of the ξ mb. isobar and mean temperature in a small interval below the ξ mb. isobar to predict the variations in hard component intensity, no one choice of ξ in the interval 500 to 80 mb. makes this function a significantly better predictor than any other. This conclusion is contrary to that of Duperier (1951).

Assuming an exponential atmosphere and a definite depth of μ-meson production, theoretical values are calculated for the barometer coefficient, meson decay coefficient and Duperier positive temperature coefficient for the hard component. It is found that the theoretical value of the barometer coefficient is numerically too high for any assumed depth of μ-meson production in the range 300 to 80 mb., that the theoretical and experimental values of the meson decay coefficient are in agreement for any assumed depth of production in the range 500 to 80 mb., and that the theoretical and experimental values of the Duperier temperature effect are in agreement only if we assume a depth of μ-meson production much greater than is to be expected from observed values of absorption length for shower-producing radiation. It is suggested that competition between capture and decay of π-mesons is not the main process responsible for the observed positive temperature effect.

It is concluded that in order to progress in the study of variations in cosmic ray intensity of atmospheric origin the simplifying assumptions above must be avoided.

Introduction. In the present section cosmic ray intensity variations of atmospheric origin will be examined under the headings used in chapter 1.

Attention will be confined mainly to the hard component, but some results will be quoted for the total intensity and soft component intensity. The purpose of this examination is to enable us to determine and study the residual variations which remain after correcting for variations in atmospheric structure and to improve our understanding of the interaction between cosmic rays and the atmosphere. A brief description of this interaction follows:

The primary cosmic radiation consists of protons and smaller numbers of α-particles and heavier nuclei. Because of collisions with nuclei of the atmosphere the heavier particles are broken up and give rise to smaller nuclear fragments, free nucleons and π-mesons (charged and neutral). The mean free path characterizing these collisions decreases with increase in atomic number of the incident nuclei ($\lambda_a = 44{\cdot}5$ gm. cm.$^{-2}$ for $Z = 2$, $21{\cdot}0$ gm. cm.$^{-2}$ for $10 \leqslant Z \leqslant 26$; Peters, 1952). The primary protons and secondary nucleons undergo further interactions, the main products of which are nucleons and mesons. The absorption thickness in the atmosphere for these particles is approximately 120 gm. cm.$^{-2}$, while the collision mean free path is close to the geometric mean free path, 60 gm. cm.$^{-2}$. (These points are discussed in detail by Rossi, 1952, Ch. 8.)

The charged π-mesons may suffer collision with nuclei, the main products of the interaction being further π-mesons and nucleons. In cases where the incident particles are charged π-mesons of energy less than about 1 Bev, nuclear interaction may sometimes yield secondary π-mesons; the probability of such events increases with increase in energy of the incident π-meson. (Camerini et al. 1951a, p. 1,255 and Camerini et al. 1951b, p. 1,274).

The charged π-mesons may also suffer decay ($\tau_{\pi^{+-}} = 2{\cdot}65 \times 10^{-8}$ sec.) giving rise to a μ-meson and a neutrino. The μ-mesons form the bulk of the penetrating radiation at sea level. They may, however, undergo decay ($\tau_{\mu} = 2{\cdot}10 \times 10^{-6}$ sec.) forming an electron and two neutrinos, the electrons contributing to the soft component of the cosmic radiation at sea level.

The neutral π-mesons arising from nuclear interactions undergo decay to two γ-rays ($\tau_{\pi^0} < 10^{-13}$ sec.) which through processes of pair production, Compton collisions, bremsstrahlung and ionization give rise to an electron-photon cascade which contributes to the soft component of the cosmic radiation at sea level.

Other particles (τ-mesons and V particles) do occur among the secondry particles but, because of their small numbers and short lifetimes, are unlikely to play an important part in determining the variations in the sea level intensity of the cosmic radiation.

In the following theoretical treatment of the problem it will be assumed that all π-mesons are formed at a definite depth and these undergo collison

with nuclei of the atmosphere or suffer decay to μ-mesons at a definite atmospheric depth. For the purpose of representing the variation of atmospheric depth with height it is assumed that the atmospere is static and isothermal, so that atmospheric depth is an exponential function of height.

All integrals in which the integrand is not given in analytical form were evaluated by graphing the integrand on a large scale and integrating with a disc planimeter, the accuracy obtained being of the order of 1 per cent.

The barometer and temperature effects—experimental results. For the purpose of calculating barometer and temperature coefficients from the Macquarie Island data, the daily mean values of cosmic ray intensity (in coincidences/hr.), barometric pressure and temperature were calculated. Denoting X_1 = cosmic ray intensity,

X_2 = pressure,

X_3 = temperature,

regression equations of the form $X_1=a+\beta_{12}x_2$ and $X_1=a+\beta_{12.3}x_2+\beta_{13.2}x_3$ were fitted and estimates b_{12}, $b_{12.3}$ and $b_{13.2}$ of the coefficients determined using standard methods described in Chapter 3.

Values of these estimates and the 95 per cent confidence limits of the coefficients calculated by standard methods described in Chapter 3 are given for Macquarie Island in Tables 2 to 6. Similar data calculated from hourly values are given for Macquarie Island in Tables 7 to 11 and for Heard Island in Tables 12 to 14.

Significance of barometer and temperature coefficients. In column 7 of these tables are listed values of χ_s^2 and the corresponding $\chi^2_{5\%}$ calculated in the manner described in Chapter 3, the values referring to regression of X_1 on X_2 and X_3. It will be seen that in nearly every case $\chi_s^2>x^2_{5\%}$ indicating that for given X_2 and X_3 the dependent variable X_1 has a variance greater than would be expected on the assumption that the number of coincidences per hour is a Poisson variate and that the expected value of X_1 is given by $a+\beta_{12.3}x_2+\beta_{13.2}x_3$. It is apparent then that the cosmic ray intensity cannot in general be accurately estimated by a linear function of barometric pressure and surface temperature alone.

This is further emphasized by the fact that in many cases where the statistic d (column 8) has been calculated, its value is less than $d_{L5\%}$ indicating positive serial correlation of the errors significant at the 5 per cent level. As pointed out in Chapter 3 this can occur only if the regression equation does not accurately describe the variations of the dependent variable. It should also be strongly emphasized that in this case the confidence limits given for the regression coefficients may be regarded only as inner limits of the true confidence intervals which may cover a much greater

TABLE 2

Barometer and Temperature Coefficients—Macquarie I.
Limits quoted are 95% confidence limits.*
$X_1 = c_{1/8}$ (mean of day); X_2 = Barometric Pressure (mean of day); X_3 = Surface Temperature (mean of day)

Month	b_{12} (%/mb)	$b_{12.3}$ (%/mb)	$b_{13.2}$ (%/°C)	$\overline{X}_1$	$\overline{X}_2$ (mb)	χ^2_s / $\chi^2_{5\%}$
1950						
June	−0·264	−0·232	−0·460	601·6	1009·1	251·6
	±0·088	±0·090	±0·538			23·7
July	−0·217	−0·217	−0·099	601·3	1008·6	79·3
	±0·038	±0·039	±0·196			31·4
Aug.	−0·201	−0·223	−0·131	599·9	1006·5	123·1
	±0·053	±0·052	±0·241			23·7
Sept.	−0·172	−0·235	−0·491	604·0	1002·4	132·0
	±0·021	±0·017	±0·241			40·1
Oct.	−0·183	−0·184	−0·081	596·8	1003·1	117·1
	±0·027	±0·028	±0·236			35·2
Nov.	−0·221	−0·221	−0·073	608·9	994·8	85·8
	±0·020	±0·020	±0·137			38·9
Dec.	−0·223	−0·216	−0·380	607·4	995·1	163·0
	±0·026	±0·024	±0·239			41·3
1951						
Jan.	−0·277	−0·288	−0·517	586·2	1006·1	487·0
	±0·058	±0·056	±0·516			41·3
Feb.	−0·257	−0·247	−0·672	585·2	1002·5	216·9
	±0·033	±0·031	±0·534			35·2
Mar.	−0·209	−0·209	−0·652	601·8	995·8	2·0
	±0·028	±0·006	±0·105			23·7
Apr.	−0·234	−0·233	−0·084	598·9	998·9	67·1
	±0·032	±0·033	±0·218			30·1
May	−0·219	−0·216	+0·082	605·1	1002·3	118·8
	±0·021	±0·023	±0·232			30·1
June	−0·270	−0·267	+0·143	599·6	1006·0	249·5
	±0·044	±0·045	±0·299			30·1
July	−0·182	−0·182	+0·008	602·2	997·3	157·4
	±0·027	±0·028	±0·252			31·4
Aug.	−0·270	−0·261	−0·117	603·6	998·1	570·9
	±0·042	±0·044	±0·347			32·7
Sept.	−0·248	−0·246	−0·038	609·3	998·3	550·5
	±0·043	±0·049	±0·315			38·9
Oct.	−0·229	−0·230	−0·110	607·1	1000·0	87·6
	±0·032	±0·031	±0·511			27·6
Nov.	−0·239	−0·215	−0·391	622·1	995·4	86·3
	±0·035	±0·026	±0·178			27·6
Dec.	−0·213	−0·200	−0·293	618·4	996·1	128·2
	±0·046	±0·040	±0·185			33·9
1952						
Jan.	−0·227	−0·224	−0·189	627·9	986·1	78·0
	±0·022	±0·021	±0·194			33·9
Feb.	−0·184	−0·179	−0·217	611·1	998·1	98·8
	±0·033	±0·035	±0·419			30·1
Mar.	−0·252	−0·259	−0·394	617·3	996·2	83·1
	±0·039	±0·030	±0·217			28·9

* In view of the possible serial correlation of the error terms these limits should be considered only as inner limits of the true confidence intervals.

TABLE 3

Barometer and Temperature Coefficients—Macquarie I.
Limits quoted are 95% confidence limits*
$X_1 = c_{3/4}$ (mean of day); X_2 = Barometric Pressure (mean of day); X_3 = Surface Temperature (mean of day)

Month	b_{12} (%/mb)	$b_{12.3}$ (%/mb)	$b_{13.2}$ (%/°C)	$\overline{X_1}$	$\overline{X_2}$ (mb)	χ^2_s / $\chi^2_{5\%}$	$d_{U5\%}$ / d / $d_{L5\%}$
1950							
June	−0·208 ±0·067	−0·180 ±0·061	−0·404 ±0·367	842·1	1009·1	81·3 23·7	0·58 1·02
July	−0·153 ±0·059	−0·154 ±0·054	−0·304 ±0·268	845·1	1008·6	110·2 31·4	0·54 1·17 1·54
Aug.	−0·144 ±0·052	−0·147 ±0·046	−0·241 ±0·214	844·2	1006·5	65·6 23·7	1·40 1·02 1·57
Sept.	−0·172 ±0·020	−0·173 ±0·016	−0·433 ±0·231	854·1	1002·4	86·9 40·1	1·32 1·28
Oct.	−0·134 ±0·021	−0·133 ±0·020	−0·166 ±0·173	848·9	1003·1	44·9 35·2	1·09 1·22
Nov.	−0·166 ±0·027	−0·165 ±0·028	−0·055 ±0·187	863·7	994·8	113·3 38·9	1·16 1·27 1·57
Dec.	−0·177 ±0·049	−0·165 ±0·037	−0·631 ±0·410	859·0	995·1	279·9 41·3	1·40 1·30
1951							
Jan.	−0·212 ±0·053	−0·230 ±0·044	−0·854 ±0·437	830·7	1006·1	212·6 41·3	0·69 1·30
Feb.	−0·187 ±0·037	−0·176 ±0·035	−0·720 ±0·602	827·9	1002·5	195·4 35·2	0·93 1·22 1·54
Mar.	−0·121 ±0·040	−0·127 ±0·038	−0·520 ±0·630	845·5	995·6	24·7 19·7	2·25
Apr.	−0·164 ±0·047	−0·160 ±0·046	−0·245 ±0·307	844·0	998·9	93·0 30·1	1·12 1·15 1·54
May	−0·156 ±0·022	−0·155 ±0·024	+0·033 ±0·248	852·3	1002·3	95·6 30·1	1·39 1·15
June	−0·217 ±0·052	−0·212 ±0·050	+0·267 ±0·333	847·2	1006·0	218·7 30·1	
July	−0·115 ±0·028	−0·116 ±0·029	+0·010 ±0·265	857·9	997·3	123·6 31·4	
Aug.	−0·208 ±0·043	−0·196 ±0·043	−0·160 ±0·343	856·4	998·1	396·9 32·7	
Sept.	−0·147 ±0·042	−0·130 ±0·045	−0·132 ±0·292	868·4	998·3	338·3 38·9	
Oct.	−0·166 ±0·033	−0·172 ±0·032	−0·167 ±0·224	855·8	1002·8	90·8 28·9	
Nov.	−0·150 ±0·033	−0·124 ±0·026	−0·434 ±0·192	880·7	953·8	79·2 31·4	
Dec.	−0·142 ±0·054	−0·142 ±0·045	−0·341 ±0·223	885·2	994·3	80·5 28·9	
1952							
Jan.	−0·141 ±0·034	−0·142 ±0·031	−0·320 ±0·285	886·2	988·1	106·5 33·9	
Feb.	−0·100 ±0·036	−0·095 ±0·039	−0·165 ±0·437	871·5	997·4	71·5 31·4	
Mar.	−0·179 ±0·044	−0·185 ±0·035	−0·413 ±0·250	876·3	996·2	78·1 28·9	

See* footnote Table 2.

TABLE 4

Barometer and Temperature Coefficients—Macquarie I.
Limits quoted are 95% confidence limits*
$X_1 = c_{s/32}$ (mean of day); X_2 = Barometric Pressure (mean of day); X_3 = Surface Temperature (mean of day)

Month	b_{12} (%/mb)	$b_{12.3}$ (%/mb)	$b_{13.2}$ (%/°C)	$\overline{X}_1$	$\overline{X}_2$ (mb)	χ^2_s $\chi^2_{5\%}$	$d_{U5\%}$ d $d_{L5\%}$
1950							
June	−0·213 ±0·054	−0·197 ±0·058	−0·232 ±0·365	655·3	1009·9	635·4 27·6	0·85 1·10 1·54
July	−0·234 ±0·028	−0·234 ±0·028	−0·058 ±0·144	662·9	1008·6	189·2 31·4	1·46 1·17 1·55
Aug.	−0·233 ±0·027	−0·222 ±0·026	−0·139 ±0·123	668·7	1003·3	503·2 33·9	1·57
Sept.	−0·218 ±0·018	−0·219 ±0·015	−0·382 ±0·216	665·2	1002·4	468·6 40·1	0·92 1·28
Oct.	−0·184 ±0·029	−0·183 ±0·029	−0·173 ±0·247	666·5	1003·1	572·0 35·2	0·91 1·22 1·54
Nov.	−0·200 ±0·019	−0·196 ±0·016	−0·147 ±0·105	676·3	996·5	131·2 30·1	1·16 1·15
Dec.	−0·204 ±0·024	−0·200 ±0·023	−0·291 ±0·246	678·3	995·7	587·6 40·1	1·21 1·28
1951							
Jan.	−0·234 ±0·032	−0·240 ±0·032	−0·285 ±0·315	660·3	1006·1	697·2 41·3	0·74 1·30
Feb.	−0·225 ±0·045	−0·214 ±0·045	−0·649 ±0·764	664·0	1002·9	1861·7 33·9	1·20 1·21 1·54
Mar.	−0·201 ±0·030	−0·201 ±0·016	−0·579 ±0·218	676·9	996·0	35·9 22·4	1·36 0·98 1·54
Apr.	−0·220 ±0·037	−0·219 ±0·037	−0·081 ±0·794	675·2	998·9	398·3 30·1	1·41 1·15 1·54
May	−0·199 ±0·019	−0·204 ±0·020	−0·137 ±0·203	663·0	1002·3	395·7 30·1	1·37 1·15
June	−0·258 ±0·033	−0·256 ±0·033	+0·122 ±0·222	651·1	1006·0	600·1 30·1	
July	−0·183 ±0·036	−0·182 ±0·037	−0·114 ±0·333	670·4	997·3	1221·5 31·4	
Aug.	−0·256 ±0·040	−0·254 ±0·043	−0·043 ±0·344	673·4	998·1	2499·0 32·7	
Sept.	−0·211 ±0·055	−0·215 ±0·063	+0·056 ±0·406	676·4	998·3	4056·1 38·9	
Oct.	−0·197 ±0·052	−0·197 ±0·053	−0·023 ±0·305	668·5	1002·4	1965·5 32·7	
Nov.	−0·204 ±0·022	−0·197 ±0·024	−0·126 ±0·173	678·9	995·4	395·9 31·4	
Dec.	−0·205 ±0·031	−0·194 ±0·022	−0·252 ±0·102	682·4	996·1	171·4 33·9	
1952							
Jan.	−0·200 ±0·031	−0·201 ±0·026	−0·396 ±0·239	683·3	988·1	460·6 33·9	
Feb.	−0·163 ±0·028	−0·154 ±0·029	−0·266 ±0·331	671·4	997·4	283·9 31·4	
Mar.	−0·235 ±0·037	−0·241 ±0·029	−0·372 ±0·204	675·1	996·2	321·3 28·9	

* See footnote Table 2.

TABLE 5

Barometer and Temperature Coefficients—Macquarie I.
Limits quoted are 95% confidence limits*
$X_1 = c_{4/32}$ (mean of day); X_2 = Barometric Pressure (mean of day); X_3 = Surface Temperature (mean of day)

Month	b_{12} (%/mb)	$b_{12\cdot3}$ (%/mb)	$b_{13\cdot2}$ (%/°C)	$\overline{X_1}$	$\overline{X_2}$	χ^2_s / $\chi^2_{5\%}$
1950						
June						
July	−0·200 ±0·034	−0·200 ±0·035	−0·044 ±0·178	664·5	1008·6	290·3 / 31·4
Aug.	−0·220 ±0·035	−0·213 ±0·039	−0·129 ±0·181	665·0	1003·7	630·8 / 30·1
Sept.	−0·184 ±0·017	−0·184 ±0·017	−0·053 ±0·242	671·5	1002·4	591·5 / 40·1
Oct.	−0·199 ±0·057	−0·201 ±0·054	−0·015 ±0·428	670·1	1007·6	298·3 / 18·3
Nov.	−0·187 ±0·019	−0·187 ±0·019	−0·042 ±0·135	688·7	995·0	330·5 / 37·7
Dec.	−0·213 ±0·015	−0·207 ±0·013	−0·260 ±0·157	680·8	993·9	160·1 / 35·2
1951						
Jan.	−0·235 ±0·054	−0·244 ±0·053	−0·445 ±0·585	654·4	1005·3	962·7 / 28·9
Feb.	−0·237 ±0·028	−0·223 ±0·021	−0·794 ±0·363	664·0	1000·7	270·7 / 28·9
Mar.						
Apr.	−0·235 ±0·051	−0·223 ±0·058	−0·273 ±0·605	667·8	998·7	23·7 / 7·8
May	−0·198 ±0·020	−0·192 ±0·020	+0·165 ±0·206	661·1	1002·3	410·9 / 30·1
June	−0·239 ±0·051	−0·238 ±0·050	+0·258 ±0·388	647·8	1006·8	1294·8 / 28·9
July						
Aug.						
Sept.	−0·222 ±0·029	−0·217 ±0·039	−0·057 ±0·270	679·4	994·9	463·2 / 25·0
Oct.	−0·253 ±0·041	−0·259 ±0·041	−0·132 ±0·195	681·0	1000·6	794·7 / 28·9
Nov.	−0·299 ±0·062	−0·276 ±0·055	−0·369 ±0·285	702·2	991·4	796·3 / 23·7
Dec.	−0·191 ±0·043	−0·179 ±0·044	−0·111 ±0·230	668·6	994·8	517·5 / 30·1
1952						
Jan.	−0·203 ±0·041	−0·201 ±0·042	−0·132 ±0·478	677·7	985·5	806·5 / 28·9
Feb.	−0·173 ±0·042	−0·149 ±0·040	−0·666 ±0·461	662·6	986·6	755·8 / 35·2
Mar.	−0·231 ±0·067	−0·242 ±0·048	−0·728 ±0·345	670·1	996·2	911·1 / 28·9

* See footnote Table 2.

TABLE 6

Barometer and Temperature Coefficients—Macquarie I.
Limits quoted are 95% confidence limits*
$X_1 = \frac{D}{4}$ (mean of day); X_2 = Barometric Pressure (mean of day); X_3 = Surface Temperature (mean of day)

Month	b_{12} (%/mb)	$b_{12.3}$ (%/mb)	$b_{13.2}$ (%/°C)	$\overline{X}_1$	$\overline{X}_2$ (mb)	$d_{U5\%}$ d $d_{L5\%}$
1950						
June	−0·428 ±0·116	−0·403 ±0·129	−0·363 ±0·770	360·3	1009·1	1·54 1·77
July	−0·362 ±0·066	−0·362 ±0·074	−0·341 ±0·377	357·6	1008·6	1·54 2·01
Aug.	−0·319 ±0·123	−0·317 ±0·128	+0·079 ±0·604	355·4	1006·5	1·54 1·28 1·02
Sept.	−0·366 ±0·038	−0·369 ±0·036	−0·501 ±0·522	353·8	1002·4	1·57 1·75
Oct.	−0·309 ±0·058	−0·309 ±0·060	+0·028 ±0·509	345·3	1003·1	1·55 1·33 1·22
Nov.	−0·362 ±0·060	−0·360 ±0·060	−0·247 ±0·407	353·3	994·8	1·56 1·71
Dec.	−0·325 ±0·066	−0·337 ±0·066	+0·566 ±0·715	356·8	995·1	1·13 1·30
1951						
Jan.	−0·440 ±0·074	−0·437 ±0·076	+0·082 ±0·752	343·1	1006·1	1·28 1·30
Feb.	−0·423 ±0·043	−0·414 ±0·037	−0·624 ±0·731	342·4	1002·5	1·55 1·74
Mar.	−0·324 ±0·121	−0·332 ±0·121	−1·279 ±2·005	358·8	995·6	1·54 1·46 0·92
Apr.	−0·420 ±0·109	−0·422 ±0·111	+0·213 ±0·739	354·1	998·9	1·08 1·15
May	−0·271 ±0·173	−0·271 ±0·190	+0·691 ±1·944	353·5	1002·3	1·54 1·51 1·15
June	−0·397 ±0·053	−0·399 ±0·056	−0·156 ±0·363	352·1	1006·0	
July	−0·347 ±0·041	−0·347 ±0·043	+0·004 ±0·390	346·4	997·3	
Aug.	−0·419 ±0·049	−0·417 ±0·056	−0·027 ±0·430	350·9	998·1	
Sept.	−0·357 ±0·036	−0·344 ±0·040	−0·189 ±0·266	355·4	998·3	
Oct.	−0·392 ±0·049	−0·394 ±0·049	−0·182 ±0·339	354·0	1000·2	
Nov.	−0·460 ±0·050	−0·445 ±0·055	−0·242 ±0·314	363·8	995·4	
Dec.	−0·327 ±0·106	−0·327 ±0·104	−0·333 ±0·518	356·6	994·3	
1952						
Jan.	−0·422 ±0·052	−0·424 ±0·054	+0·112 ±0·493	366·6	986·1	
Feb.	−0·355 ±0·083	−0·344 ±0·090	−0·411 ±1·277	351·5	998·1	
Mar.	−0·432 ±0·057	−0·438 ±0·053	−0·348 ±0·381	358·3	996·2	

* See footnote Table 2.

TABLE 7

Barometer and Temperature Coefficients—Macquarie I.
Limits quoted are 95% confidence limits*
$X_1 = c_{1/s}$; X_2 = Barometric pressure (mean of hour); X_3 = Surface Temperature (mean of hour)

Month	b_{12} (%/mb)	$b_{12\cdot3}$ (%/mb)	$b_{13\cdot2}$ (%/°C)	$\overline{X_1}$	$\overline{X_2}$ (mb)	χ^2_s / $\chi^2_{5\%}$
1950						
June	−0·199 ±0·028	−0·215 ±0·031	+0·158 ±0·138	603·7	1007·4	1810·1 509
July	−0·217 ±0·017	−0·218 ±0·017	−0·069 ±0·087	600·9	1008·8	664·2 632
Aug.	−0·221 ±0·018	−0·221 ±0·018	+0·013 ±0·067	600·5	1006·7	658·8 468
Sept.	−0·229 ±0·008	−0·231 ±0·008	−0·385 ±0·095	603·8	1002·5	934·2 776
Oct.	−0·174 ±0·010	−0·174 ±0·010	−0·021 ±0·079	595·8	1004·3	725·3 694
Nov.	−0·216 ±0·011	−0·216 ±0·011	−0·049 ±0·070	609·1	994·7	892·9 762
Dec.	−0·223 ±0·010	−0·221 ±0·010	−0·257 ±0·095	607·3	995·2	945·3 796
1951						
Jan.	−0·267 ±0·016	−0·277 ±0·016	−0·302 ±0·130	586·4	1006·1	1225·5 777
Feb.	−0·248 ±0·011	−0·243 ±0·011	−0·465 ±0·129	586·7	1001·6	934·9 695
Mar.	−0·186 ±0·016	−0·191 ±0·016	−0·280 ±0·158	601·3	996·0	581·3 498
Apr.	−0·228 ±0·020	−0·228 ±0·017	−0·057 ±0·092	598·5	999·3	702·7 617
May	−0·219 ±0·009	−0·218 ±0·009	+0·066 ±0·081	606·3	1001·3	804·5 602

TABLE 8

Barometer and Temperature Coefficients—Macquarie I.
Limits quoted are 95% confidence limits*
$X_1 = c_{2/4}$; X_2 = Barometric Pressure (mean of hour); X_3 = Surface Temperature (mean of hour)

Month	b_{12} (%/mb)	$b_{12\cdot3}$ (%/mb)	$b_{13\cdot2}$ (%/°C	$\overline{X}_1$	$\overline{X}_2$ (mb)	χ^2_8 / $\chi^2_{5\%}$
1950						
June	−0·200	−0·182	−0·182	845·1	1007·4	608
	±0·019	±0·021	±0·095			509
July	−0·156	−0·155	+0·062	845·0	1008·0	745
	±0·022	±0·022	±0·110			632
Aug.	—0·153	−0·152	−0·140	844·6	1006·7	460
	±0·018	±0·018	±0·067			458
Sept.	−0·169	−0·171	−0·290	854·0	1002·5	778
	±0·009	±0·009	±0·103			776
Oct.	−0·120	−0·121	−0·139	847·9	1004·3	748
	±0·012	±0·012	±0·095			694
Nov.	−0·157	−0·157	−0·052	864·2	994·7	835
	±0·013	±0·013	±0·080			762
Dec.	−0·174	−0·171	−0·596	859·0	994·9	1103
	±0·014	±0·013	±0·128			776
1951						
Jan.	−0·200	−0·214	−0·498	830·2	1006·3	1066
	±0·018	±0·017	±0·141			786
Feb.	−0·177	−0·174	−0·406	828·7	1001·9	874
	±0·013	±0·012	±0·150			690
Mar.	−0·141	−0·146	−0·261	843·9	995·7	491
	±0·020	±0·020	±0·214			412
Apr.	−0·155	−0·153	+0·207	843·1	999·5	729
	±0·021	±0·020	±0·105			632
May	−0·158	−0·158	+0·010	853·5	1001·3	616
	±0·009	±0·009	±0·266			602

* See footnote Table 2.

TABLE 9

Barometer and Temperature Coefficients—Macquarie I.
Limits quoted are 95% confidence limits*
$X_1 = c_{3/32}$, X_2 = Barometric Pressure (mean of hour); X_3 = Surface Temperature (mean of hour)

Month	b_{12} (%/mb)	$b_{12.3}$ (%/mb)	$b_{13.2}$ (%/°C)	$\overline{X}_1$	$\overline{X}_2$ (mb)	$\left\{ \begin{matrix} \chi^2_s \\ \chi^2_{5\%} \end{matrix} \right.$
1950						
June	−0·208	−0·195	−0·120	657·4	1008·6	1304
	±0·010	±0·012	±0·054			568
July	−0·222	−0·223	−0·124	663·2	1008·7	1014
	±0·011	±0·010	±0·051			630
Aug.	−0·277	−0·221	−0·093	669·5	1003·4	1333
	±0·007	±0·007	±0·028			652
Sept.	−0·216	−0·218	−0·278	665·1	1002·5	1327
	±0·005	±0·005	±0·004			776
Oct.	−0·167	−0·168	−0·077	664·7	1004·6	1284
	±0·006	±0·006	±0·048			722
Nov.	−0·197	−0·196	−0·093	676·9	996·1	840
	±0·007	±0·006	±0·040			598
Dec.	−0·205	−0·204	−0·196	678·6	995·4	1154
	±0·005	±0·005	±0·051			780
1951						
Jan.	−0·233	−0·236	−0·118	660·6	1006·1	1632
	±0·008	±0·008	±0·068			794
Feb.	−0·234	−0·231	−0·293	665·9	1001·7	1847
	±0·007	±0·007	±0·083			704
Mar.	−0·184	−0·186	−0·133	677·4	995·9	1262
	±0·011	±0·011	±0·110			485
Apr.	−0·214	−0·215	−0·123	675·5	999·1	792
	±0·009	±0·009	±0·047			577
May	−0·202	−0·204	−0·120	664·5	1001·3	1244
	±0·005	±0·005	±0·048			602

TABLE 10

Barometer and Temperature Coefficients—Macquarie I.
Limits quoted are 95% confidence limits*
$X_1 = c_{4/32}$; X_2 = Barometric Pressure (mean of hour); X_3 = Surface Temperature (mean of hour)

Month	b_{12} (%/*mb*)	$b_{12\cdot3}$ (%/*mb*)	$b_{13\cdot2}$ (%/°C)	$\overline{X}_1$	$\overline{X}_2$ (*mb*)	χ^2_8 / $\chi^2_{5\%}$
1950						
June	−0·109	−0·099	−0·460	644·9	1016·9	267
	±0·048	±0·042	±0·141			165
July	−0·209	−0·208	+0·044	664·5	1008·5	1091
	±0·011	±0·011	±0·057			604
Aug.	−0·219	−0·219	−0·018	665·7	1003·9	1174
	±0·007	±0·007	±0·031			593
Sept.	−0·184	−0·186	−0·328	672·0	1002·2	1634
	±0·006	±0·005	±0·062			740
Oct.	−0·171	−0·179	−0·288	670·7	1006·6	1158
	±0·009	±0·009	±0·077			453
Nov.	−0·189	−0·189	+0·372	689·3	994·6	1141
	±0·006	±0·006	±0·038			750
Dec.	−0·205	−0·204	−0·125	681·2	993·9	1414
	±0·007	±0·007	±0·063			687
1951						
Jan.	−0·236	−0·242	−0·251	653·7	1005·6	1897
	±0·011	±0·011	±0·011			606
Feb.	−0·228	−0·223	−0·338	664·9	999·9	1553
	±0·008	±0·007	±0·092			602
Mar.						
Apr.	−0·234	−0·238	−0·124	667·7	999·4	328
	±0·013	±0·013	±0·070			241
May	−0·199	−0·198	+0·055	662·9	1001·1	1333
	±0·006	±0·006	±0·053			559

* See footnote Table 2.

TABLE 11

Barometer and Temperature Coefficients—Macquarie I.
Limits quoted are 95% confidence limits.*

$X_1 = \frac{D}{4}$; X_2 = Barometric Pressure (mean of hour); X_3 = Surface Temperature (mean of hour)

Month	b_{12} (%/*mb*)	$b_{12.3}$ (%/*mb*)	$b_{13.2}$ (%/°C)	$\overline{X}_1$	$\overline{X}_2$ (*mb*)
1950					
June	−0·383 ±0·044	−0·379 ±0·055	−0·038 ±0·246	362·5	1007·4
July	−0·354 ±0·053	−0·350 ±0·053	+0·286 ±0·271	356·9	1008·8
Aug.	−0·355 ±0·051	−0·355 ±0·051	+0·062 ±0·193	356·1	1006·7
Sept.	−0·369 ±0·028	−0·371 ±0·028	−0·516 ±0·318	353·7	1002·5
Oct.	−0·311 ±0·035	−0·314 ±0·035	+0·210 ±0·264	343·9	1004·3
Nov.	−0·352 ±0·036	−0·352 ±0·036	−0·094 ±0·232	353·4	994·7
Dec.	−0·333 ±0·034	−0·337 ±0·032	+0·609 ±0·323	356·5	994·9
1951					
Jan.	−0·395 ±0·052	−0·364 ±0·054	+1·012 ±0·429	342·5	1006·1
Feb.	−0·415 ±0·030	−0·411 ±0·030	−0·584 ±0·392	343·8	0101·9
Mar.	−0·288 ±0·055	−0·283 ±0·055	+0·155 ±0·604	359·4	995·7
Apr.	−0·316 ±0·058	−0·398 ±0·058	+0·289 ±0·309	353·7	999·3
May	−0·366 ±0·025	−0·362 ±0·027	+0·142 ±0·245	358·9	1001·3

TABLE 12

Barometer and Temperature Coefficients—Heard I.
Limits quoted are 95% confidence limits*
$X_1 = c_{1/s}$; X_2 = Barometric Pressure (mean of hour); X_3 = Surface Temperature (mean of hour)

Month	b_{12} (%/mb)	$b_{12.3}$ (%/mb)	$b_{13.2}$ (%/°C)	$\overline{X}_1$	$\overline{X}_2$ (mb)	$\left\{ \begin{matrix} \chi^2_s \\ \chi^2_{1\%} \end{matrix} \right.$
1948						
Apr.	−0·196	−0·223	−0·277	556·7	999·7	158
	±0·037	±0·043	±0·237			164
May	−0·268	−0·283	−0·387	571·4	982·4	367
	±0·021	±0·023	±0·247			233
June	−0·234	−0·234	−0·114	562·2	992·8	1548
	±0·014	±0·014	±0·354			579
July	−0·189	−0·191	−0·176	569·4	990·6	1365
	±0·020	±0·020	±0·474			540
Aug.	−0·212	−0·132	−0·213	552·6	979·2	1396
	±0·029	±0·032	±0·252			319
Sept.	−0·128	−0·131	−0·143	546·1	1002·0	1000
	±0·016	±0·016	±0·112			498
Oct.	−0·267	−0·265	−0·288	570·0	988·2	1293
	±0·015	±0·014	±0·070			692
Nov.	−0·210	−0·210	+0·054	561·8	990·5	736
	±0·015	±0·015	±0·158			553
Dec.	−0·172	−0·171	−0·328	557·1	996·1	1410
	±0·011	±0·011	±0·132			786
1949						
Jan.	−0·214	−0·214	+0·010	561·3	989·3	1299
	±0·018	±0·018	±0·190			568

* See footnote Table 2.

TABLE 13

Barometer and Temperature Coefficients—Heard I.
Limits quoted are 95% confidence limits*
$X_1 = c_{2/4}$; X_2 = Barometric Pressure (mean of hour); X_3 = Surface Temperature (mean of hour)

Month	b_{12} (%/mb)	$b_{12.3}$ (%/mb)	$b_{13.2}$ (%/°C)	$\overline{X}_1$	$\overline{X}_2$ (mb)	χ^2_{s} $\chi^2_{5\%}$
1948						
Apr.	−0·115	−0·056	+0·055	821·0	999·4	120
	±0·042	±0·051	±0·284			134
May	−0·180	−0·177	+0·107	824·8	984·9	488
	±0·020	±0·021	±0·214			309
June	−0·150	−0·150	−0·080	809·7	991·7	1482
	±0·017	±0·018	±0·137			538
July	−0·148	−0·149	−0·058	822·3	991·0	732
	±0·022	±0·022	±0·184			333
Aug.	−0·188	−0·190	−0·031	839·8	978·6	556
	±0·014	±0·016	±0·131			446
Sept.	−0·159	−0·156	−0·209	809·2	998·2	962
	±0·013	±0·013	±0·077			679
Oct.	−0·206	−0·204	−0·314	822·6	988·2	938
	±0·014	±0·013	±0·067			730
Nov.	−0·178	−0·179	−0·135	814·4	990·6	558
	±0·015	±0·015	±0·158			554
Dec.	−0·132	−0·132	−0·279	809·9	996·0	834
	±0·010	±0·010	±0·117			796
1949						
Jan.	−0·172	−0·170	−0·386	812·0	989·8	672
	±0·018	±0·018	±0·189			617

TABLE 14

Barometer and Temperature Coefficients—Heard I.
Limits quoted are 95% confidence limits*
$X_1 = c_{s/s_2}$ X_2 = Barometric Pressure (mean of hour); X_3 = Surface Temperature (mean of hour)

Month	b_{12} (%/mb)	$b_{12.3}$ (%/mb)	$b_{13.2}$ (%/°C)	$\overline{X}_1$	$\overline{X}_2$ (mb)	χ^2_s / $\chi^2_{5\%}$
1948						
Apr.	−0·206	−0·238	−0·455	637·8	996·0	119·1
	±0·034	±0·043	±0·395			84·5
May	−0·236	−0·237	−0·013	654·6	982·5	465
	±0·013	±0·015	±0·176			226
June	−0·245	−0·258	−0·558	678·8	985·8	805
	±0·009	±0·008	±0·065			365
July	−0·211	−0·212	−0·091	674·3	989·1	1590
	±0·008	±0·008	±0·922			618
Aug.	−0·229	−0·223	−0·081	686·3	980·4	1476
	±0·011	±0·013	±0·089			388
Sept.	−0·214	−0·213	−0·100	654·0	998·2	2597
	±0·008	±0·008	±0·050			710
Oct.	−0·135	−0·140	+0·475	669·9	986·8	3123
	±0·032	±0·032	±0·235			663
Nov.	−0·213	−0·213	−0·081	661·4	990·4	916
	±0·008	±0·008	±0·083			532
Dec.	−0·187	−0·186	−0·115	656·5	995·8	1348
	±0·005	±0·005	±0·060			776
1949						
Jan.	−0·217	−0·214	−0·327	662·6	990·2	2070
	±0·010	±0·010	±0·105			600

*See footnote Table 2.

range. Also the values given for χ^2 must be regarded only as upper limits of the significance points of the appropriate statistic.

It will be noted that in many cases the 95 per cent confidence interval of the temperature coefficient $\beta_{13.2}$ includes zero, indicating that the estimate is not significant at the 5 per cent level. In all other cases the value is small and, in view of the above remarks on serial correlation, may not be significant. Further, the values of $b_{13.2}$ vary considerably from month to month and the values calculated using daily mean values of the variables differ considerably from those calculated from hourly data. It appears, then, that little physical significance attaches to these values; that is, in the light of considerations of the sea level temperature effect in Chapter 1, surface temperature is a very poor indicator of scale height of the atmosphere at Heard Island and Macquarie Island.

In view of the smallness and doubtful significance of the temperature coefficient and because of the small range of variation of surface temperature at Heard Island and Macquarie Island, this effect is ignored in reducing observations to standard atmospheric conditions in the following section on variations associated with solar and geomagnetic disturbance. Regression equations of the form $X_1 = a + \beta_{12}x_2$ are used.

In the case of the barometer coefficients b_{12} and $b_{12.3}$ there can be little doubt that they are statistically significant and that there are significant variations from month to month. Examination of Tables 2 to 6 and 12 to 14 shows that the values of b_{12} and $b_{12.3}$ vary from month to month in a similar manner for each measure of the cosmic ray intensity, indicating the presence of physical causes acting alike on each measure.

Barometer effect for mesons—theoretical treatment. In order to calculate the barometer effect for μ-mesons it is necessary to know their momentum spectrum at production. It will be assumed that μ-mesons are produced (by decay of π-mesons) at a definite depth, x_o gm. cm.$^{-2}$ in the atmosphere.

Define

N_o = number of μ-mesons per unit at production

N_s = number of μ-mesons per unit at sea level, the unit being (unit momentum) sec. sterad cm.^{2}

$pm_\mu c$ = momentum of a μ-meson of rest mass m_μ

τ_μ = mean life of the μ-meson

s = distance measured downwards from the production level

x = atmospheric depth in gm. cm.$^{-2}$.

H = scale height of the atmosphere

p_1 = minimum value of p for μ-mesons capable of penetrating 10 cm. of lead absorber

$p_2 = 73{\cdot}39$ ($p_2 m_\mu c = 8000$ Mev/c).

The subscript "o" will be used to denote values of a variable at the production level and the subscript "s" at sea level.

It can be readily shown that for μ-mesons of momentum p_s the probability of survival after travelling a distance s' is

$$\exp\left(-\frac{1}{\tau_\mu c}\int_0^{s'}\frac{ds}{p}\right)$$

Consequently $\mathrm{N}_s = \mathrm{N}_o \exp\left(-\frac{1}{\tau_\mu c}\int_0^{s_s}\frac{ds}{p}\right)\frac{dp_o}{dp_s}$

Assume the atmosphere to be isothermal and static

(1) $\mathrm{X} = \mathrm{X}_o \exp(S/\mathrm{H})$

This leads to

(2) $\mathrm{N}_s = \mathrm{N}_o \exp\left(-\frac{\mathrm{H}}{\tau_\mu c}\int_{\mathrm{x}_o}^{\mathrm{x}_s}\frac{d\mathrm{x}}{\mathrm{x}p}\right)\frac{dp_o}{dp_s}$

(3) $\mathrm{N}_o = \mathrm{N}_s \exp\left(\frac{\mathrm{H}}{\tau_\mu c}\int_{\mathrm{x}_o}^{\mathrm{x}_s}\frac{d\mathrm{x}}{\mathrm{x}p}\right)\frac{dp_s}{dp_o}$.

Using the Bethe-Bloch relation

$$-\frac{d\mathrm{E}}{d\mathrm{x}} = \frac{4\pi e^4 \mathrm{NZ/A}}{m_e c^2}\cdot\frac{1}{\beta^2}\left[\log\left(\frac{2m_e c^2}{\mathrm{I}}\cdot\frac{\beta^2}{1-\beta^2}\right)-\beta^2\right]$$

for energy loss per gm. cm.$^{-2}$ of a fast particle which loses energy by ionization and excitation (the most important processes for $p < 100$) and the substitution

$p = \sinh\gamma$

(4) $-\frac{d\gamma}{d\mathrm{x}} = g\,[(a+2\log\sinh\gamma-\tanh^2\gamma)/\sinh\gamma\tanh^2\gamma]$

is obtained for μ-mesons where $g = \frac{4\pi e^4 \mathrm{NZ/A}}{m_e c^2 m_\mu c^2}$ and $a = \log 2m_e c^2/\mathrm{I}$

The range R of a μ-meson is then given by

$$\mathrm{R} = \mathrm{R}_1 + \int_{\gamma_1}^{\gamma}\frac{d\gamma}{-d\gamma/d\mathrm{x}}$$

(5) $\mathrm{R} = \mathrm{R}_1 + \frac{1}{g}\int_{\gamma_1}^{\gamma}\frac{\sinh\gamma\tanh^2\gamma\,d\gamma}{a+2\log\sinh\gamma-\tanh^2\gamma}$

where e = charge of the electron ($4{\cdot}803\times10^{-10}$ esu)

m_e = mass of the electron ($9{\cdot}1\times10^{-28}$ gm.)

N = Avogadro's number ($6{\cdot}023\times10^{23}$ molecules/gm. mol)

Z/A = atomic number/atomic weight of the absorber (0·5, average value for air)

I = mean energy of excitation of the electrons of the absorber atoms (80·5 ev)

βc = velocity of the particle

R_1 = range of μ-mesons for which $p = \sinh\gamma_1$.

Using (5), Fenton (1952) has calculated a table of values of p as a function of R.

Since $\delta R = -\delta x$ this table may be used to determine $p(x)$ for any given p_s and x_s, hence using numerical or graphical methods the integral $\int_{x_o}^{x_s} \frac{dx}{xp}$ may be evaluated and dp_s/dp_o determined. Using this procedure and using values of $N_s(p_s)$ obtained by Caro, Parry and Rathgeber (1951), (see Fig. 1), $N_o(p_o)$ has been calculated for $x_o = 81{\cdot}6$ gm. cm.$^{-2}$ (80 mb.), 102 gm. cm.$^{-2}$ (100 mb.), 153 gm. cm.$^{-2}$ (150 mb.) and 306 gm. cm.$^{-2}$ (300 mb.). The values used for the constants were

$$\tau_\mu = 2{\cdot}15\ \mu\text{-sec.}$$
$$m_\mu = 215\ m_e$$
$$c = 3 \times 10^{10}\ \text{cm. sec.}^{-1}$$
$$x_s = 1026\ \text{gm. cm.}^{-2}$$
$$H = 7 \times 10^5\ \text{cm.}$$

Results of these calculations are shown in Fig. 13. It will be seen that for high momenta the variation of N_o with p_o is similar to the variation of N_s with p_s. In the discussion of this section consider the spectra $N_s = k_s p_s^{-2}$ (in line with results given by Rossi, 1948) and $N_s = k_s p_s^{-3}$ (in line with results given by Caro, Parry and Rathgeber, 1951) for $p_s > p_2 = 73{\cdot}39$ ($p_2 m_\mu c = 8000$ Mev/c). The spectra of Caro, Parry and Rathgeber and of Rossi are similar for lower momenta.

Using the spectrum $N_o(p_o)$ ($x_o = 153$ gm. cm.$^{-2}$) (curve III of Fig. 13) and (2) several values of H and x_s may be calculated. These results are shown in Fig. 14.

The differential barometer coefficient is now given by

$$B_{12} = \frac{1}{N_s}\left(\frac{\partial N_s}{\partial x_s}\right)_H = \text{const.}$$

From (2) is obtained

$$(6)\quad B_{12} = \frac{1}{N_o}\frac{dN_o}{dp_o}\frac{dp_o}{dx_s} + \frac{d}{dp_s}\left(\frac{dp_o}{dx_s}\right)\frac{dp_s}{dp_o} - \frac{N}{\tau_\mu c x_s p_s}$$

giving for any value of $\quad \frac{dp_s}{dx_s} = -\frac{dp_o}{dx} = -\frac{d(\sinh\gamma)}{dx} = -\cosh\gamma\frac{d\gamma}{dx}$

Substituting $\frac{d\gamma}{dx}$ from (4)

$$(7)\quad \frac{dp_o}{dx_s} = \frac{1}{g}\cosh\gamma\left[\frac{a + 2\log\sinh\gamma - \tanh^2\gamma}{\sinh\gamma\tanh^2\gamma}\right]$$

is obtained leading to $\frac{dp_o}{dx_s}$ for any p_o which (for given x_o and x_s) corresponds to a particular value of p_s. The term $\frac{d}{dp_s}\left(\frac{dp_o}{dx_s}\right)$ may be obtained

graphically after plotting dp_o/dx_s against p_s. Likewise $\frac{dN_o}{dp_o}$ and $\frac{dp_s}{dp_o}$ are obtained. Using this procedure the results for B_{12} shown in Fig. 15 were obtained.

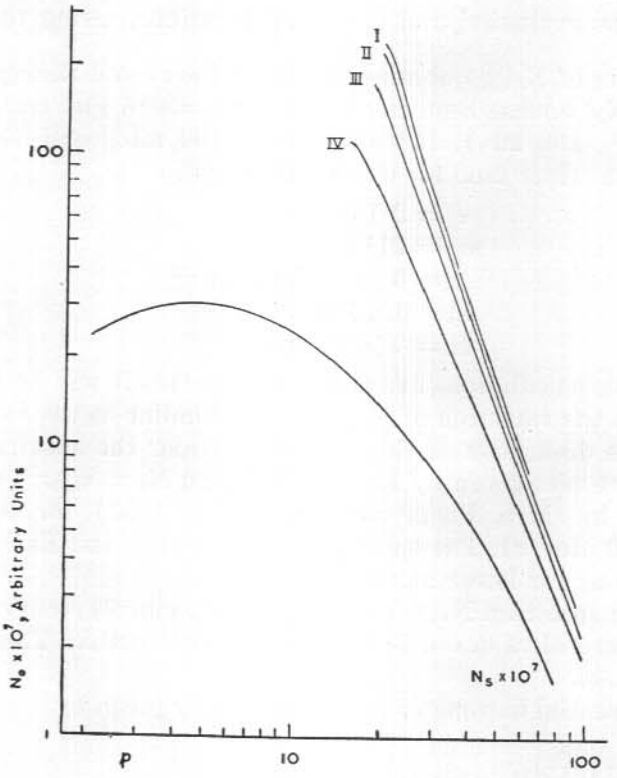

FIG. 13.
Sea level μ-meson momentum spectrum, $N_s(p_s)$—after Caro, Parry and Rathgeber (1951)—and calculated spectra at production, $N_o(p_o)$, assuming depth of production $x_o = 80$ mb., curve I; 100 mb., curve II; 150 mb., curve III; 300 mb., curve IV.

The integral barometer coefficient is now given by

$$\beta_{12} = 100 \int_{p_1}^{\infty} B_{12} N_s dp_s \Big/ \int_{p_1}^{\infty} N_s dp_s$$

Integration over the range of p_s from p_1 to p_2 may be carried out by graphical or numerical methods; the values used for N_s are of course the calculated values given in Fig. 14 for the appropriate H and x_s. In order to calculate the integrals over the range of p_s from p_2 to ∞ the following assumptions were made:

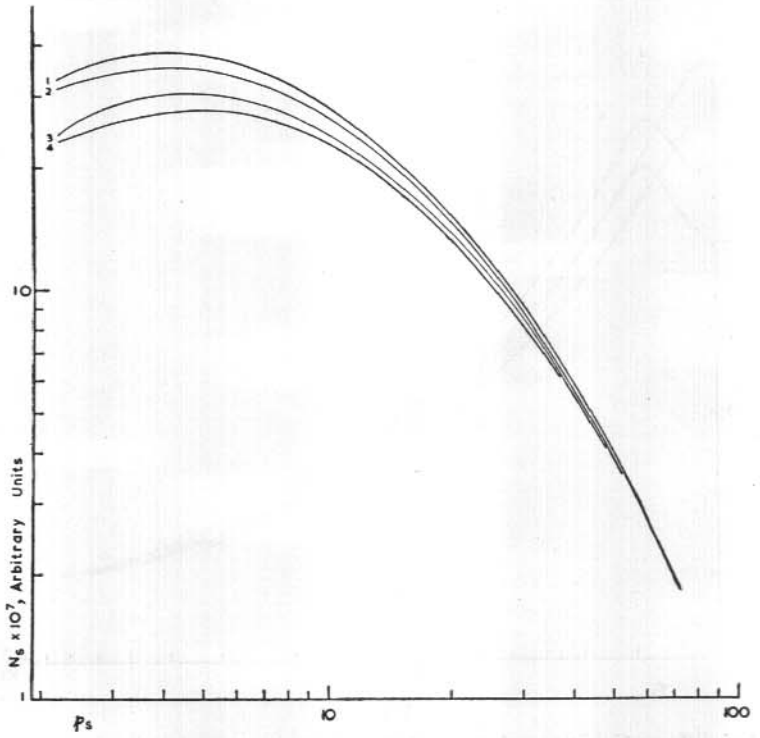

FIG. 14.

Sea level μ-meson momentum spectrum, $N_s(p_s)$, calculated from Fig. 13, curve III and (2) for

H = 6 km., x_s = 1026 gm. cm.$^{-2}$ — curve 1
H = 6 km., x_s = 1050 gm. cm.$^{-2}$ — curve 2
H = 7 km., x_s = 1026 gm. cm.$^{-2}$ — curve 3
H = 7 km., x_s = 1050 gm. cm.$^{-2}$ — curve 4

N_s/N_o = constant; the value used is that for $p_s = p_2$.

$$p_o - p_s = \text{constant}$$

$$dp_o/dx_s = g\,(a-1+2\log p) \quad \text{cf. (7)}$$

$$\frac{d}{dp_s}\left(\frac{dp_o}{dx_s}\right)\frac{dp_s}{dp_o}N_s = 0$$

This term is negligible at $p_s = p_2$ and decreases roughly as $p_s^{-1}\,N_s$.
Assuming momentum spectra

$N_o = k_o p_o^{-3}$ and $N_s = k_s p_s^{-3}$ for $p_s > p_2$ gives

$$\int_{p_2}^{\infty} B_{12} N_s dp_s = -(N_o)_2\left[\left(\frac{dp_o}{dx_s}\right)_2 + \frac{2}{3}g\right] - \frac{H(N_s)_2}{3\tau_\mu c x_s}$$

where the subscript '2' denotes values corresponding to $p_s = p_2$. Assuming momentum spectra $N_o = k_o' p_o^{-2}$ and $N_s = k_s' p_s^{-2}$ gives

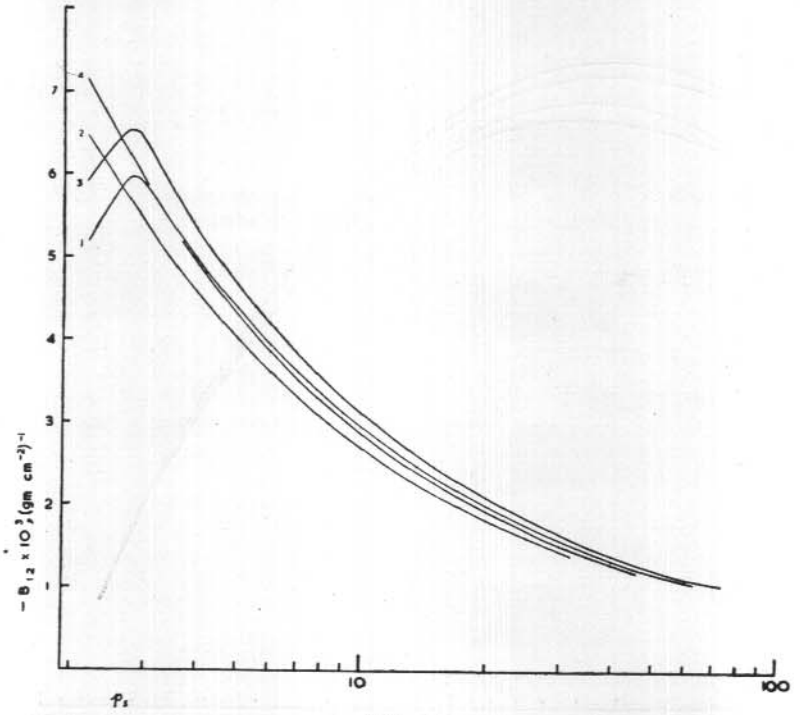

FIG. 15.
Calculated differential barometer coefficient, $B_{12}(p_s)$, assuming sea level momentum spectra as given in Fig. 14.

$$\int_{p_2}^{\infty} B_{12} N_s \, dp_s = -(N_o)_2 \left[\left(\frac{dp_o}{dx_s} \right)_2 + g \right] - \frac{H(N_s)_2}{2 \tau_\mu c x_s}$$

The final values calculated for β_{12} are given in Table 15.

TABLE 15
Calculated values of β_{12} in % per mb.

x_0 (gm. cm.$^{-2}$)	H (cm.)	x_s (gm. cm.$^{-2}$)	β_{12} ($\gamma = 2$)	β_{12} ($\gamma = 3$)
153	7×10^5	1026	−0·241	−0·261
153	7×10^5	1050	−0·220	−0·239
153	6×10^5	1026	−0·236	−0·254
153	6×10^5	1050	−0·220	−0·238
81·6	7×10^5	1026	−0·237	−0·256

Barometer effect—discussion. Comparison of the estimates, b_{12}, of the barometer coefficient for mesons given in Tables 3, 8 and 13 with the

theoretical values given in Table 15 shows that the theoretical value is too high, whatever the choice of x_o, H, x_s and γ in the ranges considered. However, it is of some interest to see whether the dependence of the barometer coefficient on H and x_s is of the form given in the table of theoretical values.

The values of b_{12} from Table 3 were plotted against mean barometric pressure for each sample. From this plot there appears to be a very small increase in numerical value of b_{12} with increase in pressure whereas, according to Table 15, β_{12} decreases numerically with increase in x_s. To examine this point further mean values of c_2 and pressure in the interval two hours before to two hours after the daily radio sonde flight were examined, using the Macquarie Island data of the period June 1950 to March 1952. These data were divided into six samples according to the values of x_s and of H defined by $H = s_s/\log \frac{x_s}{x_o}$ where $x_o = 153$ gm. cm.$^{-2}$. The estimates of the barometer coefficients for these samples are given in Table 16.

TABLE 16

Estimates of β_{12} in % per mb. from Data Grouped According to Values of x_s and H.

	$x_s < 1000$ mb $\bar{x}_s = 991$ mb	1000 mb $< x_s <$ 1010 mb $\bar{x}_s = 1005$ mb	$x_s > 1010$ mb $\bar{x}_s = 1016$ mb
H < 7 km $\bar{H} = 6{\cdot}9$ km	−0·21	−0·058	−0·15
	$x_s < 990$ mb $\bar{x}_s = 982$ mb	990mb $\leqslant x_s <$ 1010 mb $\bar{x}_s = 1001$ mb	$x_s > 1010$ mb $\bar{x}_s = 1016$ mb
H > 7 km $\bar{H} = 7{\cdot}1$ km	−0·17	−0·19	−0·28

From this table it is clear that the estimates of the barometer coefficient from the samples considered do not vary in any simple way with x_s and H as do the theoretical values summarized in Table 15.

These results strongly suggest that the assumption that the atmosphere is static and isothermal is unsatisfactory. In the following the total barometer coefficient is derived in a manner which avoids this assumption in one of the more important terms.

From the previous section, "Barometer effect for mesons—theoretical treatment" is taken

$$N_s = N_o \exp\left(-\frac{1}{\tau c}\int_0^s \frac{ds}{p}\right)\frac{dp_o}{dp_s}$$

The differential total barometer coefficient $B'_{12} = \frac{1}{N_s}\frac{dN_s}{dx_s}$

is then

$$B'_{12} = \frac{1}{N_s}\left(\frac{\partial N_s}{\partial x_s}\right)_{s_s = \text{const.}} + \frac{1}{N_s}\left(\frac{\partial N_s}{\partial S_s}\right)_{x_s = \text{const.}} \frac{dS_s}{dx_s}$$

Using the notation later described in the section "Barometer effect for μ-mesons (height of production constant)" the following is obtained

$$B'_{12} = B_{12.34} - \frac{1}{\tau c p_s}\frac{dS_s}{dx_s}$$

The first term, $B_{12.34}$, is derived using the assumption $x_s = x_o \exp(S_s/H)$ while in the second term the value of dS_s/dx_s appropriate to the sample of observations is used. The integral total barometer coefficient is given by

$$\beta'_{12} = \int_{p_1}^{\infty} B'_{12} N_s \, dp_s \Big/ \int_{p_1}^{\infty} N_s \, dp_s$$

The μ-mesons are assumed to be produced at $x_o = 153$ gm. cm.$^{-2}$.

Using the Macquarie Island data of June, 1950, to March, 1952, the values of S_s (height of 153 gm. cm.$^{-2}$ level) obtained from the daily radiosonde flight were plotted against x_s. The plotted points covered a large region with no clearly defined trend. From these points two samples were selected, one in which all points lay in a narrow band of slope $dS_s/dx_s = 953{\cdot}4$ cm./gm. cm.$^{-2}$ and another in which the points lay in a narrow band of zero slope. Using the values of c_2 and pressure (mean of the period two hours before to two hours after the time of ascent of the radiosonde) associated with the points of these samples, estimates and 95 per cent confidence limits of the barometer coefficient were calculated. These results are presented in Table 17 along with the theoretical values, β'_{12}, calculated with $x_o = 153$ gm. cm.$^{-2}$, $N_o(p_o)$ given in curve III of Fig. 13, $N_s(p_s)$ as given in Fig. 13 and $x_s = 1026$ gm. cm.$^{-2}$.

TABLE 17

Theoretical Values and Estimates of Total Barometer Coefficients, β'_{12}, in % per mb.

	Sample Estimates		Theoretical Values	
ds_s/dx_s cm/gm. cm^{-2}	$\bar{x}_s$ gm. cm^{-2}	b'_{12} %/mb	β'_{12} ($\gamma = 2$) %/mb	β'_{12} ($\gamma = 3$) %/mb
953·4	1025	$-0{\cdot}223 \pm 0{\cdot}055$	$-0{\cdot}325$	$-0{\cdot}351$
0	1021	$-0{\cdot}151 \pm 0{\cdot}052$	$-0{\cdot}204$	$-0{\cdot}221$

This table shows that the dependence of the theoretical values on ds_s/dx_s is of the form obtained in the samples but the theoretical values are still too high (numerically). This may be due to (a) the assumption that the atmosphere is static and isothermal used in deriving the first term of

B'_{12}, (b) a wrong choice of x_o (using $x_o = 81{\cdot}6$ gm. cm.$^{-2}$ reduces β'_{12} by only about 2 per cent), (c) errors in $N_o(p_o)$ (this was deduced from $N_s(p_s)$ and the assumption that the pressure height distribution in the atmosphere is given on the average by $x = x_o \exp S/H$ with $H = 7$ km. and $x_s = 1026$ gm. cm.$^{-2}$) or (d) weakness of the assumption that the μ-mesons are produced at a definite level, x_o gm. cm.$^{-2}$, in the atmosphere.

In Chapter 7, Jacklyn, from an analysis of some of the Macquarie Island measurements of c_2, has shown that the barometer coefficient characteristic of a temperate air mass is different from the value characteristic of a polar air mass, the difference being associated with different values of ds_s/dx_s for the two air masses.

As suggested by Jacklyn, it seems likely that the variations of barometer coefficient from sample to sample may be due mainly to variations in some sort of mean value of ds_s/dx_s associated with the samples.

In order to compare the estimates of the barometer coefficient for the hard component obtained in the present case with those of other workers, some values obtained in recent measurements with Geiger counter telescopes are shown in Table 18. The Macquarie Island and Heard Island values fall roughly in the middle of the range of values of this table.

Fenton (1952), from an examination of experimental and theoretical values, concludes that there is insufficient evidence to justify the view that the barometer coefficient for the hard component varies with zenith angle of incident of the particles. In that case Table 18 gives no indication of a systematic variation of the barometer coefficient with lead absorber thickness.

Several earlier theoretical calculations of the barometer coefficient have been made; of these the calculations of Rose (1951) and Fenton (1952) should be mentioned. Rose (1951) assumes variations in atmospheric structure of a type which does not in fact occur. (He assumes the change in pressure at any height h to be proportional to $x(h)/x_s$ and adjusts the density to give no change in temperature distribution). In view of earlier remarks this may lead to incorrect results. He then assumes the momentum of the mesons to be a linear function of absorber thickness traversed (in gm. cm.$^{-2}$) and proceeds to select a form of the momentum spectrum of μ-mesons at production which leads to agreement between his calculated and experimental values for the barometer coefficient. The form of the production spectrum deduced by Rose derived largely from the marked increase he found in barometer coefficient with increase in lead absorber thickness; there appears to be little other evidence for this effect (Table 18).

Fenton assumes the μ-mesons to be produced at the 100 mb. (102 gm. cm.$^{-2}$) level with a momentum spectrum of the form $p_o^{-\gamma}$ for the whole range of p_o. His method after this is essentially an approximation to the

TABLE 18

Estimates of Barometer Coefficient for the Hard Component from Different Measurements

Source	Zenith Angle	Lead Absorber	b_{12} (%/mb)
Caro et al. (1948)			
,, Lat. 38°–51°S	0°	10 cm.	−0·126(1)
,, Lat. 51°–65°S	0°	10 cm.	−0·136(1)
,, Lat. 65°–67°S	0°	10 cm.	−0·112(1)
Table 3	0°	10 cm.	−0·162(2)
Table 13	0°	10 cm.	−0·163(3)
Fenton (1952)	15°	12 cm.	−0·180
,,	30°	12 cm.	−0·192
,,	45°	12 cm.	−0·175
,,	60°	12 cm.	−0·153
,,	70°	12 cm.	−0·209
Rose (1951)	0°	18·5 cm.(4)	−0·131
Duperier (1949)	0°	25 cm.	−0·105(1)
Dolbear, Elliott (1951)	45°	35 cm.	−0·139(5)
,,	45°	35 cm.	−0·142(6)
Rose (1951)	0°	39 cm.(4)	−0·160
Duperier (1951)	0°	40 cm.	−0·123(1)

(1) Calculated from data given in reference.
(2) Mean of 22 monthly values.
(3) Mean of 10 monthly values.
(4) Mean of several values.
(5) North pointing telescope; mean of 12 monthly values.
(6) South pointing telescope; mean of 12 monthly values.

method used in the present case, the theoretical values obtained being somewhat higher than his experimental values.

The conclusions of the preceding sections may be summarized as follows:

1. If the cosmic ray intensity at sea level at Heard Island or Macquarie Island is predicted by a linear function of barometric pressure and surface temperature, the constants of the function (barometer and temperature coefficients) being estimated by the least squares method, it is found that

(a) The temperature effect is not significant,
(b) The variance of the errors of prediction is greater than is expected,
(c) The errors are serially correlated, i.e. they vary from hour to hour and from day to day in a non-random manner. If, then, the primary cosmic ray intensity is constant (apart from occasional abnormal variations, some of which are discussed in Chapter 5) there are systematic variations in sea level intensity of terrestrial (presumably atmospheric) origin which are not accounted for in terms of variation of barometric pressure and surface air temperature alone.

2. Using the simplying assumptions that all μ-mesons are produced at a definite atmospheric depth and that atmospheric depth is an exponential function of height, theoretical values of the expected barometer coefficient for the sea level μ-meson intensity have been calculated and compared with the observed values for the hard component. It is found that

(a) The theoretical values are numerically too high,

(b) The dependence of barometer coefficient on barometric pressure and scale height of the atmosphere, as determined theoretically, is not apparent in the experimental results,

(c) When the second assumption is dropped in calculating one of the important terms involved in the theoretical value for the barometer coefficient, the dependence of this value on the derivative of the assumed height of the μ-meson production level with respect to sea level pressure is similar to that obtained experimentally; the theoretical values are however still numerically too high.

One would expect the importance of inaccuracy of the assumption of an exponential atmosphere to be reduced by assuming the cosmic ray intensity to be a function of barometric pressure and height of production of the μ-mesons. This has been done by Duperier (1951) who also included a term involving the temperature in the vicinity of the μ-meson production level. A similar procedure is used in the following section.

Cosmic ray intensity and upper air data—experimental results. In order to examine further the relation between cosmic ray intensity at sea level and structure of the atmosphere, the Macquarie Island observations of June, 1950, to May, 1951, were divided into four samples:

Sample 1—Data of June, July, August, 1950, and May, 1951.

Sample 2—Data of September, October, 1950, and March, April, 1951.

Sample 3—Data of November, December, 1950, and January, February, 1951.

Sample 4—Data in which barometric pressure at the time of the daily radiosonde flight was within the limits 1005 to 1007 mb. Some of these observations were obtained by conducting additional radiosonde flights at times when the pressure was within the above limits. All of the data of Sample 4 are contained in Samples 1, 2 or 3. In these samples the values used for cosmic ray intensity and barometric pressure are mean values for the period two hours before to two hours after the time of ascent of the radiosonde. It is assumed that the pressure-height and temperature-height distributions remain constant during this period.

The following notation is used:

X_1 = cosmic ray intensity (c_1, c_2, c_3 or D defined in the section, "Notation for coincidence rates", in Chapter 2).

X_2 = barometric pressure.

$X_3(\xi)$ = height of the level at which the pressure is ξ mb.

$X_4(\xi)$ = mean temperature in the interval ξ to ξ' mb.

The values used for ξ and ξ' are $\xi = 80$, $\xi' = 100$; $\xi = 100$, $\xi' = 150$; $\xi = 150$, $\xi' = 200$; $\xi = 300$, $\xi' = 400$; $\xi = 500$, $\xi' = 600$.

Following Duperier (1951 and earlier references given in this paper) various correlation coefficients have been calculated, the values of which are given for the hard component, c_2, in Figs. 16 and 17 and for the soft component, D in Figs. 18 and 19. In the notation of the section, "Multiple regression—error term normally distributed" in Chapter 3, the partial correlation coefficients are given by

$$r_{1i(j)} = \frac{-w_{1i}}{\sqrt{w_{11}w_{ii}}}.$$

Using the regression model $X_1 = \alpha + \beta_{12\cdot34}x_2 + \beta_{13\cdot24}x_3 + \beta_{14\cdot23}x_4 + \epsilon$ the least squares estimates $b_{12.34}$, $b_{13.24}$ and $b_{14.23}$ of $\beta_{12.34}$, $\beta_{13.24}$ and $\beta_{14.23}$ were calculated. These estimates and the 95 per cent confidence limits of the regression coefficients are given for c_1, c_2, c_3 and D in Tables 19 to 22.

Significance of results. On each set of curves of Figs. 16 and 17, and 18 and 19, is marked the value of $r_{\min 5\%}$, the smallest value of r which is significant at the 5 per cent level calculated on the assumption that $\frac{r\sqrt{n-k}}{\sqrt{1-r^2}}$ has Student's distribution with $n-k$ degrees of freedom. As "d" (column 6 of Table 20) is less than $d_{U\,5\%}$ in all cases in which it has been calculated $r_{\min 5\%}$ must be regarded as only a lower limit of the appropriate statistic. However, in Figs. 16 and 17, the general form of the curves is similar for each sample, indicating a common physical cause of the variation of the correlation coefficients with choice of ξ. Also Fig. 16 showing the variation of $r_{12.3}$ and $r_{13.2}$ with choice of ξ is similar to that obtained by Duperier (1951). In particular, the decrease in numerical value of $r_{13.2}$ for $\xi < 300$ mb. ($\xi < 200$ mb. in Duperier's case) is similar.

The variations of $r_{12.3}$, $r_{13.2}$, $r_{12.34}$ and $r_{14.23}$ with choice of ξ, in the cases where $X_1 = c_1$ and $X_1 = c_3$ (not reproduced here), are similar to those for $X_1 = c_2$ (Figs. 16 and 17). In the case where $X_1 = D$ most of the values of $r_{13.2}$, $r_{13.24}$ and $r_{14.23}$ are not significant and their values vary with choice of ξ in different ways for each of the four samples. The values of $r_{12.3}$ and $r_{12.34}$ are significant (according to standard tests which ignore the possible serial

TABLE 19

Estimates of Regression Coefficients $\beta_{12.34}$, $\beta_{13.24}$ and $\beta_{14.23}$
Limits quoted are 95% confidence limits*
$X_1 = c_{1/s}$ (four hourly mean); X_2 = Barometric Pressure (four hourly mean); $X_3(\xi)$ = Height of Level of Pressure ξ mb;
$X_4(\xi)$ = Mean Temperature in interval ξ to ξ' mb.

	ξ mb.	ξ' mb.	$b_{12.34}$ (%/mb)	$b_{14.24}$ (%/km)	$b_{14.23}$ (%/°C)	$\left\{ \begin{matrix} \chi^2_s \\ \chi^2_{5\%} \end{matrix} \right.$
Sample 1	80	100	−0·175 ±0·044	−3·59 ±3·50	+0·059 ±0·118	155·4 73·0
	100	150	−0·160 ±0·047	−4·27 ±3·24	+0·077 ±0·101	149·9 73·0
	150	200	−0·180 ±0·045	−1·83 ±2·43	+0·014 ±0·067	162·5 73·0
	300	400	−0·155 ±0·060	−3·61 ±4·54	−0·016 ±0·153	151·9 73·0
	500	600	−0·202 ±0·092	+0·23 ±9·75	−0·159 ±0·186	146·0 73·0
Sample 2	80	100	−0·171 ±0·024	−4·50 ±2·00	+0·028 ±0·067	158·3 89·1
	100	150	−0·168 ±0·025	−4·88 ±2·05	+0·019 ±0·075	156·9 89·1
	150	200	−0·159 ±0·026	−5·58 ±2·08	+0·018 ±0·054	159·2 89·1
	300	400	−0·251 ±0·046	−0·27 ±4·50	−0·167 ±0·160	177·2 89·1
	500	600	−0·236 ±0·090	+6·75 ±11·28	−0·106 ±0·228	187·8 89·1
Sample 3	80	100	−0·203 ±0·017	−3·84 ±1·33	+0·251 ±0·054	272·7 118·5
	100	150	−0·201 ±0·018	−3·47 ±1·28	+0·182 ±0·052	283·7 118·5
	150	200	−0·193 ±0·019	−4·56 ±1·36	+0·094 ±0·042	290·8 118·5
	300	400	−0·196 ±0·029	−4·22 ±2·50	−0·034 ±0·088	302·4 118·5
	500	600	−0·121 ±0·048	−13·83 ±5·94	+0·100 ±0·106	300·6 118·5

* See footnote Table 2.

TABLE 20

Estimates of Regression Coefficients $\beta_{12\cdot34}$, $\beta_{13\cdot24}$ and $\beta_{14\cdot23}$
Limits quoted are 95% confidence limits*

$X_1 = c_{2/4}$ (four hourly mean); X_2 = Barometric Pressure (four hourly mean); $X_3(\xi)$ = Height of Level of Pressure ξ mb; $X_4(\xi)$ = Mean Temperature in interval ξ to ξ' mb.

	ξ mb	ξ' mb.	$b_{12\cdot34}$ (%/mb)	$b_{13\cdot24}$ (%/km)	$b_{14\cdot23}$ (%/°C)	χ^2_s / $\chi^2_{5\%}$	$d_{U5\%}$ / d / $d_{L5\%}$
Sample 1	80	100	−0·140 ±0·044	−4·13 ±3·49	+0·078 ±0·118	108·7 73·0	
	100	150	−0·127 ±0·046	−4·60 ±3·23	+0·085 ±0·101	104·4 73·0	
	150	200	−0·143 ±0·045	−2·20 ±2·40	+0·020 ±0·066	111·5 73·0	
	300	400	−0·129 ±0·060	−3·21 ±4·55	−0·039 ±0·152	107·1 73·0	
	500	600	−0·149 ±0·094	−6·18 ±10·06	−0·092 ±0·192	109·5 73·0	
Sample 2	80	100	−0·076 ±0·034	−7·85 ±3·01	+0·189 ±0·111	223·4 89·1	1·70 1·57 1·53
	100	150	−0·063 ±0·034	−8·62 ±2·93	+0·200 ±0·105	208·3 89·1	1·47 1·53
	150	200	−0·056 ±0·035	−8·89 ±2·88	+0·103 ±0·071	201·5 89·1	1·35 1·53
	300	400	−0·082 ±0·058	−4·78 ±5·65	−0·138 ±0·200	211·2 89·1	1·52 1·53
	500	600	−0·109 ±0·120	+ 0·13 ±15·03	−0·250 ±0·302	228·0 89·1	1·50 1·53
Sample 3	80	100	−0·143 ±0·032	−6·27 ±2·56	+0·271 ±0·101	292·7 118·5	1·51 1·61
	100	150	−0·141 ±0·031	−5·70 ±2·29	+0·201 ±0·093	284·5 118·5	1·47 1·61
	150	200	−0·128 ±0·033	−6·77 ±2·38	+0·115 ±0·074	278·9 118·5	1·37 1·61
	300	400	−0·123 ±0·161	−6·50 ±4·43	−0·032 ±0·153	284·5 118·5	
	500	600	−0·064 ±0·083	−13·84 ±10·35	+0·030 ±0·185	286·2 118·5	
Samples 1, 2, 3	100	150	−0·106 ±0·021	−6·23 ±1·26	+0·170 ±0·055	707·4 260·7	
	150	100	−0·108 ±0·020	−6·39 ±1·19	+0·105 ±0·046	673·6 260·7	
	150	200	−0·104 ±0·021	−5·45 ±1·17	+0·109 ±0·038	652·4 260·7	

* See footnote Table 2.

TABLE 21

Estimates of Regression Coefficients $\beta_{12.34}$, $\beta_{13.24}$ and $\beta_{14.23}$
Limits quoted are 95% confidence limits*

$X_1 = c_{3/32}$ (four hourly mean); X_2 = Barometric Pressure (four hourly mean); $X_3(\xi)$ = Height of Level of Pressure ξ mb.; $X_4(\xi)$ = Mean Temperature in interval ξ to ξ' mb.

	ξ mb.	ξ' mb.	$b_{12.34}$ (%/mb)	$b_{13.24}$ (%/km)	$b_{14.23}$ (%/°C)	χ^2_s / $\chi^2_{5\%}$
Sample 1	80	100	−0·168	−3·43	+0·060	405·1
			±0·034	±2·70	±0·091	73·0
	100	150	−0·162	−3·05	+0·062	415·3
			±0·037	±2·57	±0·081	73·0
	150	200	−0·153	−2·00	+0·061	370·7
			±0·032	±1·75	±0·048	73·0
	300	400	−0·159	−2·37	−0·114	319·3
			±0·042	±3·14	±0·105	73·0
	500	600	−0·184	+1·35	−0·160	336·9
			±0·066	±7·07	±0·135	73·0
Sample 2	80	100	−0·180	−1·65	+0·071	366·2
			±0·017	±1·48	±0·052	89·1
	100	150	−0·176	−1·93	+0·080	347·6
			±0·017	±1·43	±0·050	89·1
	150	200	−0·171	−2·12	+0·061	326·7
			±0·017	±1·41	±0·035	89·1
	300	400	−0·170	−2·74	+0·015	346·6
			±0·029	±2·76	±0·101	89·1
	500	600	−0·140	−6·38	+0·050	338·2
			±0·055	±6·97	±0·144	89·1
Sample 3	80	100	−0·196	−1·53	+0·136	560·2
			±0·019	±1·53	±0·057	112·9
	100	150	−0·193	−1·08	+0·122	547·8
			±0·018	±1·36	±0·053	112·9
	150	200	−0·187	−1·90	+0·073	559·1
			±0·020	±1·56	±0·045	112·9
	300	400	−0·154	−5·89	+0·102	510·1
			±0·029	±2·41	±0·086	112·9
	500	600	−0·112	−11·72	+0·119	570·9
			±0·049	±6·41	±0·109	112·9

* See footnote Table 2.

TABLE 22

Estimates of Regression Coifficients $\beta_{12.34}$, $\beta_{13.24}$ and $\beta_{14.23}$
Limits quoted are 95% confidence limtits*
X_1 = D/4 (four hourly mean); X_2 = Barometric Pressure (four hourly mean);
X_3 (ξ) = Height of Level of Pressure ξ' mb.; X_4 (ξ) = Mean Temperature Inverval ξ to ξ' mb.

	ξ mb.	ξ' mb.	$b_{12.34}$ (%/mb)	$b_{13.24}$ (%/km)	$b_{14.23}$ (%/°C)
Sample 1	80	100	−0·245 ±0·144	−0·31 ±6·31	+0·031 ±0·233
	100	150	−0·228 ±0·074	−4·03 ±6·31	+0·061 ±0·227
	150	200	−0·259 ±0·081	−0·52 ±6·68	−0·067 ±0·166
	300	400	−0·208 ±0·135	−4·60 ±13·35	+0·023 ±0·464
	500	600	−0·321 ±0·265	+9·34 ±33·30	−0·328 ±0·663
Sample 2	80	100	−0·384 ±0·144	+2·23 ±6·31	−0·298 ±0·233
	100	150	−0·399 ±0·074	+2·51 ±6·31	−0·348 ±0·227
	150	200	−0·382 ±0·081	+0·31 ±6·68	−0·134 ±0·166
	300	400	−0·416 ±0·135	+6·76 ±13·35	−0·146 ±0·464
	500	600	−0·508 ±0·265	+19·06 ±33·30	−0·292 ±0·663
Sample 3	80	100	−0·317 ±0·067	+1·56 ±5·41	+0·172 ±0·211
	100	150	−0·317 ±0·068	+1·53 ±4·96	+0·120 ±0·200
	150	200	−0·320 ±0·073	+0·56 ±5·24	+0·054 ±0·161
	300	400	−0·530 ±0·111	+3·75 ±9·41	−0·213 ±0·333
	500	600	−0·291 ±0·180	−4·79 ±22·51	+0·092 ±0·406

* See footnote Table 2.

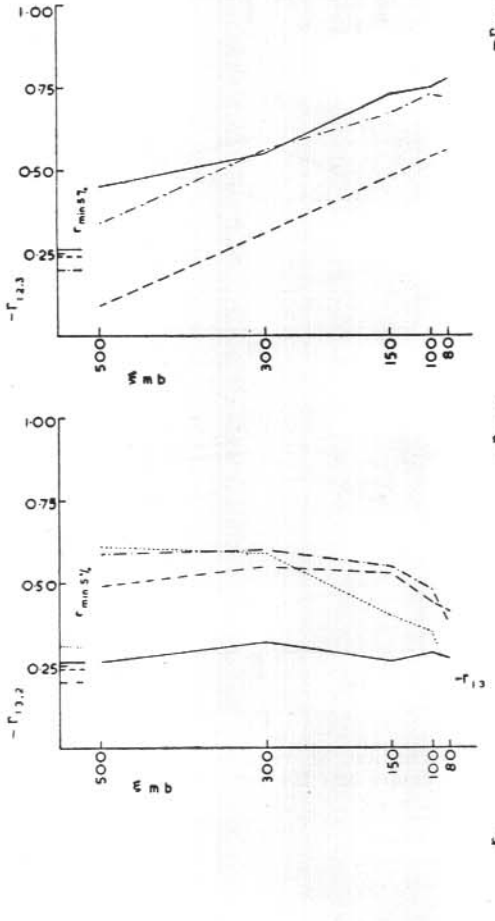

FIG. 16.

Variation of $r_{12.3}$ and $r_{13.2}$ with choice of ξ for the hard component c_2.

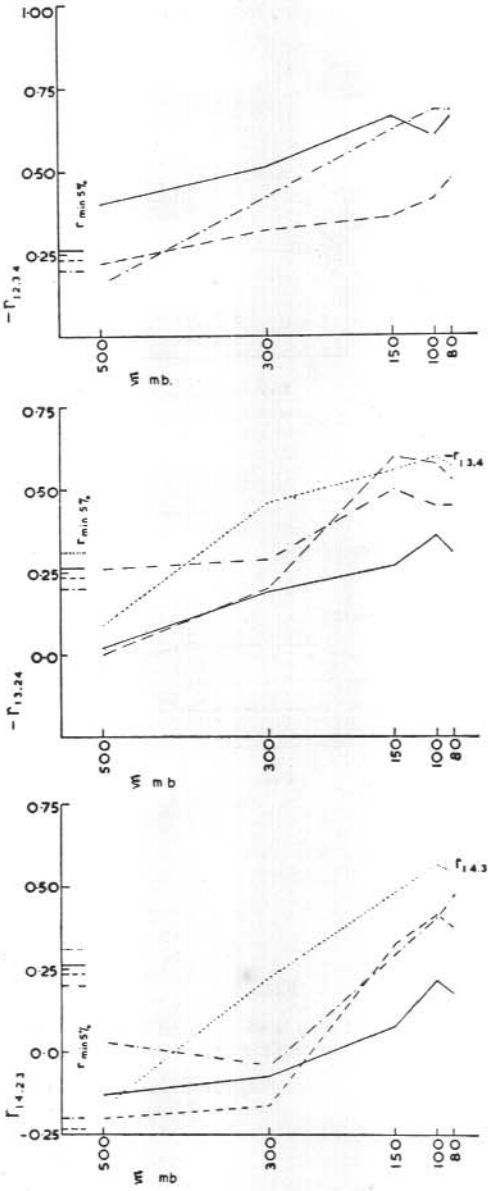

FIG. 17.

Variation of $r_{12.34}$, $r_{13.24}$ and $r_{14.23}$ with choice of ξ for the hard component c_2.

Data from Sample 1 ————————
Sample 2 — — — —
Sample 3 —·—·—·—·
Sample 4 .....

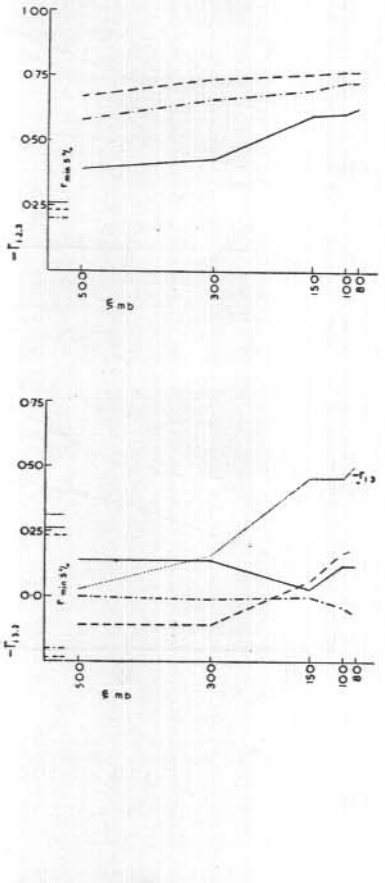

FIG. 18.

Variation of $r_{12.3}$ and $r_{13.2}$ with choice of ξ for the soft component D.

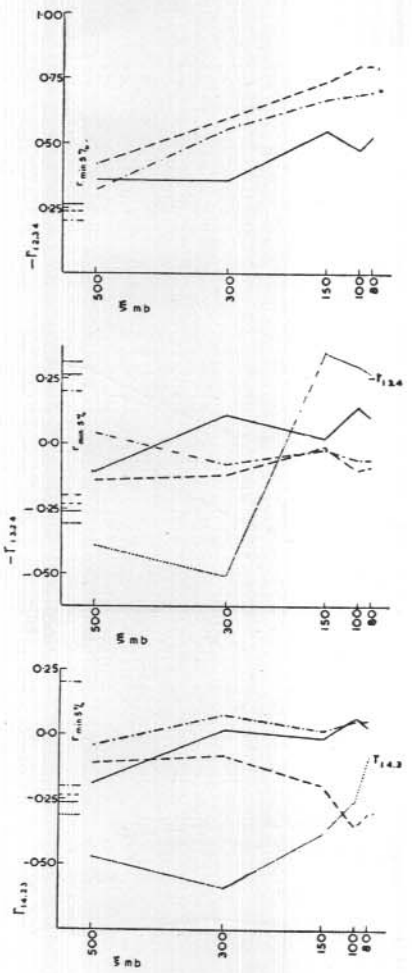

FIG. 19.

Variation of $r_{12.34}$, $r_{13.24}$ and $r_{14.23}$ with choice of ξ for the soft component D.

Data from Sample 1 ————
Sample 2 — — — —
Sample 3 —·—·—·
Sample 4 .....

correlation of the error term). These results are in qualitative agreement with those of Dawton and Elliott (1953) for the soft component measured in a similar manner.

The partial correlation coefficient $r_{1i(j)}$ ($j=2, 3, \ldots . i-1, i+1, \ldots . k$) is the coefficient of correlation between $X_{1(j)}$ (deviation of X_1 from regression on $X_{(j)}$) and $Z_{i(j)}$ (deviation of X_i from regression on $X_{(j)}$). Under certain conditions (Weatherburn, p. 252, 1947), which are probably satisfied approximately in the samples with which we are concerned, this is the coefficient of correlation between X_1 and X_i for any fixed values of the variables $X_{(j)}$.

Using this fact the decrease in numerical value of $r_{13.2}$ for $\xi < 300$ mb. may be explained. Denote

X_1 = hard component intensity
X_2 = barometric pressure
X_3 = height of the level ξ mb.
X_3' = height of the level ξ' mb. ($\xi' > \xi$)
X_4 = mean temperature in the interval $\xi - \xi'$ mb.

It can be shown then that

$$r_{13'.24} = \frac{r_{13'.2} - r_{14.2}\, r_{3'4.2}}{(1-r^2_{14.2})^{\frac{1}{2}}(1-r^2_{3'4.2})^{\frac{1}{2}}}$$

$$r_{13.24} = \frac{r_{13.2} - r_{14.2}\, r_{34.2}}{(1-r^2_{14.2})^{\frac{1}{2}}(1-r^2_{34.2})^{\frac{1}{2}}}$$

Now $r_{13'.24} = r_{13.24}$ since the variations of the heights X_3 and X'_3 are the same if the temperature X_4 between these levels is constant. Then

$$\frac{r_{13'.2}}{(1-r^2_{3'4.2})^{\frac{1}{2}}} - \frac{r_{13.2}}{(1-r^2_{34.2})^{\frac{1}{2}}} = r_{14.2}\left[\frac{r_{3'4.2}}{(1-r^2_{3'4.2})^{\frac{1}{2}}} - \frac{r_{34.2}}{(1-r^2_{34.2})^{\frac{1}{2}}}\right]$$

The values $r_{3'4.2}$ and $r_{34.2}$ which are characteristics of the atmosphere are, for $\xi \leqslant 150$ mb., both negative and $|\, r_{3'4.2}\,| > |\, r_{34.2}\,|$. Also, in the present samples, $r_{14.2}$ is positive. It follows then that $|\, r_{13.2}\,| < |\, r_{13'.2}\,|$. It appears then that the decrease in numerical value of $r_{13.2}$ for $\xi < 300$ mb. is a consequence of the positive value of $r_{14.2}$ (the coefficient of correlation between hard component intensity and temperature in the interval ξ to ξ' mb. at constant barometric pressure). The fact that $r_{12.34}$, $r_{13.24}$ and $r_{14.23}$ have their highest values (numerically) at $\xi = 150$ to 80 mb. (Fig. 17) is consistent with this explanation.

However, these findings, which are similar to those of Duperier (1951), do not justify Duperier's conclusion that the bulk of the μ-mesons are produced in the vicinity of the 100 mb. level and that the temperature in this vicinity has some controlling influence on their intensity.

If the assumption is made that the bulk of the μ-mesons is produced within a small range of atmospheric depth and that the temperature in this

region has a controlling influence on their intensity, then one would expect the value of ξ mb. chosen such that the set of variables X_2, X_3 (ξ), X_4 (ξ) is the best predictor of cosmic ray intensity X_1, to be a good approximation to the mean depth of production. The natural criterion for selection of ξ is that the multiple correlation coefficient $R_{1(234)} = \left(1 - \frac{w}{w_{11}}\right)^{\frac{1}{2}}$ has the greatest value (i.e. the variance of the errors of prediction has a minimum value).[1] Tests of the hypothesis that this greatest value is significantly greater than any or all of the values, corresponding to different selection of ξ, have not been worked out. (A similar problem has been treated by Hotelling, 1940.) However, in the samples here dealt with the variation of $R_{1(234)}$ with choice of ξ is extremely small and is different for each of the four samples (*cf.* Figs. 20 to 23). It appears then extremely unlikely that any one choice of ξ leads to significantly better prediction of X_1 than any other in the range of values of ξ considered.

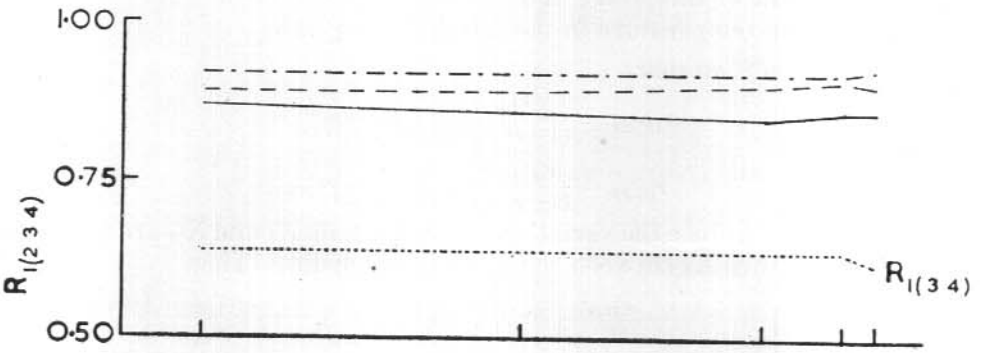

FIG. 20.

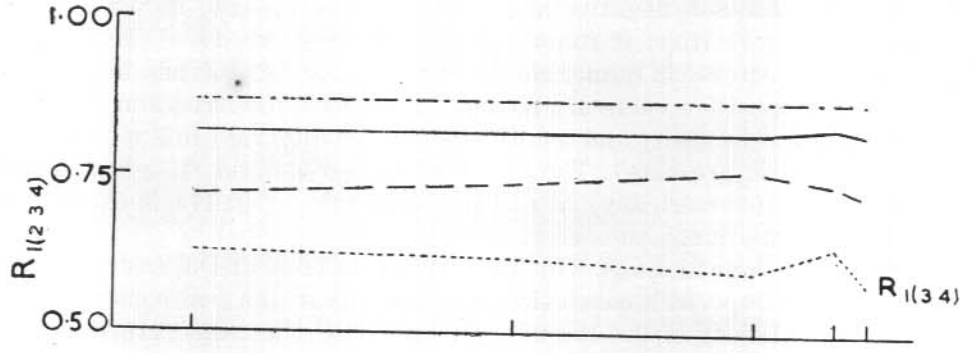

FIG. 21.

1. The criterion implied and used without justification by Duperier (1951) is that the partial correlation coefficient $r_{14.23}$ has the greatest value. The justification of the criterion used in the present case is that it is the "maximum likelihood" criterion.

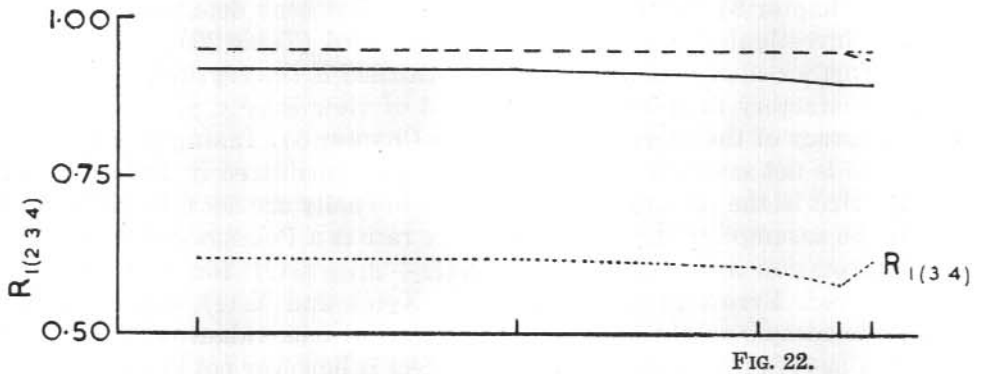

FIG. 22.

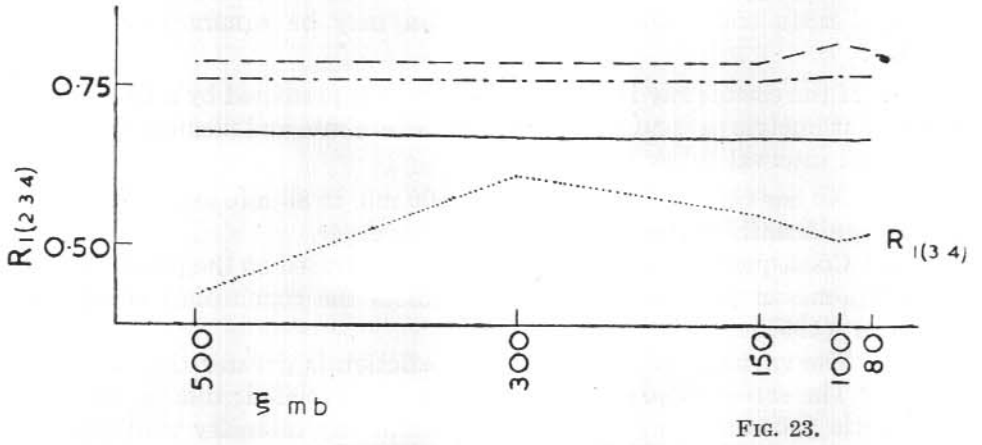

FIG. 23.

FIGS. 20, 21, 22 and 23.

Variation of $R_{1(234)}$ with choice of ξ for c_1 (20), c_2 (21), c_3 (22), D (23).
Data from Sample 1 ————, Sample 2 — — —, Sample 3 — · — · —, Sample 4 .....

It should be noted that the errors in measurement of $X_3(\xi)$ and $X_4(\xi)$ increase as ξ decreases. (Errors in measurement of air temperature due to absorption of solar radiation by the radiosonde are greatest at high altitudes.) This effect will cause the value of $R_{1(234)}$ in the samples to be less than the true value, the effect being more marked for smaller values of ξ. Also, as has been pointed out by Fisher (1948, p. 189), such errors (even if random) in the "independent" variables produce systematic errors in the partial correlation coefficients. This effect may be of some importance in determining the form of variation of the partial correlation coefficients with change of choice of ξ shown in Figs. 16 and 17, and 18 and 19.

If the regression model is to be satisfactory from the physical point of view there should be no evidence of serial correlation in the error term, that is $d > d_U$ (see section on "Effect of non-independence of successive values

of ϵ" in Chapter 3). In the cases for which it has been determined for the samples investigated this condition is not satisfied (Table 20).

A further condition which must be satisfied if the regression model is to be satisfactory from the physical point of view is $\chi_s^2 < \chi_p^2$ (see section on "Accuracy of the regression model" in Chapter 3). Taking $p = 5\%$ this condition is not satisfied in any of the samples considered in Tables 19, 20 and 21; that is, the variations in cosmic ray intensity are not fully accounted for by the assumption that the coincidence rate is a Poisson variate and X_1 has expectation $\alpha + \beta_{12.34}\, x_2 + \beta_{13.24}\, x_3(\xi) + \beta_{14.23}\, x_4(\xi)$ for any value of ξ considered. Errors in measurement of $X_3(\xi)$ and $X_4(\xi)$ will of course make the sample values of χ_s^2 greater than the true values especially for small values of ξ; the magnitude of this effect is however not known.

The main conclusions of this section may be summarized then as follows:

1. If the cosmic ray intensity at sea level is predicted by a linear function of barometric pressure, height of the level ξ mb. and mean temperature in a small interval below ξ mb. then:

(a) No one choice of ξ in the range 500 mb. to 80 mb. makes this function a significantly better predictor than any other.

(b) Consequently no new information is provided on the position of the level of μ-meson production. This contradicts the conclusions reached by Duperier (1951).

(c) The variance of the errors of prediction is greater than expected.

(d) The errors of prediction are serially correlated; that is, there are systematic (non-random) variations in cosmic ray intensity which are not accounted for by such a linear function.

In the absence of a more satisfactory model predicting the variations of sea level cosmic ray intensity, calculations will be made of the regression coefficients $\beta_{12.34}$ (barometer coefficient), $\beta_{13.24}$ (meson decay coefficient) and $\beta_{14.23}$ (Duperier temperature coefficient) of the present regression model from theoretical considerations. In the three sections which follow only the hard component will be considered, comparing the theoretical results with the estimates given in Table 20 with a view to determining which choice of ξ gives the best agreement between theoretical and experimental values of the regression coefficients.

Duperier temperature effect—theoretical treatment. It will be assumed that π-mesons are formed in a small range of atmospheric depth and that these undergo either nuclear capture or decay, giving rise to a μ-meson and a neutrino of zero rest mass at a fixed atmospheric depth x_o gm. cm.$^{-2}$. Several values of x_o will be considered.

In order to calculate the Duperier temperature effect, it is necessary to know the differential momentum spectrum of the π-mesons which decay to μ-mesons. Following the procedure used by Ascoli (1950), let

$U mc^2$ = total energy of a particle
pmc = momentum of a particle

$\overline{U}_\mu$ and $\bar{p}_\mu$ refer to the decay μ-meson in the rest frame of the π-meson
a = cosine of the angle between the π- and μ-meson tracks in the rest frame of the π-meson. This gives

(1) $U^2 = p^2+1$
$\bar{p}_\mu = \frac{1}{2}(m_\pi/m_\mu - m_\mu/m_\pi)$

(1a) $U_\mu = \overline{U}_\mu U_\pi + \bar{p}_\mu p_\pi a$

(1b) $p_\mu \simeq p_\mu \| = \bar{p}_\mu U_\pi a + \overline{U}_\mu p_\pi$

where $p_\mu \|$ is the component of p_μ in the direction of the initial π-meson track. This is, for the momenta dealt with, very close to $| p_\mu |$. From (1a) and (1b) are obtained the lower and upper limits of U_μ and p_μ for given U_π and p_π

(2a) $U_{\mu l} = \overline{U}_\mu U_\pi - \bar{p}_\mu p_\pi$, $U_{\mu h} = \overline{U}_\mu U_\pi + \bar{p}_\mu p_\pi$

(2b) $p_{\mu l} = \overline{U}_\mu p_\pi - \bar{p}_\mu U_\pi$, $p_{\mu h} = \overline{U}_\mu p_\pi + \bar{p}_\mu U_\pi$

and the upper and lower limits of U_π and p_π for given U_μ and p_μ

(3a) $U_{\pi l} = \overline{U}_\mu U_\mu - \bar{p}_\mu p_\mu$, $U_{\pi h} = \overline{U}_\mu U_\mu + \bar{p}_\mu p_\mu$

(3b) $p_{\pi l} = \overline{U}_\mu p_\mu - \bar{p}_\mu U_\mu$, $p_{\pi h} = \overline{U}_\mu p_\mu + \bar{p}_\mu U_\mu$

In the rest frame of the π-meson all directions in space are equally likely for the track of the μ-meson, consequently the probability $F(p_\mu)\, dp_\mu$ of the μ-meson having momentum p_μ in the interval dp_μ is $\frac{1}{2}\, da$; hence

(4) $F(p_\mu)\, dp_\mu = dp_\mu / 2\bar{p}_\mu U_\pi$

If now

$P\, p_\pi)$ = number of π-mesons per unit which decay to μ-mesons, $N_o(p_\mu)$ = number of μ-mesons per unit produced, the units being (unit momentum) sec. sterad cm^2.

(5) $$N_o(p_\mu) = \int_{p_{\pi l}}^{p_{\pi h}} F(p_\mu)\, P(p_\pi)\, dp_\pi = \frac{1}{2\bar{p}_\mu} \int_{p_{\pi l}}^{p_{\pi h}} \frac{P(p_\pi)}{U_\pi}\, dp_\pi$$

$$\frac{dN_o(p_\mu)}{dp_\mu} = \frac{1}{2\,\bar{p}_\mu} \left(\frac{dp_{\pi h}}{dp_\mu} \frac{P(p_{\pi h})}{U_{\pi h}} - \frac{dp_{\pi h}}{dp_\mu} \frac{P(p_{\pi l})}{U_{\pi l}} \right)$$

Using (3b), (1) and (3a) gives

$$\frac{dN_o(p_\mu)}{dp_\mu} = \frac{1}{2\bar{p}_\mu U_\mu} (P(p_{\pi h}) - P(p_{\pi l}))$$

hence if $R(p_\mu) \equiv P(p_{\pi l}) - P(p_{\pi h})$

$$(6) \qquad R(p_\mu) = -2\bar{p}_\mu U_\mu \frac{dN_o(p_\mu)}{dp_\mu}$$

The sequence $p_{\pi 1}, p_{\mu 2}, p_{\pi 3}, p_{\mu 4} \ldots$ is now defined such that $p_{\mu(2n)}$ is the highest value of p_μ for μ-mesons arising from decay of π-mesons with $p_\pi = p_{\pi(2n-1)}$ and $p_{\pi(2n-1)}$ is the highest value of p_π for π-mesons which decay to μ-mesons with $p_\mu = p_{\mu(2n-2)}$. It is clear then that

$$P(p_{\pi 1}) = R(p_{\mu 2}) + P(p_{\pi 3})$$
$$P(p_{\pi 3}) = R(p_{\mu 4}) + P(p_{\pi 5})$$

$$(7) \qquad P(p_{\pi 1}) = R(p_{\mu 2}) + R(p_{\mu 4}) + \ldots\ldots$$

Using (6) and (7) we may now calculate $P(p_\pi)$ for any values of p_π. The series (7) converges rapidly.

Values of $dN_0(p_\mu)/dp_\mu$ were obtained from the curves given in Fig. 13 and the assumption $N_o = k_o p_\mu^{-3}$ for higher values of p_μ. The assumption $N_o = k_o' p_\mu^{-2}$ for large p_μ leads to values of $P(p_\pi)$ which differ insignificantly over the range for which it has been calculated from those obtained using the exponent -3. The calculated spectra, $P(p_\pi)$, are shown in Fig. 24, the several curves having been obtained by assuming decay to occur at x_o = 81·6, 102, 153 and 306 gm. cm.$^{-2}$. For the masses of π- and μ-mesons the values 275 and 215 electron masses were assumed.

From the spectra of Fig. 24 and the assumption $P(p_\pi) = k_\pi p_\pi^{-3}$ for higher values of p_π, the mean values of p_π were calculated. (The assumption $P(p_\pi) = k_\pi p_\pi^{-2}$ leads of course to infinite $\bar{p}_\pi$). This gives $\bar{L} = \tau_\pi c \bar{p}_\pi$ for the mean distance travelled by the π-mesons before decay at the level x_o gm. cm.$^{-2}$. Using $\tau_\pi = 2{\cdot}65 \times 10^{-8}$ sec. the calculated values of $\bar{L}$ for each value of x_o are (within limits of error in calculation) all $2{\cdot}50 \times 10^4$ cm.

Using the mean atmospheric depth—height curve from the Macquarie Island data referred to in an earlier section (Samples 1, 2 and 3) one obtains x_o', the atmospheric depth at height $\bar{L}$ above the point of atmospheric depth x_o. Values of x_o', the mean depth of formation of π-mesons assuming $\pi - \mu$ decay to occur at depth x_o, are given in Table 24. We now define the "mean" density, ρ, of the region x_o' to x_o gm. cm.$^{-2}$ by $\rho = (x_o - x_o')/\bar{L}$ and the "mean" temperature by $T = \dfrac{x_o + x_o'}{2\rho R}$, R being the gas constant (2930 cm. (°K)$^{-1}$). Values of ρ and T are given in Table 24.

The atmosphere is assumed to be of constant density, ρ, between the region of π-meson production and the level at which $\pi - \mu$ decay occurs. The decrease in momentum of the π-mesons within this range is ignored.

Denoting by $\Pi(p_\pi)$ the intensity (number per unit momentum interval. sec. sterad. cm.^{2}) of π-mesons at atmospheric depth x gm. cm.$^{-2}$ and by

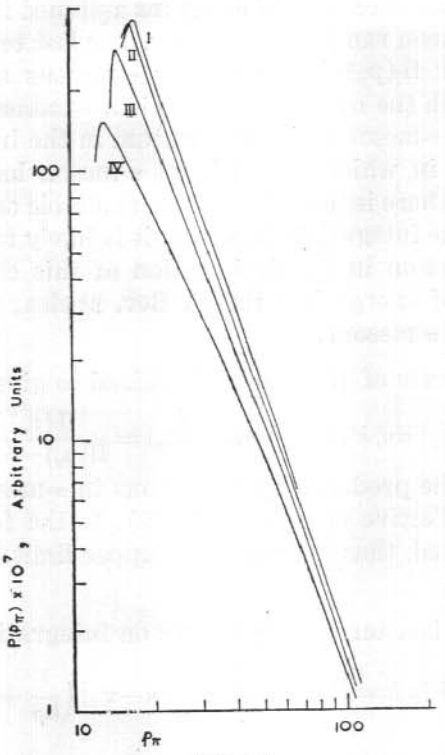

FIG. 24.

Differential momentum spectrum, $P(p_\pi)$, of π-mesons at decay calculated from $P(p_{\pi_1}) = R(p_{\mu_2}) + R(p_{\mu_4}) + \ldots$. and the curves for $N_0(p_0)$ of Fig. 13

TABLE 24

x_0 (gm. cm.$^{-2}$)	x'_0 (gm. cm.$^{-2}$)	ρ (gm. cm.$^{-3}$)	T (°K)
81·6	78·5	$1{\cdot}24 \times 10^{-4}$	220
102	98·1	$1{\cdot}55 \times 10^{-4}$	220
153	147·2	$2{\cdot}32 \times 10^{-4}$	220
306	294·5	$4{\cdot}60 \times 10^{-4}$	223

$\Pi'_0(p_\pi)$ the intensity of π-mesons produced by interactions in which the incident particles are nucleons and nuclei (but not π-mesons) which are assumed to take place at the depth x_0' gm. cm.$^{-2}$, the change in $\Pi(p_\pi)$ in the interval dx is given by

$$(8) \quad d\Pi(p_\pi) = -\Pi(p_\pi)\frac{dx}{L\rho} - \Pi(p_\pi)\frac{dx}{\lambda_\pi} + \phi(p_\pi)\frac{dx}{\lambda_\pi}$$

where $\phi(p_\pi) = \int_{p_\pi}^{\infty} S(p_\pi, p'_\pi)\,\Pi(p'_\pi)\,dp'_\pi$,

λ_π is the collision mean free path of π-mesons assumed independent of p_π, and $\mathrm{L} = \tau_\pi p_\pi c$ is their mean range before decay. The last term of (8) represents the contribution to $\Pi(p_\pi)$ by secondary π-mesons arising from nuclear interactions in which the incident particle is a π-meson. $S(p_\pi, p'_\pi)\,dp_\pi$ is the average number of π-mesons with momentum in the interval dp_π at p_π produced per collision in which the incident π-meson has momentum in the interval dp_π at p'_π. There is insufficient data available on $S(p_\pi, p'_\pi)$ to enable the calculation of the integral ϕ; however, it is likely to be of importance in view of the observation in the first section of this chapter that even for incident π-mesons of energy less than 1 Bev. nuclear interactions may involve the ejection of π-mesons.

The last two terms of (8) can be combined to give

$$-\Pi(p_\pi)\,d\mathrm{x}/\lambda'(p_\pi) \text{ where } \lambda'(p_\pi) = \frac{\Pi(p_\pi)\,\lambda_\pi}{\Pi(p_\pi) - \phi(p_\pi)}$$

Thus the effect of the production of π-mesons in π-meson-nuclear collisions is to increase the effective value of λ_π in (8). In the following calculations this effect is neglected, thus leading to an upper limit to the Duperier temperature coefficient.

Neglecting the last term of (8) gives on integration

$$\Pi(p_\pi) = \Pi'_o(p_\pi)\exp\left\{-(\mathrm{x}-\mathrm{x}'_o)\left(\frac{1}{\mathrm{L}\rho} + \frac{1}{\lambda_\pi}\right)\right\}$$

which leads to

$$\mathrm{P}(p_\pi) = \int_{\mathrm{x}'_o}^{\mathrm{x}} \frac{\Pi(p_\pi)\,d\mathrm{x}}{\mathrm{L}\rho} = \Pi'_o(p_\pi)\,\frac{\lambda_\pi}{\mathrm{L}\rho + \lambda_\pi}\left[1 - \exp\left\{-(\mathrm{x}-\mathrm{x}'_o)\left(\frac{1}{\mathrm{L}\rho} + \frac{1}{\lambda_\pi}\right)\right\}\right]$$

which for large values of $(\mathrm{x} - \mathrm{x}'_o)$ is approximated by

$$(9) \qquad \mathrm{P}(p_\pi) \simeq \Pi'_o(p_\pi)\frac{\lambda_\pi}{\mathrm{L}\rho + \lambda_\pi}$$

$\mathrm{P}(p_\pi)$ being the intensity of π-mesons which undergo decay to μ-mesons. This decay is assumed to occur at the level x_o gm. cm.$^{-2}$ in the following calculations: $(\mathrm{x}_o - \mathrm{x}'_o) = \overline{\mathrm{L}}\rho$ (see above).

The differential Duperier temperature coefficient is now given by

$$(10) \qquad \mathrm{B}_{14.23} = \frac{1}{\mathrm{N}_s}\cdot\frac{\partial \mathrm{N}_s}{\partial \mathrm{T}}$$

Now $\dfrac{\partial \mathrm{N}_s}{\partial \mathrm{T}} = \dfrac{\partial \mathrm{N}_s}{\partial \rho}\cdot\dfrac{\partial \rho}{\partial \mathrm{T}} = -\dfrac{\partial \mathrm{N}_s}{\partial \rho}\cdot\dfrac{\rho}{\mathrm{T}}$

Using (2) from the previous section. "Barometer effect for mesons—theoretical treatment" and (5) and (9) above, gives

$$(11) \qquad \mathrm{B}_{14.23} = \frac{\rho/\mathrm{T}}{2\bar{p}_\mu \mathrm{N}_o}\int_{p_{\pi l}}^{p_{\pi h}} \frac{\mathrm{LP}(p_\pi)}{(\mathrm{L}\rho + \lambda_\pi)\,\mathrm{U}_\pi}\,dp_\pi$$

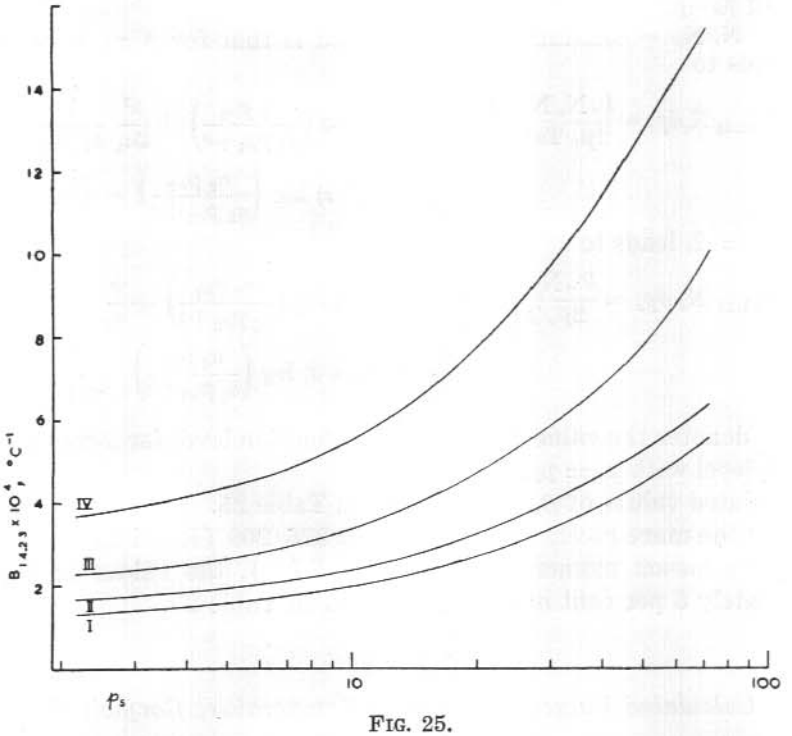

FIG. 25.

Calculated values of differential Duperier temperature effect, $B_{14.23}$ (p_s), assuming $\lambda_\pi = 60$ gm. cm.$^{-2}$ and $P(p_\pi)$ as given in Fig. 24.

Some calculated values of $B_{14.23}$ are shown in Fig. 25. These were obtained using N_o as given in Fig. 13; $P(p_\pi)$ as given in Fig 24; ρ and T as given in Table 25,

$\tau_\pi = 2{\cdot}65 \times 10^{-8}$sec (Rossi, 1952, p. 528)
$\lambda_\pi = 60$ gm. cm.$^{-2}$.

The integral Duperier temperature coefficient is given by

$$\beta_{14.23} = 100 \int_{p_1}^{\infty} B_{14.23} N_s \, dp_s / \int_{p_1}^{\infty} N_s \, dp_s$$

Integration over the range of p_s from p_1 to p_2 was carried out graphically. For $p_s > p_2$ (for which p_π is large) we have $p_\pi \simeq U_\pi$, hence

$$p_{\pi l} \simeq \alpha_1 p_\mu, \quad p_{\pi h} \simeq \alpha_2 p_\mu$$

where $\alpha_1 = (\overline{U}_\mu - \bar{p}_\mu)$, $\alpha_2 = (\overline{U}_\mu + \bar{p}_\mu)$

Assuming $P(p_\pi) = k_\pi p^{-\gamma}$ from (11) is obtained

$$B_{14.23} = \frac{k_\pi}{2\bar{p}_\mu N_o T} \int_{\alpha_1 p_\mu}^{\alpha_2 p_\mu} \frac{dp_\pi}{p_\pi^\gamma (p_\pi + s)}$$

where $s = \lambda_\pi / \tau_\pi c p$.

Assuming $p_\mu - p_s =$ constant

$N_s/N_o =$ constant; the value used is that for $p_s = p_2$ which, for $\gamma = 3$, leads to

$$\int_{p_2}^{\infty} B_{14.23} N_s dp_s = \frac{k_\pi N_s/N_o}{2\bar{p}_\mu T s^3}\left[\frac{1}{a_1}(a_1 p_{\mu_2}+s)\log\left(\frac{a_1 p_{\mu_2}}{a_1 p_{\mu_2}+s}\right)+\frac{s^2}{2a_1}\frac{1}{a_1 p_{\mu_2}}+\frac{s}{a_1}\right.$$
$$\left.-\frac{1}{a_2}(a_2 p_{\mu_2}+s)\log\left(\frac{a_2 p_{\mu_2}}{a_2 p_{\mu_2}+s}\right)-\frac{s^2}{2a_2}\frac{1}{a_2 p_{\mu_2}}-\frac{s}{a_2}\right]$$

and, for $\gamma = 2$, leads to

$$\int_{p_2}^{\infty} B_{14.23} N_s dp_s = \frac{k'_\pi N_s/N_o}{2\bar{p}_\mu T s^2}\left[\frac{1}{a_2}(a_2 p_{\mu_2}+s)\log\left(\frac{a_2 p_{\mu_2}}{a_2 p_{\mu_2}+s}\right)+\frac{s}{a_2}\right.$$
$$\left.-\frac{1}{a_1}(a_1 p_{\mu_2}+s)\log\left(\frac{a_1 p_{\mu_2}}{a_1 p_{\mu_2}+s}\right)-\frac{s}{a_1}\right]$$

where p_{μ_2} denotes the value of p_μ at the production level for μ-mesons which reach sea level with $p_s = p_2$.

Calculated values of $\beta_{14.23}$ are given in Table 25.

Using the more recent value $m_\pi/m_\mu = 276/209$ (Rossi 1952, p. 528) to derive the π-meson momentum spectrum, $P(p_\pi)$, the values of $\beta_{14.23}$ are approximately 6 per cent higher than given in Table 25.

TABLE 25

Calculated Values of Duperier Temperature Coefficient

$\beta_{14.23}$ in % per °C.

$\tau_\pi = 2{\cdot}65 \times 10^{-8}$ sec., $m_\pi/m_\mu = 275/215$

x_0 (gm. cm.$^{-2}$)	λ_π (gm. cm.$^{-2}$)	$\beta_{14.23}$ ($\gamma = 2$)	$\beta_{14.23}$ ($\gamma = 3$)
81·6	60	0·043	0·034
81·6	130		0·017
102	60	0·051	0·041
102	130	0·033	0·021
153	60	0·070	0·057
153	130		0·029
306	60	0·106	0·091
306	130		0·050

Duperier temperature effect—discussion. In Fig. 26 is shown the estimates and 95 per cent confidence intervals of $\beta_{14.23}$ (ξ) for the hard component (*cf.* Table 20) from Samples 1, 2 and 3 for the several values of ξ. The smooth curves are drawn through the theoretical values of $\beta_{14.23}$ (x_o) for $\lambda_\pi = 60$ gm. cm.$^{-2}$ (*cf.* Table 20). It is clear that the theoretical values and sample estimates are in fair agreement only if we take $x_o = 153$ gm. cm.$^{-2}$. Combining Samples 1, 2 and 3 gives for the estimate and 95 per cent

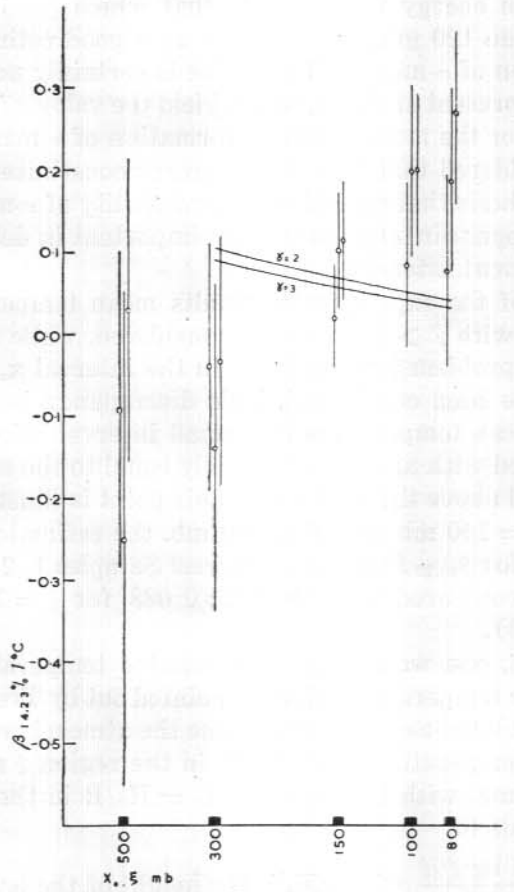

FIG. 26

Variation with choice of ξ of experimental estimates and 95 per cent confidence limits (from Samples 1, 2, 3) of Duperier temperature effect $\beta_{14.23}(\xi)$ and theoretical values $\beta_{14.23}(x_o)$ as a function of the assumed height of production of μ-mesons—smooth curves.

confidence limits of $\beta_{14.23}$ the value 0·109 ± 0·038 per cent °C. for $\xi = 150$ mb. From the trend of the experimental points one would expect better agreement for somewhat higher values of x_o, about $x_o = 170$ gm. cm.$^{-2}$, which leads to $x_o' \simeq 160$ gm. cm.$^{-2}$ for the mean depth of formation of the π-mesons.

From Fig. 26 and Table 25 it can be seen that if the theoretical and experimental values should agree for some value of x_o this value of x_o is greater if $\gamma = 3$ than if $\gamma = 2$ though the difference is not large; also it is greater the greater the appropriate value of λ_π.

Measurements of absorption thickness for shower producing radiation lead to values of about 120 gm. cm.$^{-2}$ (Rossi, 1952, p. 443). Since this radia-

tion (mainly high energy nucleons) is that which produces most of the π-mesons, the value 120 gm. cm.$^{-2}$ serves as a good estimate of the mean depth of formation of π-mesons. This value is certainly not consistent with the results of the present analysis, which yield the value $x_o' = 160$ gm. cm.$^{-2}$ as a lower limit for the mean depth of formation of π-mesons in the atmosphere. It is considered that this disagreement constitutes strong evidence against the hypothesis that variations in probability of π-meson capture due to variations in upper air temperature are important in determining the sea level hard component intensity.

In analysis of the experimental results mean temperatures in an interval ξ to ξ' mb. with $\xi' > \xi$ have been considered, while in the theoretical treatment of the problem temperatures in the interval x_o to x_o' gm. cm.$^{-2}$ with $x_o' < x_o$ have been considered. This discrepancy is however not important, as the mean temperature in a small interval below the level ξ mb. is highly correlated with and approximately equal to the mean temperature in a small interval above the level ξ mb. This point is illustrated by the fact that on taking $\xi = 150$ mb. and $\xi' = 100$ mb. the estimate and 95 per cent confidence limits for $\beta_{14.23}$ from the combined Samples 1, 2 and 3 is $0{\cdot}105 \pm 0{\cdot}046$ %/°C. as compared with $0{\cdot}109 \pm 0{\cdot}038$ for $\xi = 150$ mb. and $\xi' = 200$ mb. (Table 20).

If $\xi' > x_o > \xi$, one would expect a positive temperature effect apart from the Duperier temperature effect as pointed out by Trefall (1953). This effect may be calculated as follows: Assume the atmosphere to be static and isothermal with temperature $T_1 = H_1/R$ in the region ξ mb. to ξ' mb. and static and isothermal with temperature $T_2 = H_2/R$ in the region ξ' mb. to sea level. This leads to

$$(1)\quad H_2 = \frac{X_3 - H \log \xi'/\xi}{\log x_s/\xi'} \quad \text{where } X_3 \text{ is the height of the level } \xi \text{ mb.}$$

Now from (2) from the previous section, "Barometer effects for mesons—theoretical treatment"

$$(2)\quad N_s = N_o \exp\left(-\frac{H_1}{\tau c}\int_{x_o}^{\xi'} \frac{dx}{xp} - \frac{H_2}{\tau c}\int_{\xi'}^{x_s} \frac{dx}{xp}\right)\frac{dp_o}{dp_s}$$

Trefall's temperature effect (which he denotes $c_2 + c_3$) is now given by

$$B'_{14.23} = \frac{dN_s}{dT_1}/N_s = \frac{dN_s}{dH_1}\frac{dH_1}{dT_1}/N_s$$

From (1) and (2) with X_3 and x_s constant this leads to

$$B'_{14.23} = \frac{R}{\tau c}\left(\log\frac{\xi'}{\xi}/\log\frac{x_s}{\xi'}\int_{\xi'}^{x_s}\frac{dx}{xp} - \int_{x_o}^{\xi'}\frac{dx}{xp}\right)$$

Evaluation of integrals of the type occurring in this expression was discussed in the previous section referred to above.

The integral temperature coefficient is now given by

$$\beta'_{14.23} = 100 \int_{p_1}^{\infty} B'_{14.23} N_s \, dp_s / \int_{p_1}^{\infty} N_s \, dp_s$$

Evaluation of integrals of the type occurring in this expression is discussed in the next section. Using $\xi = 100$ mb. (102 gm. cm.$^{-2}$), $\xi' = 150$ mb. (153 gm. cm.$^{-2}$) and following Trefall, $x_0 = 120$ gm. cm.$^{-2}$ and assuming $N_s = k_s p_s^{-\gamma}$ for large p_s gives

$$\beta'_{14.23} = 0.040\% \text{ per } ^\circ\text{C for } \gamma = 2$$
$$\beta'_{14.23} = 0.044\% \text{ per } ^\circ\text{C for } \gamma = 3$$

From the smooth curves of Fig. 25 we have for $\lambda_\pi = 60$ gm. cm.$^{-2}$, $x_0 = 120$ gm. cm.$^{-2}$.

$$\beta_{14.23} = 0{\cdot}058 \ \% \text{ per } ^\circ\text{C. for } \gamma = 2$$
$$\beta_{14.23} = 0{\cdot}047 \ \% \text{ per } ^\circ\text{C. for } \gamma = 3$$

For the total temperature coefficient $\beta^\circ_{14.23} = \beta_{14.23} + \beta'_{14.23}$ is obtained

$$\beta^\circ_{14.23} = 0{\cdot}098 \ \% \text{ per } ^\circ\text{C. for } \gamma = 2$$
$$\beta^\circ_{14.23} = 0{\cdot}091 \ \% \text{ per } ^\circ\text{C. for } \gamma = 3$$

which should be compared with the estimate

$b_{14.23} = 0{\cdot}170 \pm 0{\cdot}055$ % per °C derived from the combined Samples 1, 2 and 3 for $\xi = 100$ mb., $\xi' = 150$ mb. and $X_1 = c_2$ (Table 20).

The theoretical values are much too low.

Taking $\xi = 150$ mb. (153 gm. cm.$^{-2}$), $x_0 = 170$ gm. cm.$^{-2}$ and $\xi' = 200$ mb. (204 gm. cm.$^{-2}$) gives

$$\beta^\circ_{14.23} = \beta_{14.23} + \beta'_{14.23} = 0{\cdot}105 \ \% \text{ per } ^\circ\text{C. for } \gamma = 2$$
$$= 0{\cdot}094 \ \% \text{ per } ^\circ\text{C. for } \gamma = 3$$

which should be compared with the estimate

$$b_{14.23} = 0{\cdot}109 \pm 0{\cdot}038 \ \% \text{ per } ^\circ\text{C.}$$

obtained from the combined Samples 1, 2 and 3 with $\xi = 150$ mb., $\xi' = 200$ mb. (Table 20).

The agreement here is good. However, we have still neglected the effects of the last term of (8) from the last section, "Duperier temperature effect—theoretical treatment".

Before concluding this discussion of the positive temperature effect for the hard component the following criticism of Duperier (1951) should be made:

Duperier finds that on taking $\xi = 50$ mb., $\xi' = 200$ mb., the experimental value for the positive temperature coefficient is roughly twice that obtained on taking $\xi = 100$ mb, $\xi' = 200$ mb. From this he concludes that the layer 50 to 100 mb. is as effective (in meson production) as the layer 100 to 200 mb. No justification is offered. However, it may be that the expected value of the hard component intensity is given accurately as a function of one particular set of variables, the value of which is approximated

by different linear functions of the two sets of variables considered by Duperier. As an example of this type of relationship consider the following: The average number N, of words per page of books in a library might be given more or less accurately by the expression $N = \alpha A$ where A is the area of the front cover. The number N could also be given (probably less accurately) by the expression $N = \beta H$ or $N = \beta' W$ where H and W are the height and width of the front cover. We would then find that $\beta'/\beta \simeq 2$. This does not imply that the width is more "effective" than the height in determining the number of words per page. It is merely a consequence of the fact that $H/W \simeq 2$ for most books.

In view of the earlier discussion of this section it does appear likely that the fact that significant values are obtained for the upper air temperature effects may be due to these temperatures being indicators of some other factor which has a controlling influence on the cosmic ray intensity at sea level.

For the purpose of comparing estimates of $\beta_{14.23}$ in the present case with those of other workers some values are summarized in Table 26.

TABLE 26

Estimates of $\beta_{14.23}$ in %/°C. for the Hard Component from Different Measurements

Source	Lead Absorber	Telescope Aperture	ξ (mb)	ξ' (mb)	$b_{14.23}$ %/°C
Dawton, Elliott (1953)	10cm.	58° × 58°	100	100	0·056
Duperier (1951)	40cm.	36° × 71°	100	200	0·075
,, ,,	25cm.	23° × 59°	100	200	0·124
Table 20 (Samples 1, 2, 3)	10cm.	33° × 33°	100	150	0·170

Since $B_{14.23}$ (p_s) is small for small p_s and increases rapidly with increase in p_s one would not expect $b_{14.23}$ to vary greatly with lead absorber thickness in the range 10 to 40 cm. Also because of the high correlation which exists between values of temperature in neighbouring layers in the atmosphere one would not expect $b_{14.23}$ to vary greatly with ξ'. Table 26 then demonstrates an increase in positive temperature coefficient with decrease in telescope aperture. This can be explained as follows: The formation of π-mesons occurs after the primary particles have traversed a certain thickness of air; this occurs at greater heights (lower densities) for inclined than for vertical directions of arrival. Since $B_{14.23}$ is roughly proportional to air density for particles of moderate momenta, the temperature coefficient would be expected to decrease with increase in zenith angle (or telescope aperture).

For the total intensity Dawton and Elliott obtain the value (0·054 ± 0·011 (s.e.)) %/°C. for $\xi = \xi' = 100$ mb., as estimate of $\beta_{14.23}$. This is somewhat less than the values found in the present case for the total intensity as measured by c_3 using $\xi = 100$ mb., $\xi' = 150$ mb. (see Table 21). However, the difference may not be statistically significant.

For the soft component Dawton and Elliott obtain the non-significant value (0·021 ± 0·020 (s.e.)) %/°C. for $\xi = \xi' = 100$ mb., as estimate of $\beta_{14.23}$. In the present case for the soft component as measured by D and taking $\xi = 100$ mb., $\xi' = 150$ mb. the estimates of $\beta_{14.23}$ are positive but not significant at the 5% level in the case of Samples 1 and 3 while in the case of Sample 2 the estimate is negative and (according to standard tests which ignore the possible serial correlation of the error term) significant (see Table 22).

μ-meson decay effect (barometric pressure constant). The differential μ-meson decay effect is given by

$$B_{13.24} \equiv \frac{1}{N_s}\left(\frac{\partial N_s}{\partial S_s}\right) x_s = \text{const.}$$

From (1) and (2) in the previous section, "Barometer effect for mesons—theoretical treatment", is obtained

$$B_{13.24} = -\frac{1}{\tau_\mu c \log x_s/x_o}\int_{x_o}^{x_s}\frac{dx}{x p_\mu}$$

Using values of the integral calculated in the section referred to above and 2.15×10^{-6} sec., $x_s = 1026$ gm. cm.$^{-2}$ the results shown in Fig 27 were obtained for $B_{13.24}$

The integral coefficient is given by

$$\beta_{13.24} = 100\int_{p_1}^{\infty} B_{13.24}\, N_s\, dp_s \Big/ \int_{p_1}^{\infty} N_s\, dp_s$$

Integration over the range of p_s from p_1 to p_2 was carried out graphically.

To calculate $\int_{p_2}^{\infty} B_{13.24}\, N_s dp_s$ the approximation $p_\mu(x) = p_s + \delta$ is made where $2\delta = (p_o)_2 - p_2$ for $p_s > p_2$. This leads to $\int_{x_o}^{x_s}\frac{dx}{x p_\mu} = \frac{1}{p_s+\delta}\log\frac{x_s}{x_o}$.

Hence $\int_{p_2}^{\infty} B_{13.24}\, N_s\, dp_s = \frac{-1}{\tau_\mu c}\int_{p_2}^{\infty}\frac{N_s}{p_s+\delta}\, dp_s$.

Assuming $N_s = k_s p_s^{-3}$ for $p_s > p_2$ gives

$$\int_{p_2}^{\infty} B_{13.24}\, N_s\, dp_s = \frac{k_s}{\tau_\mu c}\left(\frac{1}{\delta^3}\log\frac{p_2}{p_2+\delta} + \frac{1}{\delta^2}\, p_2^{-1} - \frac{1}{2\delta}\, p_2^{-2}\right)$$

and assuming $N_s = k'_s p_s^{-2}$ gives

$$\int_{p_2}^{\infty} B_{13.24}\, N_s\, dp_s = \frac{k'_s}{\tau_\mu c}\left(\frac{1}{\delta^2}\log\frac{p_2+\delta}{p_2} - \frac{1}{\delta}\, p_2^{-1}\right).$$

The calculated values of $\beta_{13.24}$ are given in Table 27.

TABLE 27

Calculated values of $\beta_{13.24}$ in % per km.

x_0 gm. cm.$^{-2}$	$\beta_{13\cdot24}$ ($\gamma = 2$)	$\beta_{13\cdot24}$ ($\gamma = 3$)
81·6	−5·22	−5·59
102	−5·43	−5·81
153	−5·62	−6·03
306	−6·41	−6·88
510	−7·61	−8·17

To facilitate comparison of the theoretical values (Table 27) and sample estimates (Table 20) of $\beta_{13.24}$ these are shown graphically in Fig. 28. It will be seen that for any choice of x_0 in the range considered the agreement is satisfactory for either $\gamma = 2$ or $\gamma = 3$.

The sample estimates are in satisfactory agreement with that of Duperier (1951), $(-3\cdot48 \pm 0\cdot45$ (s.e.)) %/km. for $\xi = 100$ mb., $\xi' = 200$ mb.,

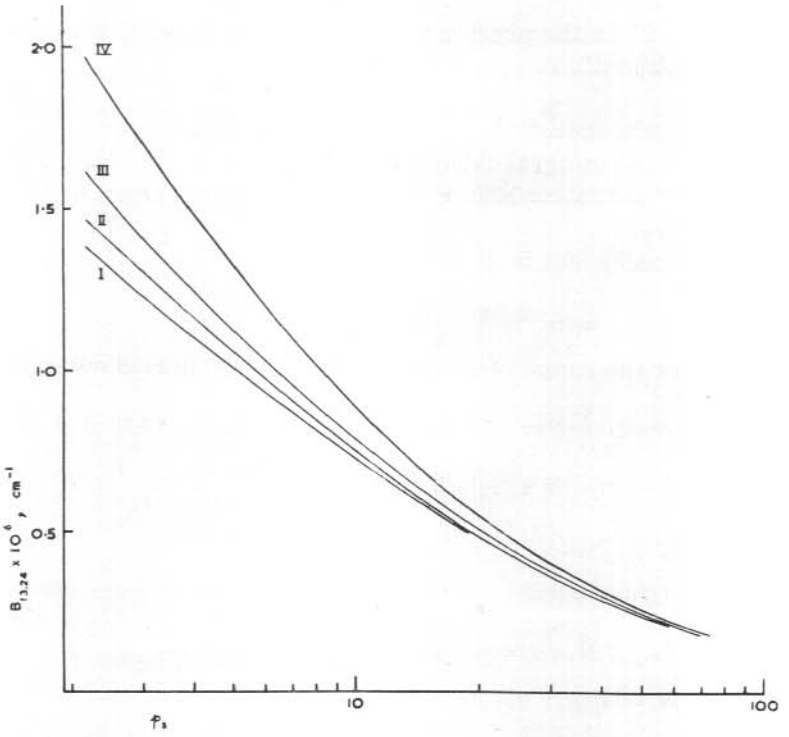

FIG. 27.

Differential μ-meson decay coefficient, $B_{13.24}$ (p_z), assuming μ-meson production to occur at 80 mb.—curve I; 100 mb.—curve II; 150 mb.—curve III; 300 mb.—curve IV.

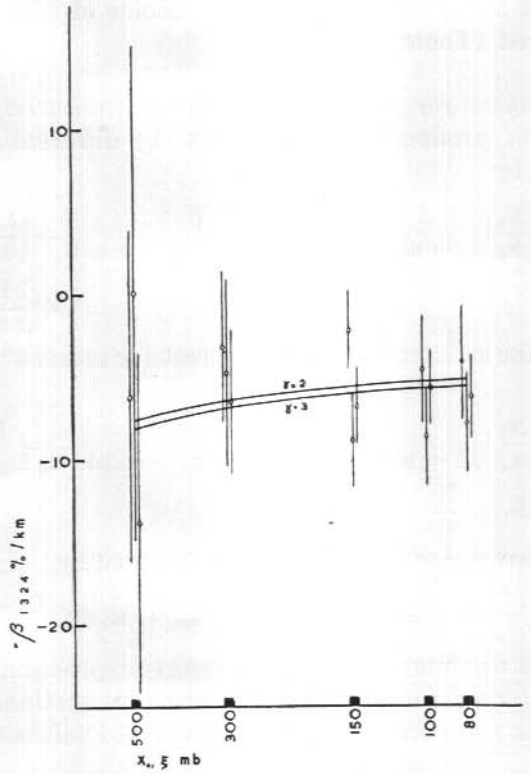

FIG. 28.

Variation with choice of ξ of experimental estimates and 95 per cent confidence limits (from Samples 1, 2, 3) of μ-meson decay effect, $\beta_{13.24}(\xi)$, and smooth curves showing theoretical values, $\beta_{13.24}(x_0)$, as a function of the assumed height of production of μ-mesons

when one considers the greater thickness of lead absorber used by Duperier (40 cm. as against 10 cm. in the present case). They are also in satisfactory agreement with the value $(-4{\cdot}00 \pm 0{\cdot}43$ (s.e.)) %/km. for $\xi = \xi' = 100$ mb. obtained by Dawton and Elliot (1953) using 10 cm. of lead.

For the total intensity Dawton and Elliot (1953) obtained the value $(-3{\cdot}02 \pm 0{\cdot}49$ (s.e.)) %/km. for $\xi = \xi' = 100$ mb. as estimate of $\beta_{13.24}$. This is consistent with the values obtained in the present case using $\xi = 100$ mb. $\xi' = 150$ mb. for the total intensity as measured by c_1 or c_3 (Tables 19 and 21). It will be noticed that the estimates for c_1 are greater (numerically) than for c_3; this difference may not be significant however.

For the soft component intensity Dawton and Elliott (1953) obtain $(-1{\cdot}05 + 0{\cdot}43$ (s.e.)) %/km. for $\xi = \xi' = 100$ mb. as estimate of $\beta_{13.24}$. In the present case the estimates of $\beta_{13.24}$ for the soft component, D, are not

significant at the 5 per cent level for any choice of ξ in any of the three samples considered (Table 22).

Barometer effect for μ-mesons (height of production constant). For constant height of production of μ-mesons the differential barometer coefficient is given by

$$B_{12.34} = \frac{1}{N_s}\left(\frac{\partial N_s}{\partial x_s}\right)_{s_s = \text{const.}} = \frac{1}{N_s}\left[\left(\frac{\partial N_s}{\partial x_s}\right)_{H = \text{const.}} + \left(\frac{\partial N_s}{\partial H}\right)_{x_s = \text{const.}} \times \left(\frac{\partial H}{\partial x_s}\right)_{s_s = \text{const.}}\right]$$

Using (1) from the section, "Barometer effect for mesons—theoretical treatment" leads to

$$B_{12.34} = \frac{1}{N_s}\left(\frac{\partial N_s}{\partial x_s}\right)_{H = \text{const.}} - \frac{1}{N_s}\left(\frac{\partial N_s}{\partial H}\right)_{x_s = \text{const.}} \cdot \frac{H}{x_s \log x_s/x_o}$$

$$B_{12.34} = B_{12} - B_{13.24}\frac{H}{x_s}$$

The integral barometer coefficient, $\beta_{12.34}$ is given by

$$\beta_{12.34} = 100 \int_{p_1}^{\infty} B_{12.34}\, N_s\, dp_s \Big/ \int_{p_1}^{\infty} N_s\, dp_s .$$

The calculation of the integrals involved in this expression has been treated in the section referred to above and the previous section, "μ-meson decay effect (barometric pressure constant)". Calculated values of $\beta_{12.34}$ are given in Table 28.

TABLE 28

Calculated Values of $\beta_{12.34}$ in % per mb.

x_0 gm. cm.$^{-2}$	$\beta_{12.34}$ ($\gamma = 2$)	$\beta_{12.34}$ ($\gamma = 3$)
81·6	−0·201	−0·217
153	−0·204	−0·221

To facilitate comparison of the theoretical values (Table 28) and sample estimates (Table 20) of $\beta_{12.34}$ these are shown graphically in Fig. 29. The theoretical values are much too high (numerically) for any choice of $x_o \geqslant 81{\cdot}6$ gm. cm.$^{-2}$ (80 mb.). This may be due to the assumption that the atmosphere is static and isothermal, to errors in N_o (p_o) (which was derived by using this assumption) or to weakness of the assumption that all μ-mesons are formed at a definite level x_o gm. cm.$^{-2}$ in the atmosphere.

The sample estimates (Table 20) of $\beta_{12.34}$ are in satisfactory agreement with the value ($-0{\cdot}091 \pm 0{\cdot}004$ (s.e.)) %/mb. for $\xi = 100$ mb., $\xi' = 200$ mb. obtained by Duperier (1951) when one considers the higher momentum

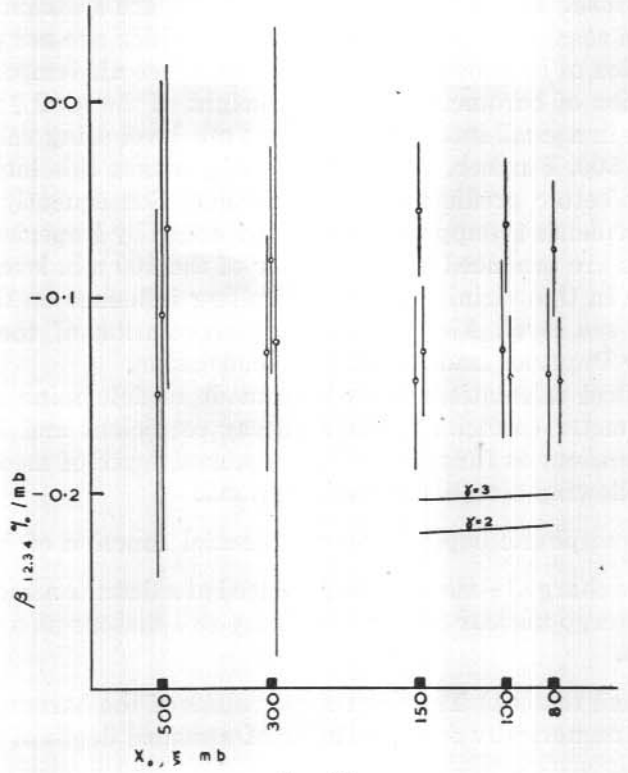

FIG. 29.

Variation with choice of ξ of experimental estimates and 95 per cent confidence limits (from Samples 1, 2, 3) of barometer effect, $\beta_{12.34}(\xi)$, for μ-mesons and smooth curves showing theoretical values $\beta_{12.34}(x_0)$, as a function of the assumed height of production of μ-mesons.

of the particles recorded in his case. They are also in good agreement with that of Dawton and Elliott (1953), $(-0{\cdot}125 \pm 0{\cdot}012$ (s.e.)) %/mb. for $\xi = \xi' = 100$ mb., obtained using the same absorber thickness as in the present case.

For the total intensity Dawton and Elliott obtain the value $(-0{\cdot}187 \pm 0{\cdot}014$ (s.e.)) %/mb. for $\xi = \xi' = 100$ mb. as estimate of $\beta_{12.34}$. This is in good agreement with the values obtained in the present case for $\xi = 100$ mb., $\xi' = 150$ mb. using c_1 or c_3 as measures of the total intensity (Tables 19 and 21).

For the soft component Dawton and Elliot obtain the estimate $(-0{\cdot}353 \pm 0{\cdot}017$ (s.e.)) %/mb. for $\xi = \xi' = 100$ mb. This is in good agreement with the estimates obtained in the present case for the soft component, D, using $\xi = 100$ mb., $\xi' = 150$ mb. (Table 22).

Conclusions. It has been shown that there are systematic day to day variations in cosmic ray intensity at sea level which are not predicted by a linear function of barometric pressure and surface air temperature or by a linear function of barometric pressure, height of the level ξ mb. and mean temperature in a small interval below the ξ mb. level using values of ξ in the range 80 to 500. Further, no one choice of ξ makes this latter function a significantly better predictor than any other. Consequently these results provide no evidence to support the view, advanced by Duperier (1951), that the μ-mesons are produced in the vicinity of the 100 mb. level and that the temperature in this vicinity has a controlling influence on the cosmic ray intensity at sea level. Also, a proper interpretation of the observations presented by Duperier leads to the same conclusion.

Theoretical calculations have been made to determine the hard component barometer coefficients, meson decay coefficient and Duperier temperature coefficient as functions of the assumed depth of meson production using the following simplifying assumptions:

(1) Atmospheric depth is an exponential function of height.

(2) The charged π-mesons are produced at a definite atmospheric depth and then undergo nuclear collision or decay to μ-mesons at a definite atmospheric depth.

It is found that (a) The theoretical values of the barometer coefficient are too high numerically for any choice of assumed depth of production of μ-mesons.

(b) The theoretical and experimental values of meson decay coefficient are in satisfactory agreement for any choice of assumed depth of production of μ-mesons.

(c) Assuming the geometrical value for the collison mean free path of π-mesons and neglecting the effect of production of π-mesons in π-nuclear interactions, the value 160 gm. cm.$^{-2}$ is obtained as a lower limit to the choice of assumed depth of production of π-mesons, which gives agreement between the theoretical and experimental values for the Duperier temperature effect. This value is much greater than the mean depth of production of π-mesons as indicated by the absorption length (120 gm. cm.$^{-2}$) for high energy nucleons in the upper atmosphere. The value 120 gm. cm.$^{-2}$ leads to theoretical values of the positive temperature effect which are too low even after allowing for an additional effect described by Trefall (1953).

It must be concluded, then, that the significant values obtained for the Duperier temperature effect cannot be ascribed entirely to the effects on the cosmic ray intensity of variations in probability of π-meson capture asso-

ciated with variations in temperature of the upper atmosphere. It is suggested that this temperature may be a (more or less poor) indicator of some other factor which has a controlling influence on the sea level cosmic ray intensity (see also the appendix to this chapter).

Using assumption (2) above, a qualitative explanation can be given of the dependence of Duperier temperature effect on counter telescope aperture.

In calculating barometer coefficients, meson decay coefficient and Duperier temperature coefficient, the μ-meson momentum spectrum was assumed to be of the form $p^{-\gamma}$ for large values of p. The values $\gamma = 2$ and $\gamma = 3$ were considered. No evidence has been found to favour either value of γ.

The fact that significant values have been obtained in some cases for the coefficients in the regression equations describing the variations of the soft component may be ascribed to the fact that the soft component consists in part of low energy μ-mesons and electrons which are secondary to the μ-mesons—decay products and knock-on products. It is considered that a quantitative treatment of the soft component behaviour must await a satisfactory treatment of the hard component.

It is considered that further studies along the lines of the present work are likely to be fruitless and that the approximations involved in assumptions (1) and (2) above should be avoided in any future work. Using the actual temperature-pressure curve obtained from radiosonde measurements and a particular μ-meson production spectrum (for example, that suggested by Sands, 1950), it is straight-forward, although laborious, to calculate the expected hard component intensity. The predicted values could be compared with observed values obtained with a high counting rate narrow-angle telescope and the errors of prediction tested for evidence of serial correlation. If the errors were serially correlated, it may then be possible (after smoothing the errors) to discern a similarity of variation of the errors with some other physical quantity, the effects of which could then be allowed for. This may of course involve a modification of the proposed μ-meson production spectrum. However, the possibility should not be overlooked that there may be systematic day-to-day variations in the primary cosmic ray intensity even apart from the occasional known effects of certain solar and geomagnetic disturbances.

This procedure is not practicable when the constants in the predicting function are determined by the least squares method (as in the present work) from the actual sample of data. This is because the errors are then uncorrelated with any of the "independent" variables (Cramer 1946, Chapter 23·3) and these "independent" variables specifying the structure of the atmosphere are highly correlated with other variables.

APPENDIX: COMMENTS ON A PAPER BY OLBERT (1953)[1]

In a recent paper Olbert (1953) calculates the expected atmospheric effects on cosmic ray hard component intensity at sea level.

Olbert states that a quantitative estimate of the Duperier positive temperature effect (interpreted as due to the competing processes of nuclear capture and decay of π-mesons), based on recent data for the mean life and the cross section for nuclear capture of π-mesons, has shown that the observed value of this effect is much too high to be ascribed exclusively to the finite life span of π-mesons. This finding is in agreement with the conclusions of Chapter 4.

For the temperature-depth variation in the atmosphere Olbert uses a mean curve derived from data for 40° geographic latitude (in Chapter 4 an isothermal atmosphere was assumed). For the variation of momentum with range of μ-mesons he uses an analytical formula which reproduces the theoretical curve within an accuracy of 1 per cent in the range considered (in Chapter 4 exact numerical data were used).

Whereas in Chapter 4 the simplifying assumption is made that the μ-mesons are produced at a definite atmospheric depth, Olbert allows for continuous production throughout the atmosphere. Following Sands (1950) the differential μ-meson intensity at sea level (x_o gm. cm.$^{-2}$) is given by

$$(1)\quad i(R) = \int_o^{x_o} G(R_s) e^{-x/L}\, w(x, R)\, dx$$

where L is the absorption mean free path of the meson producing radiation and $G(R_s)$ (assumed to be a function of residual range $R_s = R + x_o - x$ only) is the range spectrum at production. The empirical expression

$$(2)\quad G(R_s) = \frac{7.31 \times 10^4}{(520 + R_s)^{3.58}} \text{ gm.}^{-2} \text{ cm.}^2 \text{ sec.}^{-1} \text{ sterad}^{-1}$$

is used; Olbert claims that this expression is more accurate than that used by Sands (1950). The term $w(x, R)$ in (1) is the probability that a μ-meson produced at atmospheric depth x-gm. cm.$^{-2}$ will reach sea level, depth x_o gm. cm.$^{-2}$, with residual range R gm. cm.$^{-2}$. The calculation of $w(x, R)$ involves the approximations mentioned in the last paragraph.

Using the mean value theorem

$$\int_a^b g(z) f(z)\, dz = g(\xi) \int_a^b f(z)\, dz, \quad \xi \int_a^b f(z)\, dz \simeq \int_a^b z f(z)\, dz$$

where $g(z)$ varies slowly in (a, b) and $f(z)$ displays a sharp maximum in (a, b), to evaluate his integrals, Olbert then proceeds analytically to show that the variations of μ-meson intensity I at sea level, can be given by

1. This paper was received after Chapter 4 of this report was completed.

(3) $\delta I/I = A_H \delta H(\bar{x}_1) + A_K [\delta T_{(2)}]\bar{x}_{av.} + A_P \delta x_o$ where $\delta H(\bar{x}_1)$ is the deviation from its mean of the height of the $\bar{x}_1$ gm. cm.$^{-2}$ isobar,

$$[\delta T(\bar{x}_2)]_{av.} = \frac{1}{x_o - \bar{x}_2} \int_{\bar{x}_2}^{x_0} \delta T(x')\, dx'$$

$T(x')$ is absolute temperature at x' gm. cm.$^{-2}$, x_o = sea level pressure, and A_H, A_K, A_P, $\bar{x}_1$ and $\bar{x}_2$ are functions of the minimum residual range of particles detected by the apparatus. For minimum residual range of a few hundred gm. cm.$^{-2}$ Olbert finds $\bar{x}_1 \simeq 115$ gm. cm.$^{-2}$, $\bar{x}_2 \simeq 190$ gm. cm.$^{-2}$. Olbert presents curves for A_H, A_K and A_P from which are obtained, for particles which can penetrate 10 cm. lead absorber, the values

$$A_H = -3{\cdot}8 \quad \%/\text{km.}$$
$$A_K = -0{\cdot}10 \quad \%\,^\circ\text{C.}$$
$$A_P = -0{\cdot}16 \quad \%/\text{mb.}$$

Duperier (1951) considered the μ-meson intensity variations at sea level to be given by the expression

(4) $\delta I/I = A'_H \delta H(\xi) + A'_K \delta T(\xi) + A'_P \delta x_o$

where $H(\xi)$ is the height above sea level of the ξ mb. (taken by Duperier as 100 mb.) isobar and $T(\xi)$ is the mean temperature in a small interval below the ξ mb. isobar. Duperier and the present writer (in Chapter 4) find that for $\xi = 100$ mb. the coefficient A'_K is positive while Olbert's coefficient A_K is negative. Olbert explains this difference of sign of A_K and A'_K as due to the fact that temperature changes in the stratosphere and in the troposphere are usually negatively correlated and the tropopause is usually in the vicinity of the $\bar{x}_2 \simeq 190$ gm. cm.$^{-2}$ isobar. This explanation is consistent with the finding of Chapter 4 that for ξ greater than about 300 mb. (which is almost always below the tropopause) the coefficient A'_K is negative.

This work is consistent with the view suggested in Chapter 4 that the temperature in a small interval below the ξ mb. isobar is a more or less poor indicator of another quantity which has a direct effect in determining the μ-meson intensity at sea level, this quantity being, according to Olbert, the "mean" temperature between sea level and the level $\bar{x}_2 \simeq 190$ gm. cm.$^{-2}$.

In order to determine which of equations (3) and (4) is the better predictor of the intensity of the hard component of cosmic radiation at sea level, use has been made of some recent measurements of N. R. Parsons at Hobart.[1] These measurements were made with a vertically directed threefold coincidence telescope in which the counter trays were 1m. × 1m., the upper and lower traps were 1·5m. apart, and the lower two trays were separated by 10cm. of lead absorber. The mean counting rate was approximately 76,000 per hour.

1. These records have been published for limited distribution by the Antarctic Division, Department of External Affairs.

The meteorological data were obtained from the Hobart daily radiosonde flight. The value used for the cosmic ray intensity was the mean value for the period two hours before till two hours after the flight. However, only those days were selected (during the period September 1953—April 1954) in which no rapid change occurred in atmospheric structure and in which no "anomalous" variations in cosmic ray intensity occurred. This selection was based on visual inspection of graphs of cosmic ray intensity and barometric pressure against time. A total of 151 days' records was selected.

It was shown in Chapter 4 that no one choice of ξ in the range 500 to 80 mb. makes (4) a significantly better predictor than any other. The writer has therefore chosen, for convenience, $\xi = 115$ mb. and $T(\xi)$ = mean temperature in the interval 115-190 mb. In (3) the values $\bar{x}_1 = 115$ mb., $\bar{x}_2 = 190$ mb. are used which are very close to the values given by Olbert.

The least squares estimates and 95 per cent confidence limits of the coefficients in (3) and (4) as determined from the sample of 151 days' records are then

$$\begin{aligned}
A_H &= +4{\cdot}05 \pm 1{\cdot}50 \ \% \text{ per km.} \\
A_K &= -0{\cdot}085 \pm 0{\cdot}018 \ \% \text{ per °C.} \\
A_P &= -0{\cdot}165 \pm 0{\cdot}012 \ \% \text{ per mb.} \\
A'_H &= -0{\cdot}539 \pm 1{\cdot}085 \ \% \text{ per km.} \\
A'_K &= +0{\cdot}073 \pm 0{\cdot}032 \ \% \text{ per °C.} \\
A'_P &= -0{\cdot}141 \pm 0{\cdot}013 \ \% \text{ per mb.}
\end{aligned}$$

The values of A_K and A_P are in good agreement with Olbert's theoretical values but the value of A_H is not.

Hotelling (1940) has shown that the magnitude of the multiple correlation coefficient can be used as a criterion to indicate which of (3) and (4) is the better predictor of the dependent variate—in this case the cosmic ray intensity I. He also devised a means to test whether the difference between the two multiple correlation coefficients is significant.

Using the notation $\delta I = x_1$, $\delta x_o = x_2$, $\delta H(\bar{x}_1) = \delta H(\xi) = x_3$, $[\delta T(\bar{x}_2)]_{av.} = x_4$ $\delta T(\xi) = x_5$, Hotelling's test can be expressed in the form

$$(5) \quad t = (r_{14.23} - r_{15.23}) \sqrt{\frac{\nu(1+r_{45.23})}{2D}} \quad \text{where } D = \begin{vmatrix} 1 & r_{14.23} & r_{15.23} \\ r_{14.23} & 1 & r_{45.23} \\ r_{15.23} & r_{45.23} & 1 \end{vmatrix}$$

and t has Student's 't' distribution with $\nu = n-5$ degrees of freedom.

From the present sample (3) yields the greater value of the multiple correlation coefficient. From (5) is obtained $|t| = 6{\cdot}34$, $\nu = 146$. The probability P of obtaining such a large value of $|t|$ is less than 0·1 per cent if the true values of the multiple correlation coefficient from (3) and (4) are

equal (Hald 1952, Table IV). On the basis of Hotelling's test, then, (3) is a significantly better predictor of cosmic ray intensity than is (4).

However, the validity of Hotelling's test and of the calculated values of the 95 per cent confidence limits of the regression coefficients of (3) and (4) quoted above are dependent on the assumption that the error terms of the regression models defined by (3) and (4) are not serially correlated (see the section, "Effect of non-independence of successive values of ϵ" in Chapter 3). In the present case using Durbin and Watson's test in both (3) and (4) the assumption of serial independence of the error terms is untenable; for (3) $d = 0{\cdot}78 < d_{L5\%} > 1{\cdot}61$, for (4) $d = 0{\cdot}76 < d_{L5\%} > 1{\cdot}61$.

It is concluded that the values quoted for P above and for the 95 per cent confidence limits of the regression coefficients are only lower limits of the true values. The conclusion that (3) is a better predictor than (4) is then somewhat uncertain and the good agreement between the experimental values and Olbert's theoretical values for the coefficients A_K and A_P may be fortuitous.

5. COSMIC RAY INTENSITY VARIATIONS ASSOCIATED WITH SOLAR AND GEOMAGNETIC DISTURBANCES

by F. JACKA

Abstract. The Heard Island and Macquarie Island cosmic ray records are examined for evidence of variations associated with magnetic storms and solar radio noise emission. During one period, in which a solar radio noise storm (on 98 Mc/sec.) and an intense geomagnetic storm coincided, there was a decrease of approximately 2 per cent in the total intensity and hard component intensity of cosmic rays at Macquarie Island. No effect was found at other times of noise storms while the average effect of a number of geomagnetic storms shows a decrease of approximately 0·5 per cent in the cosmic ray intensity.

The cosmic ray total intensity at Macquarie Island is found to be uncorrelated with the intensity of 10 cm. solar radiation. No significant variation is found at times of "outstanding short duration occurrence" of solar radio noise on 62 or 98 Mc/sec.

Introduction. In Chapter 4 the problem was considered of predicting the variations in sea-level cosmic ray intensity in terms of a function of variables specifying the structure of the atmosphere. It was found that that there are systematic day-to-day variations which are not predicted by any of the functions examined.

It was considered nevertheless that these systematic variations are due to changes in atmospheric structure, the assumption being made that there are no significant day-to-day changes in the primary intensity apart from occasional abnormal values associated with certain solar and geomagnetic disturbances. It is consequently difficult to recognize these occasional "abnormal" values (unless they are "very abnormal") even after the predicted atmospheric effects have been subtracted; in fact, in the Heard Island and Macquarie Island records, only one such "abnormal" value (that of 14-18 June, 1951) has been identified.

However, the average effect associated with many occurences of a particular type of solar or geomagnetic disturbance may be determined approximately by a form of the "superposed epoch" method introduced by Chree (1912). This involves subtracting the predicted atmospheric effect, listing the residual values in columns numbered according to the time measured from an origin at the time of the particular solar or geomagnetic disturbance, then averaging the columns of figures. The variance of the errors (due

to unpredicted atmospheric effects and random fluctuations) in these average figures then decreases approximately as 1/N, N being the number of rows (the number of occurrences of the disturbance considered).

In the following sections this method is used to examine the variations in cosmic ray intensity at Heard Island and Macquarie Island, associated with solar radio noise outbursts and magnetic storms. A brief description of the variations found to be associated with magnetic storms and other disturbances is given in Chapter 1.

The solar diurnal variation in cosmic ray intensity has been determined from the Macquarie Island records by Ford and Parsons (see Chapter 6).

Variations associated with magnetic storms. The records of cosmic ray intensity available for the present investigation cover the periods April 1948 to January 1949 at Heard Island, and August 1948 to January 1949 and June 1950 to March 1952 at Macquarie Island. Daily mean values of the hard component intensity, c_2, and total intensity, c_3, are examined.

The times of occurrence of magnetic storms with sudden commencement during these periods were obtained from I.A.T.M.E. Bulletins (Bartels and Veldkamp, 1949-52) and in the case of 1952 data from J. Geophys. Res. (Bartels and Veldkamp, 1952).

Deviations (Z_{12}) of the observed cosmic ray intensity from regression on barometric pressure were calculated for the period four days before to four days after each magnetic storm sudden commencement for which cosmic ray records were available. The barometer coefficients used were those calculated from monthly samples (see the section, "The barometer and temperature effects—experimental results", in Chapter 4). On only one occasion was a significant variation of intensity associated with the magnetic storm. This was during the period 12 June to 22 June 1951 in which three sudden commencements occurred. During the same period a significant decrease in hard component intensity was also observed at Manchester and at Thule (Singer, private communication). The variation for c_2 and c_3 measured at Macquarie Island is shown in Fig. 30. These curves were calculated using values of the barometer coefficients derived from three months' data, viz. May, June and July 1951.

On taking the average variation associated with 14 magnetic storms in the case of c_2 and 18 in the case of c_3 measured at Macquarie Island during the period September 1950 to December 1951 (but not including June 1951) the amplitude of the statistical fluctuations is reduced and the magnetic storm effect shown in Fig. 31 is found.

Cosmic ray intensity and solar radio noise. Solar radio noise may be divided into three apparently distinct categories; (1) A slowly varying

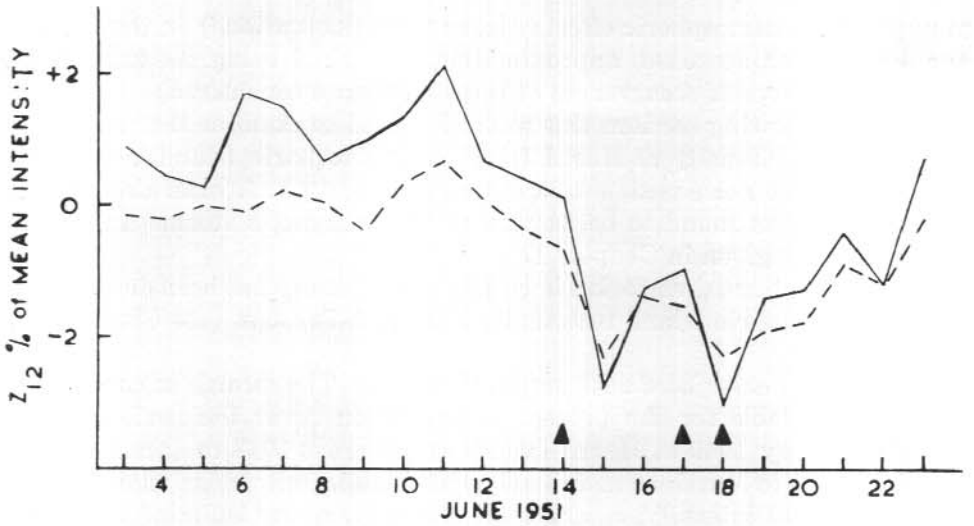

FIG. 30.

Variation of hard component c_2 (full curve), and total intensity c_3 (dashed curve), at Macquarie Island associated with magnetic storms with sudden commencement at times indicated by ▲.

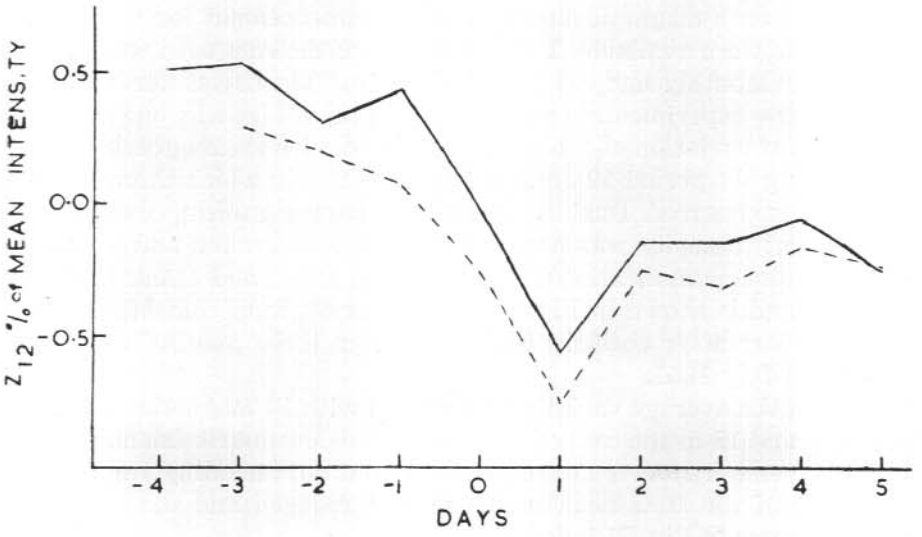

FIG. 31.

Mean variation of hard component c_2 (full curve), and total intensity c_3 (dashed curve), at Macquarie Island, associated with a number of magnetic storms with sudden commencement on day O.

component (decimetre wave-length), (2) Noise storms (metre wave-lengths) of duration a few days, and (3) Outstanding short duration (order of minutes) occurrences on metre wave-lengths. These include "outbursts" of the type normally associated with solar flares.

Using five-day means the regression of cosmic ray total intensity (measured at Macquarie Island) on barometric pressure and 10 cm. solar radiation intensity (measured at Sydney) was examined using data of August to December 1950. The regression coefficient of solar radiation intensity is not significant at the 5 per cent level.

During the period June 1950 to June 1951 at times when cosmic ray records were obtained at Macquarie Island eight noise storms (on 98 Mc/sec.) occurred. One of these, lasting from 9 June to 22 June 1951, had its maximum intensity on 16 June 1951. The variations in hard component intensity, c_2, and total intensity, c_3, of the cosmic radiation at these times is shown in Fig. 30. It is not possible to say whether the variations shown in this curve should be attributed to the solar radio noise storm or to the magnetic storms with sudden commencements during the same period. Not one of the other seven noise storms was associated with a significant change in cosmic ray intensity as measured by c_2 or c_3.

From the Macquarie Island records of total intensity of cosmic radiation, c_3, during the period June 1950 to January 1952, data were selected at times of the 80 most energetic (energy defined by "smoothed maximum intensity" $\times$ "duration") outstanding short duration occurrences of solar radio noise on frequencies of 62 and/or 98 Mc/sec. measured at Sydney.

The mean variation (of 80 occasions) over the period 10 hours before to 12 hours after the occurrence was corrected for variations in barometric pressure using a barometer coefficient calculated from the whole sample. No significant variation is found in the corrected cosmic ray intensities. The standard error of any one point is approximately 0·1 per cent.

These results should be contrasted with those of Dolbear, Elliot and Dawton (1951) who find an increase on the average, of 0·3 per cent in the cosmic ray intensity at times of Dellinger type radio fade-outs which are usually associated with solar flares of moderate intensity.

The data on solar radio noise used in this investigation were supplied by Dr. J. L. Pawsey, Division of Radiophysics, C.S.I.R.O.

Conclusions. The preceding analysis of solar and geomagnetic disturbance effects on cosmic ray intensity is regarded only as a preliminary to a more detailed discussion of the problem. It is considered that a satisfactory treatment of this problem can be expected only when extensive cosmic ray records are available from a number of stations distributed over

a wide range of latitude and longitude. Also this problem must be treated together with a study of geomagnetic variations and the aurora.

Measurements of the hard component similar to those discussed in this report are being continued at Macquarie Island. Measurements of the hard component intensity with a narrow angle telescope and counting rate approximately 75,000 particles per hour are now being made in co-operation with the Physics Department of the University of Tasmania at Hobart. Two similar telescopes, one directed vertically and the other directed alternately in different azimuths at a fixed zenith angle, were installed early in 1955 at Mawson, Antarctica.

It is proposed to examine the present records together with records from these new projects in a detailed study of the variations in cosmic ray intensity associated with solar and geomagnetic disturbances.

6. DIURNAL VARIATION IN COSMIC RAY INTENSITY

by P. W. FORD AND N. R. PARSONS

Records of c_2 (narrow angle hard component) and of c_3 (wide angle total intensity), obtained at Macquarie Island during the period June 1950-April 1952 have been examined for evidence of diurnal variations.

For this purpose the data were divided into bi-monthly groups (months (1, 2), (3, 4), etc.) and each group examined separately in order that any significant seasonal changes in amplitude and phase of the daily intensity wave might be apparent.

For each bi-monthly group, mean bi-hourly values of cosmic ray intensity and barometric pressure were calculated using only those days when the records were complete. This yielded 12 values of the variables equally spaced over a period of one solar day. Correction of the 12 cosmic ray intensity values to standard pressure conditions was then carried out using a barometer coefficient computed from daily mean values of intensity and pressure from the complete-days records of the bi-monthly group.

For the period June 1950-May 1951 only c_2 records were reduced in this manner. For the period May 1951-March 1952 both c_2 and c_3 records were reduced using only those days on which both records were complete. March 1952 records were taken as representative of the bi-monthly period March-April since recording ceased at the end of March.

The 12 corrected intensity values were then subjected to harmonic analysis and the amplitudes and phases of the 24-hr. and 12-hr. components determined. Mean values for the year were obtained by analysing the 12 means of the six sets of bi-monthly corrected figures.

The results of this analysis are presented in Fig. 32, which shows the amplitude (as % of the mean intensity) and time of maximum on harmonic dials—24-hr. dials for the diurnal component and 12-hr. dials for the semi-diurnal component.

It will be noted that there is a cyclic progression of points on the 24-hr. harmonic dial for c_3. Such an effect can be caused by an annual variation in amplitude and phase of the true solar diurnal variation or by the superposition of a sidereal diurnal variation on a solar variation of constant phase and varying amplitude. With the present data alone it is not possible to distinguish the two cases (*cf.* Elliot and Dolbear, 1951).

In order to obtain some idea of the significance of the bi-monthly points, several were chosen and the diurnal variation calculated for the individual

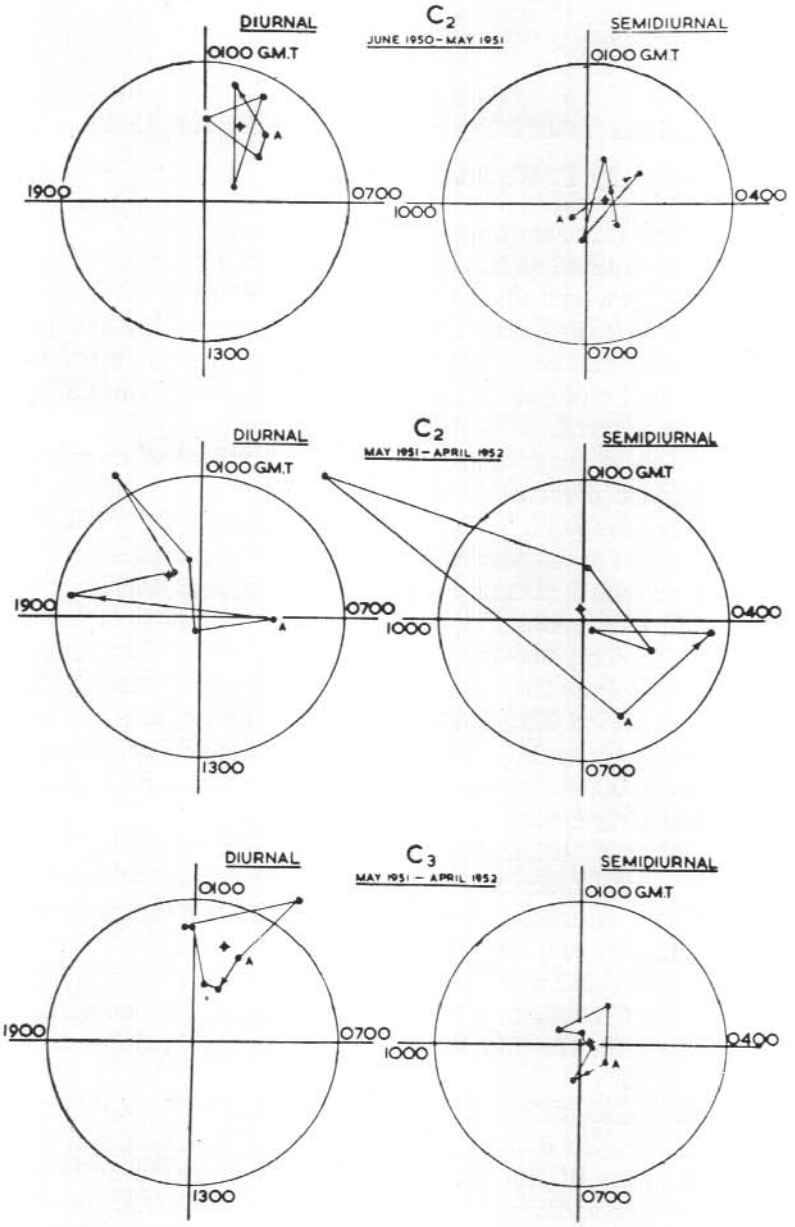

FIG. 32.

Harmonic dials showing the amplitudes (in % of the mean intensity) and times of maximum of the diurnal and semi-diurnal variations in cosmic ray intensity at Macquarie Island.

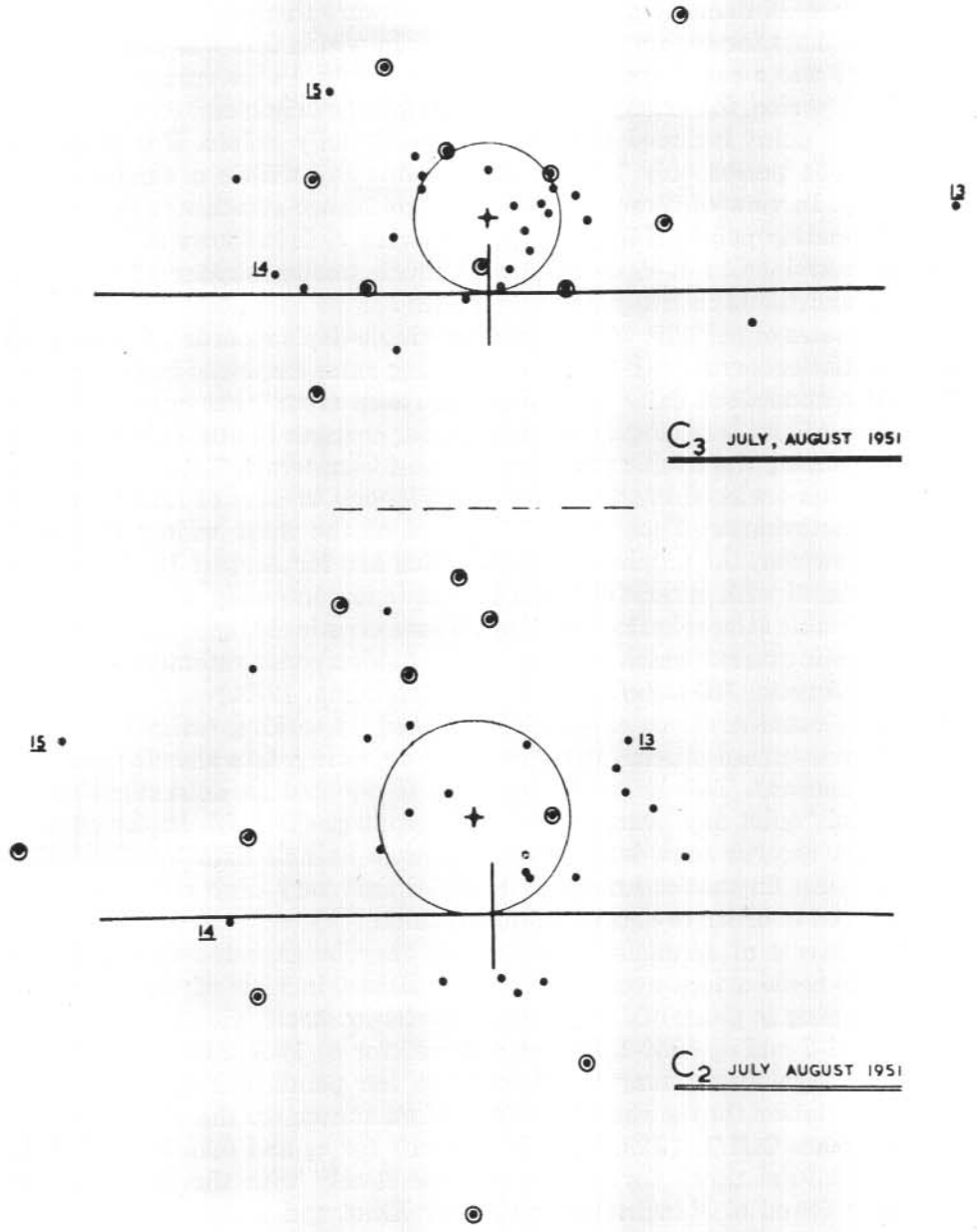

FIG. 33.

Harmonic dials showing the relative amplitudes and times of maxima of the diurnal variations in cosmic ray intensity at Macquarie Island for individual days of a bi-monthly period. The point indicated by + is the mean point for the whole period.

days of these bi-monthly groups. The results were then plotted on separate harmonic dials for each group. In all cases in which this was done with c_2 data there was a considerable scatter of the points. In the case of the May-June 1951 period, for example, a circle through the origin and centred on the bi-monthly point included only one of the 37 daily points. For the July-August 1951 period only 7 of 33 daily points lay within a similar circle (Fig. 33). In view of these results little significance attaches to the individual bi-monthly points of the harmonic dials for c_2 data shown in Fig. 32. A similar examination of c_3 data shows a much smaller scatter of the daily points about the bi-monthly point (Fig. 32).

Estimates of periodic variations from single-day's records are subject to large statistical error with the small counting rates employed in the present case. Also anomalous daily variations can result from other causes. Important among these is inadequate correction for changes in atmospheric structure influencing the cosmic ray intensity (see Chapters 4, 7 and 8). On Fig. 33 the points enclosed in small circles correspond to days of marked atmospheric disturbance. These include several of the most widely scattered points. However, the numbered points which are for August 13, 14 and 15 are associated with erratic changes in cosmic ray intensity at times of apparently stable atmospheric conditions. These erratic changes may be due to the magnetic storms which occurred with sudden commencements on 13th and 15th August, 1951. (*cf.* Bartels and Veldkamp, 1952.)

These considerations emphasize the need, in seeking estimates of the normal undisturbed diurnal variations, for rejecting data showing anomalous fluctuations. This sort of procedure is adopted in determination of the normal "quiet day" variations in the geomagnetic field. In the case of cosmic ray records such drastic restrictions in useable data together with the statistical fluctuations make it essential that very high counting rates be employed in order to obtain reliable results.

The effects of anomalous fluctuations may be expected to cancel one another to some extent over long periods. Hence, in view of the relatively close grouping in phase of the points on the 24-hr. harmonic dials (Fig. 31) for c_3, 1951-2 and c_2, 1950-1 (not reproduced for c_2, 1951-2 however), some degree of significance may be attached to the points showing the mean diurnal variation for the year. The times of maximum for these mean points are 02h. 00m. G.M.T. (12h. 30m. local time) for c_2 and 02h. 30m. G.M.T. (13h. 00m. local time) for c_3. These agree closely with the local time of maximum found at Manchester in 1949 by Elliot and Dolbear (1951) and are consistent with the systematic change in phase shown by Thambayahpillai and Elliot (1953) to have taken place over the last 20 years.

There is no evidence in the present results for a significant semi-diurnal variation in cosmic ray intensity.

7. THE BAROMETER COEFFICIENT AND AIR MASS EFFECTS ON COSMIC RAYS AT MACQUARIE ISLAND

by R .M. JACKLYN

Abstract. The changes in cosmic ray intensity associated with the passage of weather fronts over the observing station are investigated, using data from Macquarie Island. The effects can be explained in terms of the different way in which the height of the production layer for mesons varies with surface pressure for warm moist and cold dry air masses. The barometer coefficients found for these air masses are respectively $-0{\cdot}120$ $\pm 0{\cdot}058$ per cent per mb. and $-0{\cdot}220$ $\pm 0{\cdot}041$ per cent per mb. for the penetrating component. These results indicate that the frequently observed fluctuations in short term barometer coefficients may be traceable to changes in air mass types.

Introduction. During the past ten to fifteen years several workers (Loughridge and Gast, 1940; Nishina et al. 1940a, 1940b; Trumpy, 1949; Lindholm, 1950) have commented on the marked changes which cosmic ray intensities undergo with the passage of fronts over the recording station. This effect was studied in the Macquarie Island 1950-1 records.

The weather at Macquarie Island is typically overcast with a yearly average humidity of 88 per cent. Daily and seasonal surface temperature fluctuations are comparatively small, but large variations of surface pressure occur, often accompanied by a change of air mass. (The phrase "air mass", for the purpose of this study, refers to a characteristic combination of surface and upper air temperatures, humidity and surface wind direction, which usually persists over the station for several days at a time, and with the passage of a surface of discontinuity, the front, changes to another typical set of the quantities.)

A change of air mass is generally associated with a cold or an occluded cold front. The origin and orientation of fronts and the tracks of major depressions in the Southern Ocean are still matters of conjecture, partly because there are very few observing stations in the area. Gibbs (1952) has assumed that the major source region of fronts is in the close neighbourhood of the Antarctic Continent. Briefly, they appear to develop as follows: Outbursts of cold dry air move northwards behind antarctic fronts until they become the polar fronts of middle latitudes. Wave developments in these fronts result in the growth of major depressions. One of the two main tracks

followed by these depressions, and their associated fronts, is in a SE direction from the SW coast of Australia to the vicinity of Macquarie Island, reaching maximum development at 60°S. As they approach the antarctic coastline and gradually dissolve, the depressions cause fresh outbreaks of antarctic air to occur, with new antarctic fronts as their forward boundaries. So it seems likely that cold fronts at Macquarie Island are either well developed polar fronts associated with depressions tracking from the north west, or else antarctic fronts associated with fresh air masses from the continent.

Data and methods of analysis. The data used in the present study are the Macquarie Island 1950-1 records of c_3 (wide angle total intensity), c_1 (narrow angle total intensity) and c_2 (narrow angle hard component intensity). These records were each analysed for the average effects produced by the passage of fronts, following a procedure used by Loughridge and Gast (1940). For an individual front, the counting rates were collected into 6-hour groups, referred to the time of passage over the station. Thus the 6-hour group immediately preceding the change of air mass was centred about the time three hours before the passage of the front. The counting rates were corrected to a standard pressure of 940 mb. using the appropriate bi-monthly barometer coefficient, derived from the daily mean rates and surface pressures.

To minimize the effects of fluctuations in the general level of intensity between one front and another, the corrected rates were normalized to the second 6-hour group preceding the front. Thus only the mean differences were plotted between this and other groups.

Records of c_1 and c_2 were analysed for six well defined cold fronts and five double cold fronts (for each of which the frontal changes occurred in two distinct stages several hours apart) recorded between June and November 1951. These have been treated as a single group of eleven cold type fronts, to obtain a better estimate of the post-front changes. Over the same period, records of c_3 were available for fourteen cold type fronts.

The Macquarie Island records for 1950 were also analysed for the effect of fronts, but in this case it was decided to consider only the occasions for which records were available for c_1, c_2 and c_3 simultaneously. This restricted the results to twelve marked cold fronts. No double fronts were included in this group.

The front effects. The average effects on the corrected counting rates for each of the years 1950 and 1951 are shown graphically in Figs. 34 and 35, together with the mean surface pressure variations. The post-front increases in the level of corrected intensities for each measure of the cosmic

ray intensity as well as the percentage increases are set out in Table 29. It can be seen that the increases are consistent for both years, and they are in qualitative agreement with the ionization chamber measurements made by Loughridge and Gast. The increases in corrected intensities c_2 and c_1, the

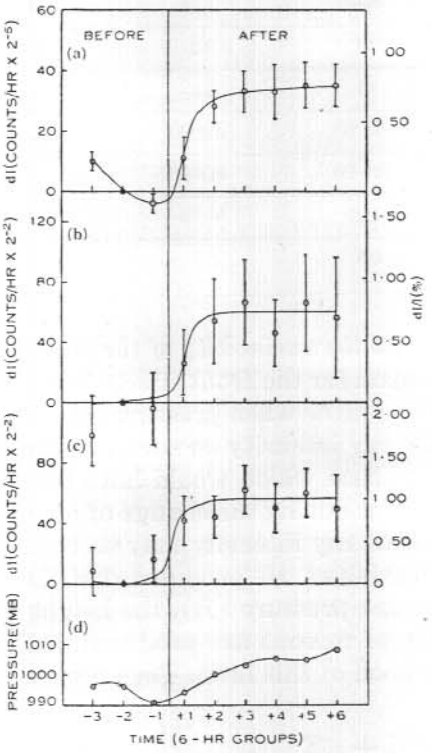

FIG. 34.

The average effect of the passage of cold fronts during 1950 on (a) the wide-angle total intensity c_3, (b) the narrow-angle total intensity c_1, (c) the narrow-angle hard component c_2, together with (d) the mean surface pressure variations. The error tails shown are the 95 per cent fiducial limits.

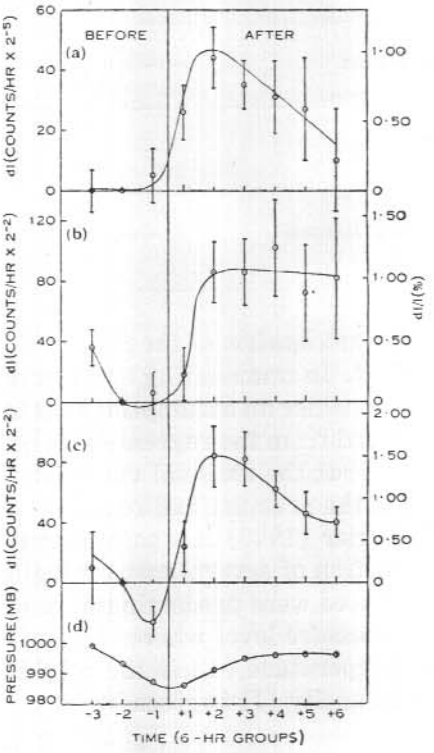

FIG. 35.

The average effect of the passage of cold type fronts during 1951. (a)-(d) as for Fig. 34.

penetrating radiation and total radiation, are the same for the two telescopes with the same geometry. The smaller per cent increase in total radiation is practically the same for both the narrow-angle and the wide-angle telescopes. Thus it appears that the post-front effects are almost entirely due to variations in the penetrating radiation.

TABLE 29

Post-front increases in cosmic ray intensities corrected for pressure using a total barometer coefficient

	Year	$c_2/4$	$c_1/4$	$c_3/32$
No. of Fronts	1950	12	12	12
	1951	11	11	14
Total Increase	1950	50–60	50–60	
	1951	80–90	80–90	
Percentage Increase	1950	0·93	0·75	0·75
	1951	1·5	1·0	1·0

The mechanism of the front effects and the variability of the barometer coefficient. In commenting on the mechanism for the front effects it is necessary to consider an assumption that is often made when pressure corrections are derived from the regression of cosmic ray intensity on surface pressure. That is, that the residual variations are those which would have been observed if the pressure had remained constant during the change of air mass. As Duperier (1949) has pointed out, cosmic ray intensity may be regarded as a function of several meteorological variables. He proposed that the following three were predominant: the surface pressure (B), the height (H) of the pressure level where the majority of mesons are produced, and the mean temperature (T) in the neighbourhood of this level. Thus a variation of the intensity (I) is given by

$$\delta I = \mu \delta B + \mu' \delta H + a \delta T$$

On the other hand, if cosmic ray intensity is regarded as a function of surface pressure only, and

$$\delta I = \beta \delta B$$

where β is the total barometric regression coefficient, then

$$(1) \qquad \beta = \mu + \mu' \frac{\delta H}{\delta B} + a \frac{\delta T}{\delta B}$$

Evidently then, the pressure coefficient varies with the upper air meteorological conditions, and may undergo marked and consistent changes when one type of air mass replaces another.

With this in mind, the total pressure coefficients for the pre-front moist warm air and the post-front polar air for the months June to November were obtained from the 1951 records (unfortunately it was not possible to extract this kind of data for the 1950 results). The coefficients for the total

intensity, c_1, and the hard component, c_2, are set out in Table 30 (the errors given being the 95 per cent fiducial limits) together with the bi-monthly coefficients used for the analysis described above. In the passage from a temperate to a polar air mass there is a significant increase in the pressure coefficient for the penetrating radiation, and that for the total intensity shows a similar trend. Notably, all the bi-monthly coefficients have values lying between the two air mass values.

TABLE 30

Barometer Coefficients in counts per hr./mb. 1951 Data

	Narrow Angle Hard Component c_2	Narrow Angle Total Intensity c_1
Temperate air mass	$-4{\cdot}072 \pm 1{\cdot}96$ ($-0{\cdot}120 \pm 0{\cdot}058\%$/mb)	$-8{\cdot}744 \pm 3{\cdot}28$ ($-0{\cdot}184 \pm 0{\cdot}069\%$/mb
Polar air mass	$-7{\cdot}508 \pm 1{\cdot}40$ ($0{\cdot}220 \pm 0{\cdot}041\%$/mb)	$-12{\cdot}504 \pm 1{\cdot}84$ ($-0{\cdot}260 \pm 0{\cdot}037\%$/mb)
Bi-monthly means		
May–June	−6·364	−11·52
July–August	−5·704	−11·52
September–October	−4·924	−11·52

If the counting rates are corrected using the appropriate coefficients for the air masses (Fig. 36), it is obvious that the change in corrected rates on passing through a front is arbitrary, depending on the choice of a standard pressure. If in the case of c_2 the standard pressure is chosen corresponding to the point of intersection of the regression lines (1005 mb.), there should be no change in corrected rates on passing from the temperate to the polar air mass. But it is clear that if a single average pressure coefficient is used, its value lying somewhere between the values for the polar and temperate air mass coefficients, the rates corrected to a standard pressure must increase after the passage of a cold front. This accounts for the fact that the pattern of variation of penetrating and total radiation, corrected using the same barometer coefficient before and after cold type fronts, is consistent for both years on Macquarie Island, and is in qualitative agreement with the observations made by Loughridge and Gast. This being so, referring to eqn. (1) the ratios $\frac{\delta H}{\delta B}$ and $\frac{\delta T}{\delta B}$ must vary consistently on passing from warm moist to cold dry air.

Now, Trumpy (1949) has successfully accounted for variations in meson counting rate due to the passage of fronts by assuming that the surface pressure (B) and the height of the 100 mb. level (H) are the predominantly effective variables, so that

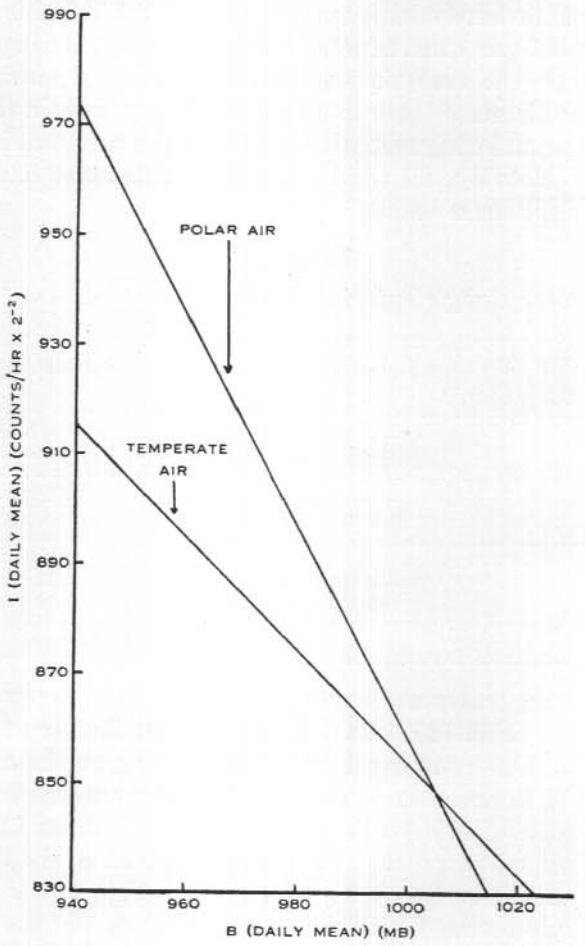

FIG. 36.

The line of regression of hard component intensity c_2 on surface pressure under different air mass conditions.

$$\delta I = \mu \delta B + \mu' \delta H$$

The corresponding expression for the barometer coefficient β is

$$\beta = \mu + \mu' \frac{\delta H}{\delta B}$$

Using the suffixes P and T to denote polar air mass and temperate air mass conditions respectively, we have

$$(2) \qquad \beta_P = \mu + \mu' \left(\frac{\delta H}{\delta B}\right)_P$$

$$(3) \qquad \beta_T = \mu + \mu' \left(\frac{\delta H}{\delta B}\right)_T$$

Since β, μ and μ' are negative, and $|\beta_P| > |\beta_T|$ one would expect $\left(\frac{\delta H}{\delta B_P}\right)$ to be greater than $\left(\frac{\delta H}{\delta B}\right)_T$. With the data obtained from the daily radiosonde flights conducted at Macquarie Island, values of $\left(\frac{\delta H}{\delta B}\right)_P$ and $\left(\frac{\delta H}{\delta B}\right)^T$ were found using the least squares method. Over the same period for which β_P and β_T had been calculated, they are as follows:

$$\left(\frac{\delta H}{\delta B}\right)_T = -3{\cdot}048 \times 10^{-5} \text{ km./mb. } (-0{\cdot}194 \times 10^{-3} \text{ per cent/mb.})$$

$$\left(\frac{\delta H}{\delta B}\right)_P = +1{\cdot}612 \times 10^{-2} \text{ km./mb. } (+0{\cdot}1028 \text{ per cent/mb.})$$

The mass absorption coefficient μ, the decay coefficient μ', and the mean range for mesons before decay, L, obtained by substitution in eqns. (2) and (3), compare favourably with the values found by Trumpy in Norway, as shown in Table 31.

TABLE 31

	μ (per cent/mb.)	μ' (per cent/km.)	L (km.)
Macquarie Island	−0·120	−5·52	18·1
Norway	−0·151	−5·8	17·3

Conclusions. Summing up, it appears that the marked changes in cosmic ray intensities which occur following the passage of cold fronts can be traced through the variation of the barometer coefficient to the different way in which the height of the production layer for mesons changes with surface pressure for warm moist and cold dry air masses, $\frac{\delta H}{\delta B}$ having the greater value (in the positive sense) for the latter.

The frequently observed fluctuations of short-term barometer coefficients may be largely traceable to this cause.

8. COSMIC RAYS AND AIR MASS EFFECTS AT MACQUARIE ISLAND

by R. M. JACKLYN

In Chapter 7 it was shown that the barometer coefficient for cosmic rays at Macquarie Island varied consistently according to the type of air mass present over the station. This was found to be due to the different average values of $\frac{\delta H}{\delta B}$ (the rate of change of the height of the assumed production level for mesons with surface pressure) in the two air mass types considered. For temperate air $\frac{\delta H}{\delta B}$ was practically zero (+0·0002 per cent/mb.) and for polar air had the value +0·1028 per cent/mb. An analysis of these air mass types has now shown why one should expect the ratio to vary in the way it does.

For each type of air mass the total regression of height (H) on surface pressure (B) was calculated for the following pressure levels: 100, 200, 400, 600, and 800 millibars using data obtained from the daily radiosonde flights at Macquarie Island. The regression and correlation coefficients are set out in Table 32. From these, and from Figure 37, it can be seen that $\frac{\delta H}{\delta B}$ progressively increases as one proceeds upwards in polar air, and in temperate air it progressively decreases. In other words, there is a tendency for polar air to expand at all levels, and for temperate air to contract, as surface pressure increases.

TABLE 32

Pressure level (mb)	800	600	400	200	100
Polar air $\frac{\delta H}{\delta B}$ (km/mb × 10^2)	+0·85	+0·975	+1·128	+1·189	+1·341
r	0·992	0·963	0·917	0·904	0·833
Temperate air $\frac{\delta H}{\delta B}$ (km/mb × 10^2)	+0·762	+0·701	+0·640	+0·366	0
r	0·958	0·875	0·686	0·330	0·106

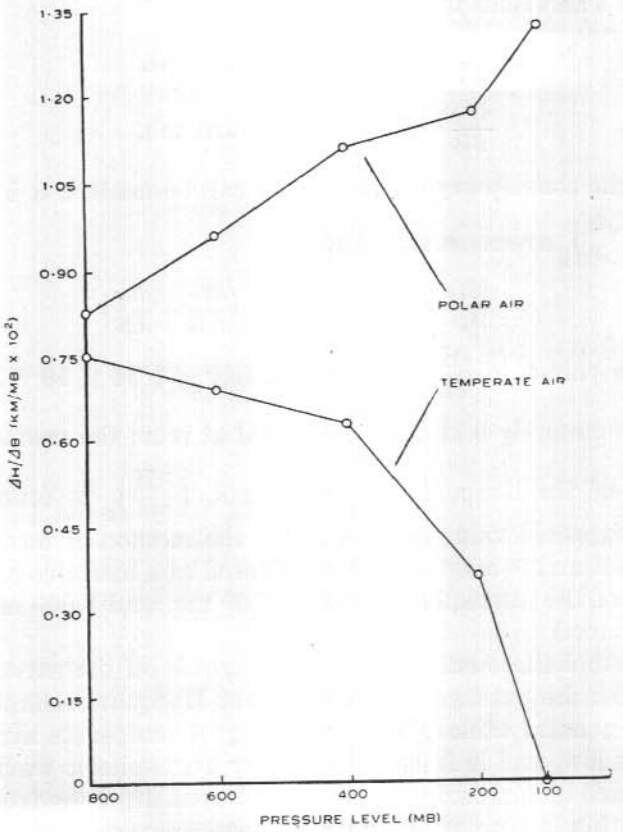

FIG. 37.

Variation of $\frac{\delta H}{\delta B}$ with pressure at height H for polar and temperate air mass conditions.

If then, the height of production (H), of mesons, is considered as a function of the mean atmospheric temperature (θ) and the surface pressure (B), and

$$\frac{dH}{dB} = \left(\frac{\partial H}{\partial \theta}\right)_B \frac{d\theta}{dB} + \left(\frac{\partial H}{\partial B}\right)_\theta$$

it seems that $\frac{d\theta}{dB}$, the rate of expansion with surface pressure, would be positive in polar air and negative in temperate air. As a measure of the mean atmospheric temperature, θ, the thickness of the atmosphere between 100 mb. and 1,000 mb. was taken, and the regression coefficients $\frac{d\theta_P}{dB}$ and $\frac{d\theta_T}{dB}$ were found, the suffixes P and T referring to polar and temperate air

respectively. The values were

$$\frac{d\theta_P}{dB} = +0.521 \times 10^{-2} \text{ km/mb.}$$

$$\frac{d\theta_T}{dB} = -0.808 \times 10^{-2}. \text{ km/mb.}$$

A check on the consistency of the figures can be made if it is assumed that $\left(\frac{\partial H}{\partial \theta}\right)_B$ and $\left(\frac{\partial H}{\partial B}\right)_\theta$ are constants. Then

$$\frac{\delta H_P}{\delta B} - \frac{\delta H_T}{\delta B} = \left(\frac{\partial H}{\partial \theta}\right)_B \left(\frac{d\theta_P}{dB} - \frac{d\theta_T}{dB}\right)$$

Knowing the values of $\frac{\delta H_P}{\delta B}$ (approximately $+1{\cdot}34 \times 10^{-2}$ km./mb.) and $\frac{\delta H_T}{\delta B}$ (approximately 0 km./mb.) arrived at from the radiosonde data independently of the temperature coefficients, $\left(\frac{\partial H}{\partial \theta}\right)_B$ is found to be 1·01, close to the expected value of unity. (i.e. the method of measurement of θ implies that δH and $\delta\theta$ may each be considered as a measure of the variation of the depth of the atmosphere between 100 mb. and 1,000 mb. at constant surface pressure.)

It seems that these effects are characteristic off the pattern of weather associated with the passage of cold fronts at Macquarie Island during winter. That is, general atmospheric warming of temperate air precedes the arrival of the low, and is followed again by atmospheric warming of polar air accompanied by increasing surface pressures, after the front has passed. Presumably, this is true of other places where marked increases of cosmic ray intensities, "corrected" for pressure, have followed the passage of cold fronts. Since the Macquarie Island measurements agree substantially with those found by Loughridge and Gast (1940), using a shielded ionization chamber at sea off the West Coast of North America, a similar maritime weather pattern probably held there. But Nishina et al. (1940), using an ionization chamber at Tokyo, found no significant effect for cold fronts, and this may have been due to the modifying effect of the neighbouring land on the temperature characteristics of the air masses.

ACKNOWLEDGMENTS

The writers wish to express their thanks to Mrs. U. Brent, Miss J. Gregory and Mrs. P. James for their assistance with the extensive numerical computations and preparation of diagrams. Much of the computing was carried out with the aid of "Hollerith" tabulating and sorting machines kindly made available by the Secretary, Department of the Army and the Director, Commonwealth Meteorological Bureau.

Meteorological data were supplied by the Director, Commonwealth Meteorological Bureau, and Mr. K. Stibbs (formerly meteorologist at Macquarie Island) assisted through several valuable discussions on these data.

The construction and operation of the equipment was made possible largely through the work of the technical staffs of the Physics Department, University of Melbourne and of the A.N.A.R.E. at the Heard Island and Macquarie Island Stations; their co-operation is greatly appreciated.

A grant from the C.S.I.R.O. enabled R. M. Jacklyn to continue work at the University of Tasmania after his return from Macquarie Island.

The writers are greatly indebted to Dr. H. D. Rathgeber (formerly of University of Melbourne), Mr. P. G. Law (Director of the Antarctic Division) and Professor A. L. McAulay and Dr. A. G. Fenton (of the University of Tasmania) for valuable discussion and encouragement during the course of the work.

REFERENCES

ALAOGLU, L., and SMITH, N. M., 1938. Phys. Rev. **53**, 832.
ALFVEN, H., 1950. Cosmical Electrodynamics, Ch. 7 (Clarendon Press, Oxford).
ASCOLI, G., 1950. Phys. Rev. **79**, 812.
BAEHNE, G. W. (Editor), 1935. Practical Applications of the Punched Card Method in Colleges and Universities.
BARTELS J., and VELDKAMP, J., 1949-52. Geomagnetic Indices K and C, I.A.T.M.E. Bulletins No. 12b-12f.
BARTELS, J., and VELDKAMP, J., 1952. International Data on Magnetic Disturbances, J. Geophys. Res. **57**.
CAMERINI, U., et al., 1951a. Phil. Mag. **42**, 1241.
CAMERINI, U., et al., 1951b. Phil. Mag. **42**, 1261.
CARO, D. E., LAW, P. G., and RATHGEBER, H. D., 1948. Aust. J. Sci. Res. Series A, **1**, 261.
CARO, D. E., PARRY, J. K., and RATHGEBER, H. D., 1951. Aust. J. Sci. Res. Series A, **4**, 16.
CHAPMAN, S., and FERRARO, V. C. A., 1933. Terr. Mag. Atmos. Elect. **38**, 79.
CHREE, C., 1912. Phil. Trans. Series A, **212**, 75
CRAMER, H., 1946. Mathematical Methods of Statistics (Princeton Univ. Press).
DAWTON, D. I., and ELLIOT, H., 1953. J. Atmos. Terr. Phys. **3**, 295.
DOLBEAR, D. W. N., and ELLIOT, H., 1951. J. Atmos. Terr. Phys. **1**, 215.
DOLBEAR, D. W. N., ELLIOT, H., and DAWTON, D. I., 1951. J. Atmos. Terr. Phys. **1**, 187.
DUPERIER, A., 1949. Proc. Phys. Soc. Series A, **62**, 684.
DUPERIER, A., 1951. J. Atmos. Terr. Phys. **1**, 296.
DURBIN, J., and WATSON, G. S., 1950. Biometrika **37**, 409.
DURBIN, J., and WATSON, G. S., 1951. Biometrika **38**, 159.
ELLIOT, H., 1952. Progress in Cosmic Ray Physics, Ch. 8 (North-Holland).
ELLIOT, H., and DOLBEAR, D. W. N., 1951. J. Atmos. Terr. Phys. **1**, 205.
FENTON, K. B., 1952. Thesis, University of Tasmania.
FISHER, R. A., 1948. Statistical Methods for Research Workers (Oliver and Boyd).
FORBUSH, S. E., 1938. Terr. Mag. Atmos. Elect. **43**, 203.
FORBUSH, S. E. STINCHCOMB, T. B., and SCHEIN, M., 1950. Phys. Rev. **79**, 501.
GIBBS, W. J., GOTLEY, A. V., and MARTIN, A. R. 1952. Aust. Nat. Ant. Res. Exp. Reports Series D, Meteorology, **1**, Part 1(e).
HALD, A., 1952. Statistical Tables and Formulas. (Wiley and Sons).
HAYAKAWA, S., NAGATA, T., NISHIMURA, J., and SUGIURA, M., 1950. J. Geophys. Res. **55**, 221.
HOGG, A. R., 1949. Memoirs of the Commonwealth Observatory No. 10 Aust.
HOTELLING, H., 1940. Ann. Math. Statist. **11**, 271.
JACKLYN, R. M., 1954. Aust. J. Phys. **7**, 315.
JACKLYN, R. M., 1955. Aust. J. Phys. **8**, 190.
JELBART, J. E., 1949. Thesis, University of Melbourne.
LANGE, I., and FORBUSH, S. E., 1948. Carnegie Institute of Washington, Publication 175.
LAW, P. G., MCKENZIE, C. D., and RATHGEBER, H. D., 1949, Aust. J. Sci. Res. Series A, **1**, 493.
LINDHOLM, F., 1950. Tellus **2**, 63.
LOUGHRIDGE, D. H., and GAST, P. F., 1940. Phys. Rev. **58**, 583.
MYSSOWSKY, L., and TUWIM, L., 1928. Z. Phys. **50**, 273.
NISHINA, Y., SEKIDO, Y., SIMAMURA, H., and ARAKAWA, H., 1940a. Phys. Rev. **57**, 663.
NISHINA, Y., SEKIDO, Y., SIMAMURA, H., and ARAKAWA, H., 1940b. Phys. Rev. **57**, 1050.
NORMAN, R., 1950. Thesis, University of Melbourne.
OLBERT, S., 1953. Phys. Rev. **92**, 454.
PARSONS, N. R., 1951. Thesis, University of Melbourne.
PETERS, B., 1952. Progress in Cosmic Ray Physics, Ch. 4 (North-Holland).
ROSE, D. C., 1951. Canad. J. Phys. **29**, 97.
ROSSI, B., 1948. Rev. Mod. Phys. **20**, 537.
ROSSI, B., 1952. High Energy Particles (Prentice-Hall Inc.).
SEKIDO, Y., and KODAMA, M., 1952. Report of Ionospheric Research in Japan. **6**, No. 2.
THAMBYAHPILLAI, T., and ELLIOT, H., 1953. Nature **171**, 918.
TREFALL, H., 1953. Nature **171**, 888.
TRUMPY, B., 1949. Univ. Bergen Arb. 1949, No. 3.
WEATHERBURN, C. E., 1947. Mathematical Statistics (Cambridge Univ. Press).